

1996

## Mechanisms and control of mine floor heave.

Yajie Wang

Follow this and additional works at: <https://researchrepository.wvu.edu/etd>

---

### Recommended Citation

Wang, Yajie, "Mechanisms and control of mine floor heave." (1996). *Graduate Theses, Dissertations, and Problem Reports*. 9979.

<https://researchrepository.wvu.edu/etd/9979>

This Thesis is protected by copyright and/or related rights. It has been brought to you by the The Research Repository @ WVU with permission from the rights-holder(s). You are free to use this Thesis in any way that is permitted by the copyright and related rights legislation that applies to your use. For other uses you must obtain permission from the rights-holder(s) directly, unless additional rights are indicated by a Creative Commons license in the record and/ or on the work itself. This Thesis has been accepted for inclusion in WVU Graduate Theses, Dissertations, and Problem Reports collection by an authorized administrator of The Research Repository @ WVU. For more information, please contact [researchrepository@mail.wvu.edu](mailto:researchrepository@mail.wvu.edu).

## INFORMATION TO USERS

This manuscript has been reproduced from the microfilm master. UMI films the text directly from the original or copy submitted. Thus, some thesis and dissertation copies are in typewriter face, while others may be from any type of computer printer.

**The quality of this reproduction is dependent upon the quality of the copy submitted.** Broken or indistinct print, colored or poor quality illustrations and photographs, print bleedthrough, substandard margins, and improper alignment can adversely affect reproduction.

In the unlikely event that the author did not send UMI a complete manuscript and there are missing pages, these will be noted. Also, if unauthorized copyright material had to be removed, a note will indicate the deletion.

Oversize materials (e.g., maps, drawings, charts) are reproduced by sectioning the original, beginning at the upper left-hand corner and continuing from left to right in equal sections with small overlaps. Each original is also photographed in one exposure and is included in reduced form at the back of the book.

Photographs included in the original manuscript have been reproduced xerographically in this copy. Higher quality 6" x 9" black and white photographic prints are available for any photographs or illustrations appearing in this copy for an additional charge. Contact UMI directly to order.

# UMI

A Bell & Howell Information Company  
300 North Zeeb Road, Ann Arbor MI 48106-1346 USA  
313/761-4700 800/521-0600



# **MECHANISMS AND CONTROL OF MINE FLOOR HEAVE**

by

**Yajie Wang**

**A Dissertation  
Submitted to the Faculty of  
Department of Mining Engineering  
College of Engineering and Mineral Resources  
West Virginia University**

**In Partial Fulfillment of the Requirements  
for the Degree of  
Doctor of Philosophy  
in  
Mining Engineering**

**Morgantown, WV  
November 1996**

**UMI Number: 9716388**

---

**UMI Microform 9716388**  
**Copyright 1997, by UMI Company. All rights reserved.**

**This microform edition is protected against unauthorized  
copying under Title 17, United States Code.**

---

**UMI**  
**300 North Zeeb Road**  
**Ann Arbor, MI 48103**

## **ABSTRACT**

Floor heave has been one of the important ground control problems in the underground coal mining industry. However, the mechanisms of floor heave have not been fully understood although some efforts have been made by many researchers. In this research, two mines experiencing floor heave are selected to study the mechanisms of floor heave. By insitu observation, two types of floor heave are identified: Type I floor heave caused by buckling failure of floor, and the Type II floor heave caused by plastic failure and plastic flow of floor material. Based on the observation results, the mechanisms of floor heave are analyzed and the mechanical models for two types of floor heave are established. The model for type I floor heave is based on composite slab theory and the model for type II floor heave is based on foundation theory. Using the models established, the floor heaves in two mines were analyzed and one of them was redesigned. Results show that the floor heaves predicted by the models are quite accurate. The mine has eliminated the floor heave problems after it had been redesigned.

## ACKNOWLEDGMENTS

The Author wishes to express his sincere appreciation and gratitude to his academic/research advisor, Dr. Syd S. Peng for his instruction, encouragement, and support during the course of this research.

Sincere thanks are due to the other members of the Ph.D. advisory committee, Dr. A. W. Khair, Dr. H. Rauch, Dr. Mo Gabr, and Dr. D. Thompson for their great support and suggestions.

The author wishes to thank all of the faculty and staff members, and graduate students in the Department of Mining Engineering.

Special thanks are extended to my wife and daughter for their love, patience, and understanding throughout the course of this research.

Finally, I would like to thank my parents for their great encouragement and moral support.

## TABLE OF CONTENTS

<b>COVER PAGE .....</b>	<b>i</b>
<b>ABSTRACT.....</b>	<b>ii</b>
<b>ACKNOWLEDGEMENTS.....</b>	<b>iii</b>
<b>TABLE OF CONTENTS .....</b>	<b>iv</b>
<b>LISTS OF FIGURES.....</b>	<b>vii</b>
<b>LIST OF TABLES .....</b>	<b>xi</b>
<b>CHAPTER 1. INTRODUCTION .....</b>	<b>1</b>
1.1 General .....	1
1.2 Literature Review .....	2
1.2.1 In-situ Observations .....	3
1.2.2 Mechanisms of Floor Heave .....	13
1.3 Objectives .....	15
<b>CHAPTER 2. FIELD STUDY .....</b>	<b>16</b>
2.1 Floor Heave in Smoot Mine .....	16
2.2 Floor Heave in Marson Mine .....	30
<b>CHAPTER 3. MECHANISMS OF TYPE I FLOOR HEAVE.....</b>	<b>37</b>
3.1 Modelling of Floor Strata as a Composite Slab Model .....	37
3.1.1 Mechanistic Model of Floor Heave.. .....	37
3.1.2 Elastic Solution .....	39



3.2	Floor Failure Initiation and Propagation .....	42
3.3	Buckling Failure Analysis .....	43
3.4	Floor Heave Analysis .....	45
3.5	Numerical Solution of the Composite Slab Model .....	47
3.5.1	Finite Difference Equation for Governing Differential Equation .....	47
3.5.2	Boundary Conditions .....	50
3.5.3	Stress Calculation .....	52
3.6	A Case Study - Floor Heave in Smoot Mine.....	53
<b>CHAPTER 4. MECHANISMS OF TYPE II FLOOR HEAVE .....</b>		<b>73</b>
4.1	Mechanistic Model of Floor Heave .....	73
4.2	Floor Bearing Capacity .....	75
4.2.1	Floor Failure Mechanism.....	75
4.2.2	Floor Bearing Capacity.....	79
4.3	Residual Floor Bearing Capacity .....	85
4.4	Performance of Floor Bearing Capacity Equation in Coal Mine .....	89
4.5	Relation between Pillar Punching and Floor Heave .....	93
4.6	Floor Failure and Floor Heave Analysis and Control Methods .....	95
4.7	Floor Heave Analysis and Mine Design - A Practical Application .....	96
4.7.1	Geological and Mining Condition in Mine A .....	96
4.7.2	Investigation of the Floor Heave .....	98
4.7.3	Rock Properties .....	101
4.7.4	Floor Bearing Capacity .....	103

4.7.5 Residual Bearing Capacity of Floor .....104

4.7.6 Finite Element Modelling .....105

**CONCLUSIONS** .....130

**REFERENCE** .....134

**VITA** .....137

**APPROVAL PAGE** .....138

### Lists of Figures

Fig. 1.1 Mine map of King #4 Mine	4
Fig. 1.2 Floor heave at location F, panel 6 in King #4 Mine	6
Fig. 1.3 "Core diskings" of Immediate mine floor core sample taken at Glen Roggers Mine	7
Fig. 1.4 Floor heave at the center of an entry at the Glen Roggers Mine	9
Fig. 1.5 Floor heave at the rib side of an entry at the Glen Roggers Mine	9
Fig. 1.6 Differential horizontal displacement in an observation hole at the Glen Roggers Mine	10
Fig. 1.7 Section layout in Big John #4 Mine	11
Fig. 1.8 Schematic diagram of typical observed floor heave in Big John #4 Mine	12
Fig. 2.1 Geological column of immediate floor of Smoot Mine	17
Fig. 2.2 Mine map for Smoot Mine	18
Fig. 2.3 Panels selected for field study in Smoot Mine	20
Fig. 2.4 Floor instrumentation plan for the Smoot Mine	21
Fig. 2.5 Measured floor deformation at Site 1, Smoot mine	23
Fig. 2.6 Measured floor deformation at Site 2, Smoot mine	24
Fig. 2.7 Cross-section of floor heave at Site 2 in Smoot Mine	26
Fig. 2.8 Separation between layer 1 and layer 2 at Site 2, Smoot Mine	27
Fig. 2.9 Differential horizontal displacement observed in an observation hole at Site 2, Smoot Mine	28

Fig. 2.10 Floor heave sequence of events	30
Fig. 2.11 Mine map of Marson Mine	31
Fig. 2.12 Geological column of Marson Mine	32
Fig. 2.13 Floor heave in Marson Mine	35
Fig. 2.14 Sequence of floor heave in Marson Mine	36
Fig. 3.1 Mechanistic model of floor heave	38
Fig. 3.2 Bending moments and shear stresses	41
Fig. 3.3 Buckling failure model	44
Fig. 3.4 Floor heave model	46
Fig. 3.5 Finite difference grid system	48
Fig. 3.6 Fixed boundary condition	51
Fig. 3.7 Panel 1 Left of Smoot Mine	54
Fig. 3.8 Floor deflection in inches before pillar retreating	59
Fig. 3.9 Maximum tensile stress distribution in psi before pillar retreating	60
Fig. 3.10 Maximum shear stress distribution in psi on bedding plane 1 before pillar retreating	61
Fig. 3.11 Floor deflection in inches after pillar retreating	62
Fig. 3.12 Maximum tensile stress distribution in psi after pillar retreating	63
Fig. 3.13 Maximum shear stress distribution in psi on bedding plane 1 after pillar retreating	64
Fig. 3.14 Maximum shear stress distribution in psi on bedding plane 2 after pillar retreating	65

Fig. 3.15 Maximum shear stress distribution in psi on bedding plane 3 after pillar retreating	66
Fig. 3.16 Maximum tensile stress distribution in psi on layer 1	67
Fig. 3.17 Maximum tensile stress distribution in psi on layer 2	68
Fig. 3.18 Maximum tensile stress distribution in psi on layer 3	69
Fig. 3.19 Maximum tensile stress distribution in psi on layer 4	70
Fig. 3.20 Maximum tensile stress distribution in psi on layer 5	71
Fig. 3.21 Maximum tensile stress distribution in psi on layer 6	72
Fig. 4.1 Mechanistic model of type II floor heave	74
Fig. 4.2 Slip-line field	76
Fig. 4.3 Formation of the problem of bearing capacity	80
Fig. 4.4 Generalized curve of relation between floor stress and settlement	86
Fig. 4.5 Mining method for the studied mine	90
Fig. 4.6 Floor heave calculation	94
Fig. 4.7 Geological column of Mine A	97
Fig. 4.8 Mine map of mine A	99
Fig. 4.9 Floor heave in first west section	100
Fig. 4.10 Simulation of floor failure initiation	106
Fig. 4.11 Vertical stress distribution on floor before failure initiation	108
Fig. 4.12 Floor average stress distribution and failure initiation	109
Fig. 4.13 Simulation of floor failure propagation	110
Fig. 4.14 Vertical stress distribution after floor failure initiation	111

Fig. 4.15 Floor average stress distribution and failure propagation	112
Fig. 4.16 Tensile stress distribution in the immediate roof after floor failure initiation	113
Fig. 4.17 Simulation of floor heave	115
Fig. 4.18 Vertical stress distribution after all the wet floor fails	116
Fig. 4.19 Floor average stress distribution and failure propagation	117
Fig. 4.20 Tensile stress distribution in the immediate roof after all of the wet floor area fails	118
Fig. 4.21 Maximum shear stress distribution in the immediate roof after all of the wet floor area fails	119
Fig. 4.22 Maximum shear stress distribution on the surface after all of the wet floor area fails	120
Fig. 4.23 Mining plan analysis	122
Fig. 4.24 Floor heave and pillar punching for the seven-entry system	123
Fig. 4.25 Floor heave and pillar punching for the six-entry system	124
Fig. 4.26 Floor heave and pillar punching for the five-entry system	126
Fig. 4.27 Proposed mining plans	127

### Lists of Tables

Table 1.1 Examples of floor heave	3
Table 2.1 Mechanical Properties of floor rocks, Smoot mine	19
Table 3.1 Mechanical properties of floor rocks for Smoot mine	55
Table 3.2 The maximum shear stress on each bedding plane	56
Table 3.3 Maximum redistributed tensile stress on each layer	56
Table 3.4 Buckling failure analysis	57
Table 3.5 Calculated floor heave	58
Table 4.1 Moisture effect on floor bearing capacity in Mine 1	83
Table 4.2 Moisture effect on floor bearing capacity in Mine 2	84
Table 4.3 Determination of deduction ratio for residual floor bearing capacity	87
Table 4.4 Determination of deduction ratio for residual floor bearing capacity	88
Table 4.5 Floor mechanical properties for the studied mine	91
Table 4.6 Pillar performance and stability factor	92
Table 4.7 Floor fireclay properties for Mine A	102
Table 4.8 Rock properties for Mine A	103
Table 4.9 Floor bearing capacity for Mine A	104
Table 4.10 Residual floor bearing capacity for Mine A	105
Table 4.11 Floor safety factor for mining plans shown in Fig. 4.27	128

# CHAPTER 1

## INTRODUCTION

---

### 1.1 General

Traditionally, pillar design and roof support are the two main tasks for underground mine design. Many efforts have been made to study the mechanism of pillar and roof failure and develop their design methods. However, floor heave, one of the ground control problems, has not received its due attention as compared to the roof and pillar problems. Floor heave occurs in many coal mines and causes many types of problems including:

1. Delay in entry development;
2. Disruption of haulage systems such as tracks and conveyer support systems;
3. Closure of entries. In some cases, the floor heaves so badly that the entries are totally filled up and the panels have to be abandoned;
4. Difficulty in ventilation; and
5. Roof failure and subsidence as a result of floor heave.

In order to control the floor heave, the mechanisms of floor failure and floor heave should be understood and floor failure and floor heave should be predicted before any control measure is applied. Unfortunately, there is no method available to predict floor failure and floor



heave although some floor failure and floor heave mechanisms have been proposed. Therefore, it is necessary to study the mechanism of floor heave further and develop a model to predict floor heave and to design floor heave control methods.

## 1.2 Literature Review

Initial investigations to characterize floor heave were conducted by Freer (1892), Jones (1897), Hall (1909), Young (1917), Nelson (1947), Jenkins (1957, 1958, 1960), Holland (1962) and Wilson (1965). However, these studies did not investigate the failure mechanisms and consider the mine layout and the mining sequence. Within the past twenty years researchers have started to study the mechanisms of floor failure and floor heave. These researchers include: Peng (1981, 1986), Peng, et al (1992), Peng and Wang (1993), Aggson (1978), Afrouze (1975), and Chugh (1986, 1990).

Some studies have been conducted on floor heave in recent years in which much effort has been devoted to observe floor heave in underground mines and to study the mechanisms of floor heave. Through in-situ observation, two kinds of floor heaves have been observed in underground mines: one is floor rock layer buckling which is called type I floor heave, while the other is plastic failure and flow of floor material which is called type II floor heave. Correspondingly, there are two kinds of floor heave mechanisms proposed: one is that floor heave is caused by the immediate floor rock buckling which can be considered as a composite beam failure and buckling. The other is that floor rock is squeezed into the entry by plastic

flow of the floor rock as a result of the pillar punching into the floor.

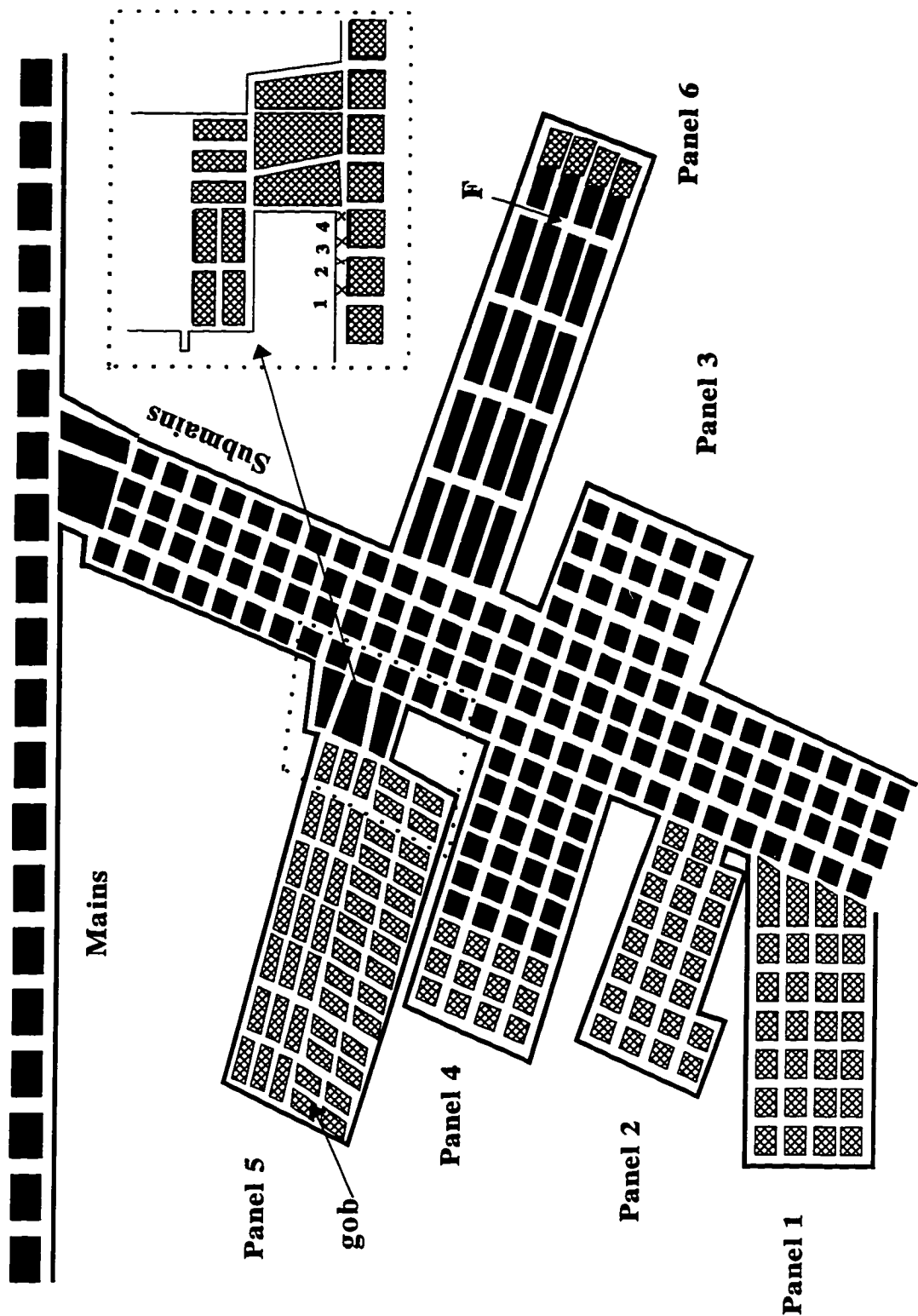
### 1.2.1 In-situ Observations

There are many coal mines in the U.S. that have experienced the floor heave problems. Some of them were so bad that a section or panel had to be abandoned. In order to study the mechanisms of the floor heave and design its control methods, many in-situ observations have been performed. Table 1 shows some of the mines in which floor heave was experienced and study was performed. Details of the floor heave in those mines are described as follows:

Table 1 Examples of floor heave

Mine	State	Floor structure	Type of floor heave	Overburden depth (ft)	Horizontal stress (psi)
King #4	Utah	shale and sandstone interbedded	I	1,200	1,085
Glen Rogers	WV	shale and sandstone interbedded	I	800	4,000
Smoot	WV	shale/fireclay	I	800	N/A
Marson	WV	massive mudstone	II	350-600	N/A
Big John #4	WV	massive coal with soft shale	II	250-500	N/A
Mary Lee	AL	soft fireclay	II	500	N/A

#### Case 1. Floor Heave in King #4 Mine

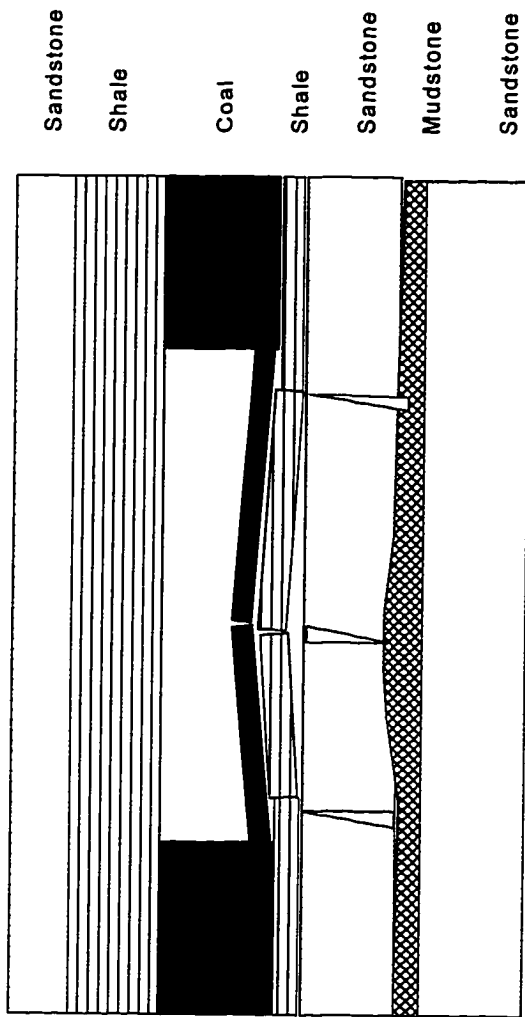


**Fig. 1.1 Mine map of King #4 Mine  
(after Conover, 1988)**

King #4 mine is located in the Wasatch Plateau coal field in Carbon County, Utah, west of the town of Hiawatha. As shown in Fig. 1.1, a room-and-pillar mining method with full pillar extraction was used. The overburden depth was about 1,200 ft. The pillar sizes in panels 1 through 4 was 70 ft x 70 ft. Pillar size in Panel 6 was 35 ft x 90 ft. The immediate floor consisted of very strong shale and interbedded with sandstone. The maximum principal horizontal stress measured by the U.S. Bureau of Mines (Conover et al., 1988) was 1,085 psi. Floor Heave in King #4 mine was also observed by Conover et al.(1988). The floor heave problems in this mine were very severe during retreat and had caused abandonment of some panels. Floor heaves typically occurred from one to three crosscuts outby the caving line. Panel 4 was abandoned due to floor heave during pillaring. Panel 5 was fully extracted with floor heave at convergence stations 2, 3, and 4. Panel 6 was abandoned soon after the retreat operation began. In order to study the mechanism of floor heave, a trench was dug at location F in panel 6. It can be concluded by examination of the trench cross-section (Fig. 1.2) that (1) the immediate floor consisted of shale interbedded with sandstone, and the main floor is massive sandstone; (2) the floor behaved like a composite beam; (3) shear failures on the bedding planes and separations between layers occurred during floor heave; and (4) the immediate floor had horizontal displacements caused by high horizontal stress.

#### Case 2. Floor Heave in Glen Rogers Mine (Aggson, 1978)

Glen Rogers mine is located on the Raleigh-Wyoming County boundary line in West Virginia, and is operated by the Raleigh-Wyoming coal Co. This mine had experienced extensive floor heave problems since it opened in the 1920's. The immediate floor was



**Fig. 1.2 Floor heave at location F, panel 6 in King #4 Mine  
(after Conover 1988)**

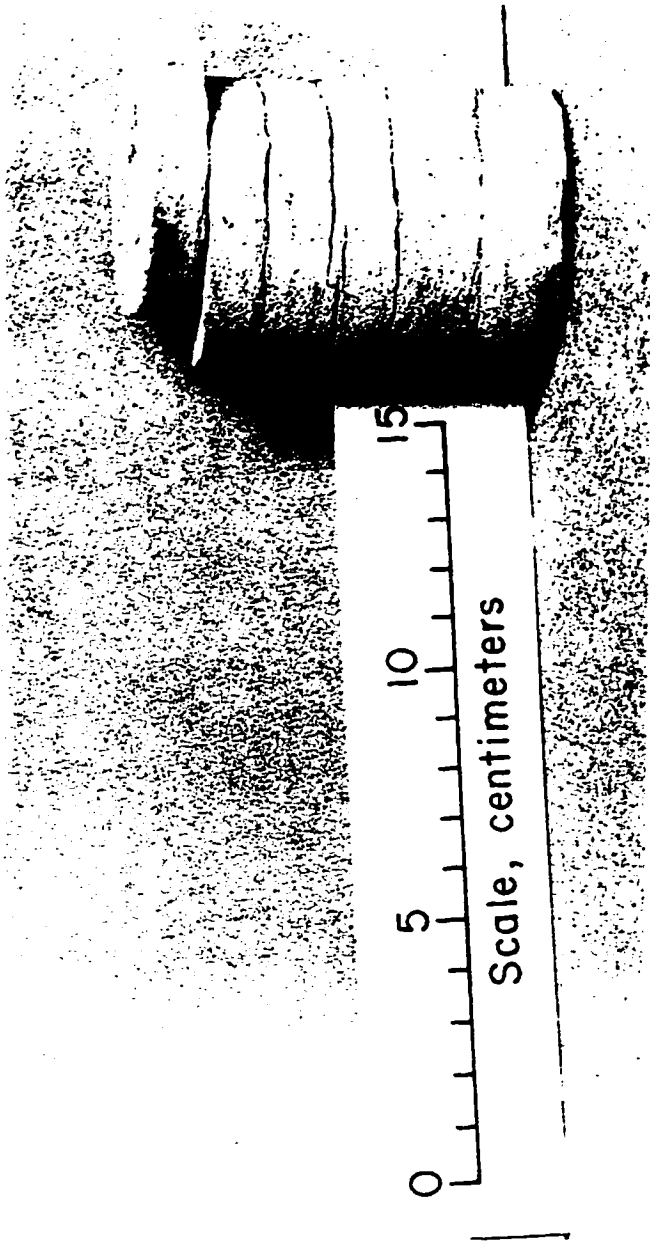


Fig. 1.3 "Core dinking" of immediate mine floor core sample taken from Glen Roggers Mine (after Aggonson, 1978)

composed of very thinly bedded strong shale. "Core diking" or breaking up of the core along bedding planes (Fig. 1.3) occurred when coring the floor, which means the shear strength of the bedding plane is very weak. The maximum horizontal stress was measured to be 4,000 psi by Aggson (1978). Floor heave usually occurred as arching near the center of the floor span (Fig. 1.4) or as a break near the rib followed by vertical deflection of the floor at the rib and sloping of the floor across the entry (Fig. 1.5). The shear failure and differential horizontal displacement between layers was also observed through an observation hole (Fig. 1.6).

### Case 3. Floor Heave in Big John #4 mine

Fig. 1.7 is a section layout of Big John #4 mine in the Cedar Grove coal seam where floor heave occurred. The immediate floor in this section was highly slickensided claystone 2-5 ft thick. Pillars were 40 ft square and the entry and crosscut were 20 ft wide. The average overburden depth was 250 ft in section 1R and was 500 ft in section 1L. During mine development there were no apparent floor heave problems. Similarly, there were no floor heave problems during retreat pillaring in section 1R. When the pillar line reached position F in section 1L, however floor heave began outby the pillar line. Once started, floor heave spread quickly to the remaining area which had to be abandoned. The floor heave in this area was due solely to the fact that pillars had punched into the floor. Peng (1986) indicated: the initial stage of floor failure was caused by the pillar punching followed by floor heave around the edges of the pillars. As the pillars penetrated into the floor, the floor heave extended to the central area and then spread across the whole entry area. Where pillar penetration continued, the broken floor rock would gradually fill the mine entry (Fig. 1.8).

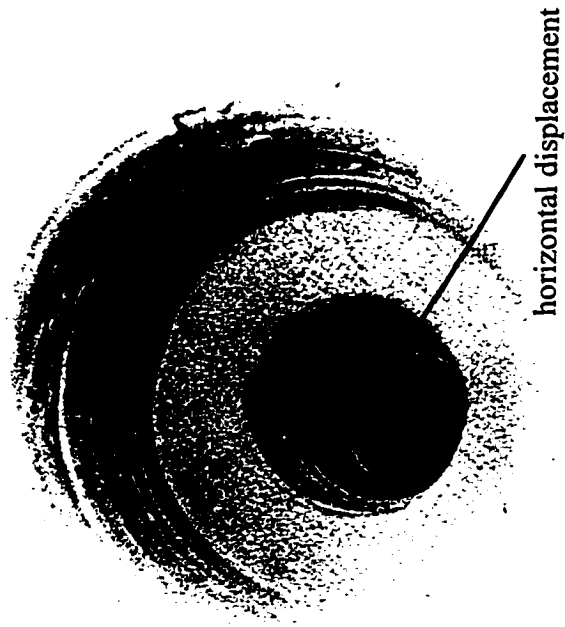


Fig. 1.4 Floor heave at the center of an entry at the Glen Rogers Mine  
(after Aggson, 1978)

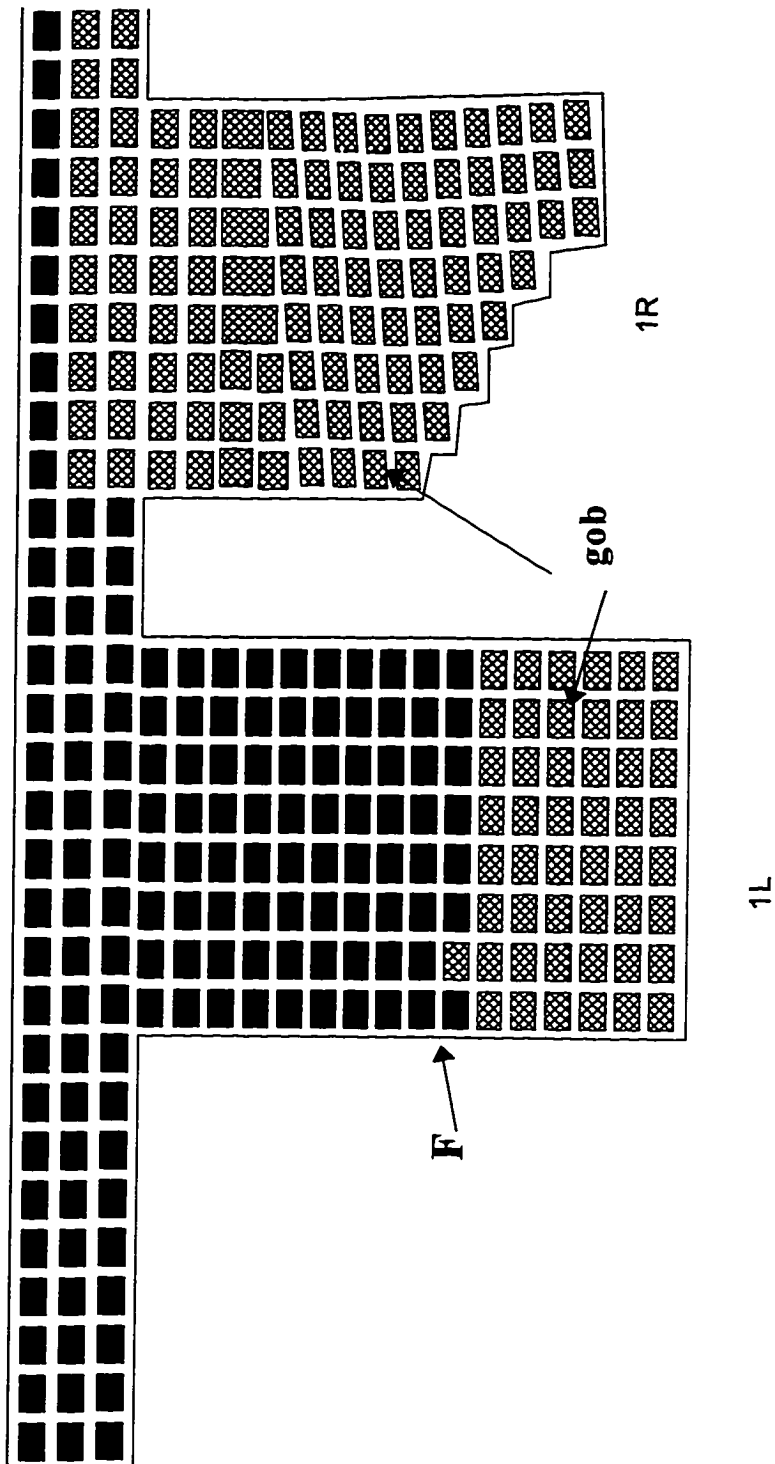


Fig. 1.5 Floor heave at the rib Side of an entry at the Glen Rogers Mine  
(after Aggson, 1978)

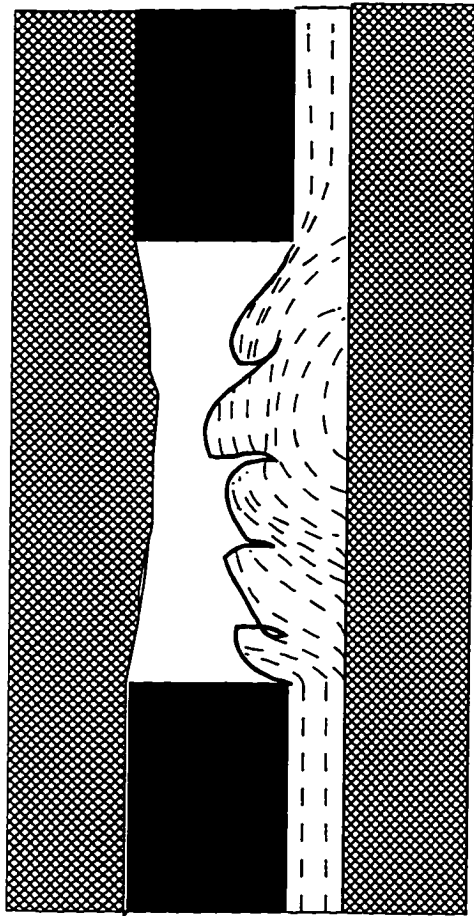




**Fig. 1. 6 Differential horizontal displacement in observation hole at the Glen Rogers Mine  
(after Aggson, 1978)**



**Fig. 1.7 Section layout in Big John #4 Mine (after Peng, 1986)**



**Fig.1.8 Schematic diagram of typical observed floor heave in Big John #4 Mine  
(after Peng, 1986)**

## 1.2.2 Mechanism of Floor Heave

Case 1 and case 2 presented above have typical type I floor heave. They share the following common features both in geological conditions and floor behavior: 1) the immediate floor is composed of several thin layers of relatively strong rock; 2) high horizontal stress is present; and 3) the floor behaves like a beam or a slab.

Case 3 is typical type II floor heave. The immediate floor consists of very soft rock such as claystone and mudstone. The floor heave is caused by pillar punching into the mine floor.

So far, there has been no systematic study about the mechanisms of floor heave. Some researchers (William, 1992) have proposed some basic concepts and procedures associated with floor heave. Since the mechanisms are different for the two types of floor heave, the mechanical models are different.

### 1. Mechanism of Type I floor heave

For the type I floor heave, it is commonly believed that the floor behaves like a composite beam and there are excessive horizontal stresses acting on the floor. Aggson (1978) reported that in a West Virginia coal mine, where the pillar stress was less than the strength of the floor and a high horizontal stress was present, the immediate floor layers were detached from each other along the bedding planes because of shear stress on the bedding planes. The floor behaved like a Euler's column and buckled up so floor heave occurred. Conover et al.,(1988) described that in King # 4 mine, the cause of the floor heave can be attributed to a high horizontal stress acting on the floor layers and the vertical stress on the pillars. Before the entry

was mined, the floor layers were loaded and deformed uniformly. When the entry was mined, confinement on the floor layers was removed, and the layers then expanded vertically and deformed into the entry. Expansion of the layers was increased by the presence of horizontal stress. The lower layer of the floor could not fully expand due to confinement provided by the upper layers. Bending of the upper layers into the entry permitted partial strain relief and induced tensile stress on the top surface of the layers at the center of the entry. Increased pillar loads caused by stress transfer from nearby mining or caving, resulted in increased induced horizontal stresses and associated vertical stress and bending stresses in the floor layers.

All of these descriptions are conceptual. There has been no mechanical model developed yet to predict the floor heave and design the mine panels to prevent floor heave. Therefore, it is necessary to develop a mechanical model to predict when the floor will fail and how much the floor can heave up.

## 2. Mechanism of the Type II floor heave

Based on the conditions of Type II mine floors, the mechanism of floor heave is more or less similar to the foundation failure in civil engineering. Based on the slip-line theory, Terzaghi (1943) developed a general bearing capacity equation. For different types of foundations, the bearing capacity equation has been modified. However, the floor heave problem is more complicated than foundation failure. In order to predict and prevent floor heave, some other factors must be considered such as roof condition, panel size, residual bearing capacity of floor, magnitude of pillar punching, relationship between pillar punching and floor heave, and magnitude of floor heave.

### **1.3 OBJECTIVES**

Through the literature review, it has been found that although some research has been done on floor heave, there are still many problems remaining to be resolved. This dissertation will concentrate on the mechanisms of both kinds of floor heave experienced frequently in underground coal mines. The objectives of this dissertation are:

- 1: Through in-situ observation of floor heave, analyze floor heave mechanisms for the two type of floor heave.
- 2: Develop a mechanistic model for type I floor heave.
- 3: Develop a mechanistic model for type II floor heave.
- 4: Model validation.
- 5: Recommendations for panel design to prevent and control the floor heave.

## **CHAPTER 2**

### **FIELD STUDY**

---

---

In order to study the mechanisms of floor heave and to verify the theoretical models developed, two mines, Smoot mine which was experiencing the Type I floor heave and Marson mine which was experiencing the Type II floor heave, were chosen as the study sites.

#### **2.1 Floor Heave in Smoot Mine**

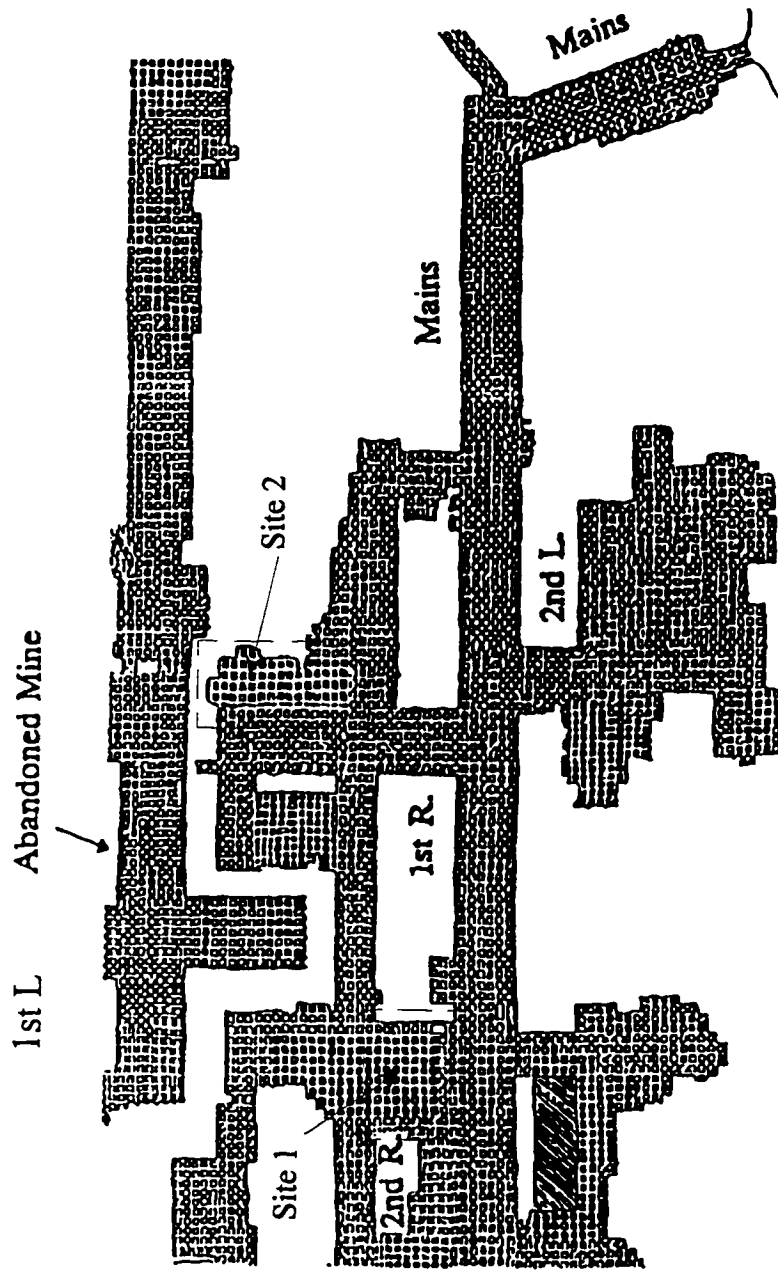
##### **Geological and Mining Conditions**

Smoot mine, located near Bolair, West Virginia, was developed in the Fire Creek coal seam using the room-and-pillar mining method. The overburden varies from 600 to 900 ft, and the seam thickness ranges from 4 to 7 ft. The immediate roof is a thick layer of sandy shale or sandstone. The immediate floor is mainly composed of shale and fireclay with coal streaks or bony coal. A geological column is shown in Fig. 2.1. The immediate floor rock type and mechanical properties are shown in Table 1. In general, four to six rows of chain pillars were developed at 60 x 80 ft centers during development and the entry width was 20 ft. Those pillars were completely recovered during retreating. The mine layout is shown in Fig. 2.2.

Symbol	Bedding plane	Rock type	Thickness
		coal	5'
layer 1		shale	4"
layer 2	1	bony coal	2"
layer 3	2	fireclay	6"
layer 4	3	bony coal	6"
layer 5	4	fireclay	3"
layer 6	5	fireclay	3"
	6	fireclay	

Fig. 2.1 Geological column of the immediate floor of Smoot Mine





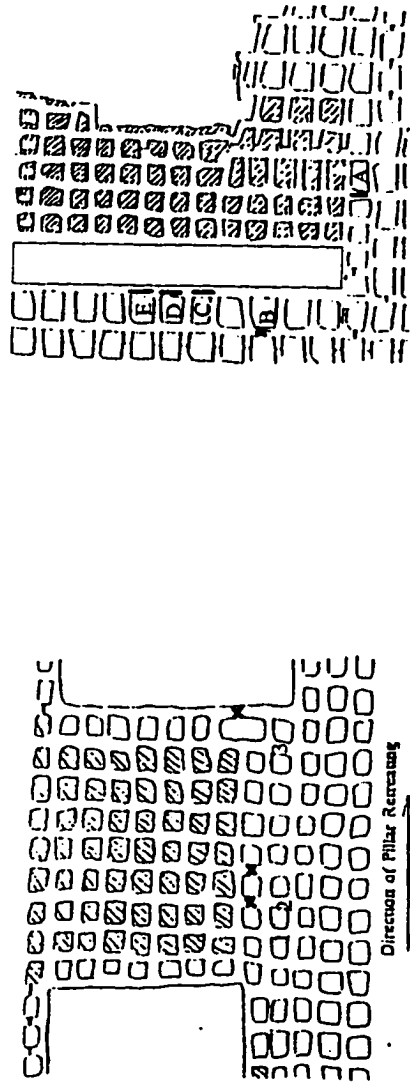
**Fig. 2.2 Mine map for Smoot Mine  
(Not to scale)**

Table 2.1 Mechanical Properties of Rocks

Rock Type	Young's Modulus (10 <sup>6</sup> psi)	Poisson's Ration	Compressive Strength (psi)	Tensile Strength (psi)	Shear Strength (psi)
Shale	1.85	0.23	11,498	1,168	1,175
Coal	0.29	0.33	1,922		
Fireclay	1.19	0.27	5,720	811	1,456

### Instrumentation Plan

In order to study the mechanism of floor heave in this mine, it was decided to monitor the floor heave at two sites. Site 1 was in the second right panel as shown in Fig. 2.3a and Site 2 was in the first left panel as shown in Fig. 2.3b. The instrumentation plan is shown in Fig. 2.4. The floor was monitored with mechanical bolts anchored at the 6 in., 18 in., and 40 in. horizons below the mine floor. The instrumentation plan is designed to monitor the floor profile for various horizons at various time periods after mining and subsequently identify the strata horizons above which heaving occurs.

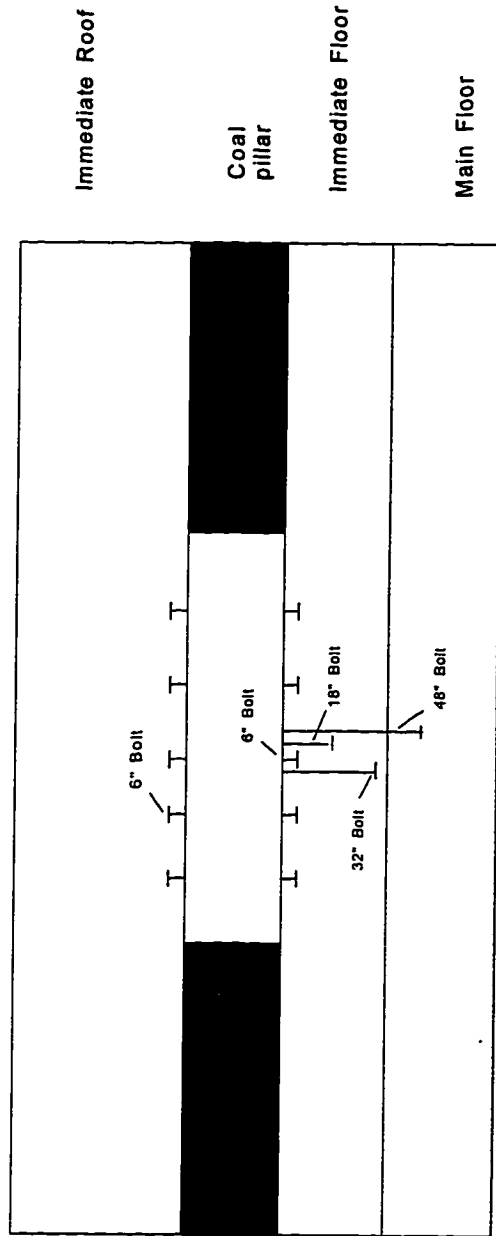


a

b

- X Instrumentation Station
- ▨ Mined out
- Floor Heave

**Fig. 2.3 Panels selected for field study in Smoot Mine  
(Not to scale)**



**Fig. 2.4 Floor instrumentation plan for the Smoot Mine**

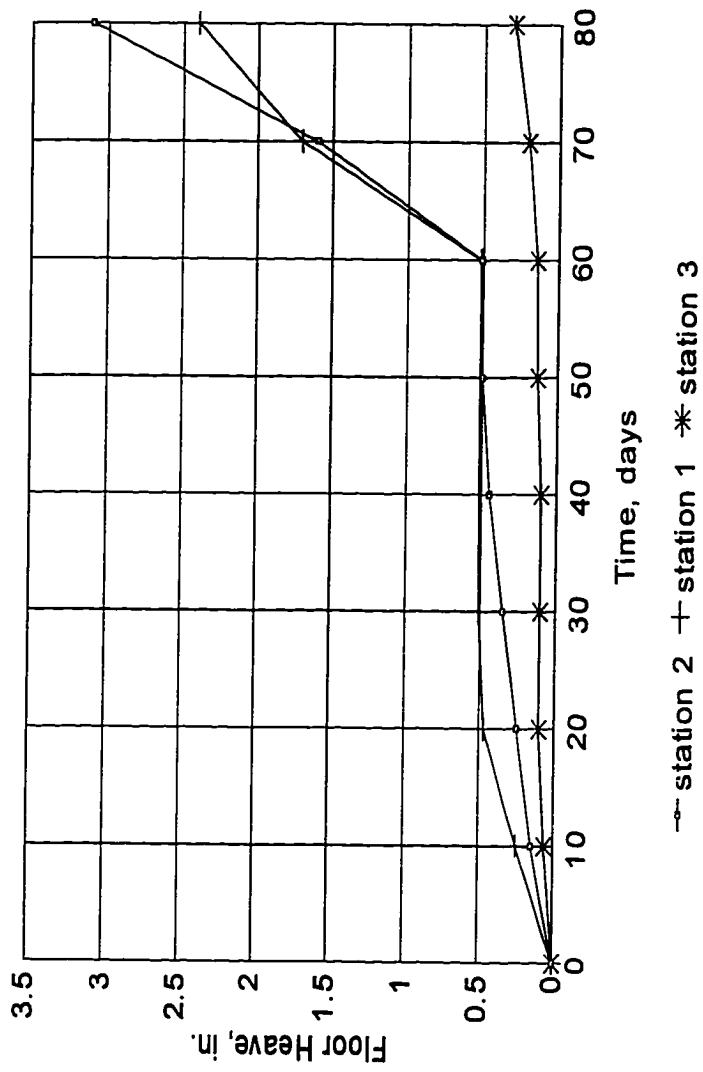
## **Floor Observation Results**

### **1. Floor Heave at site 1**

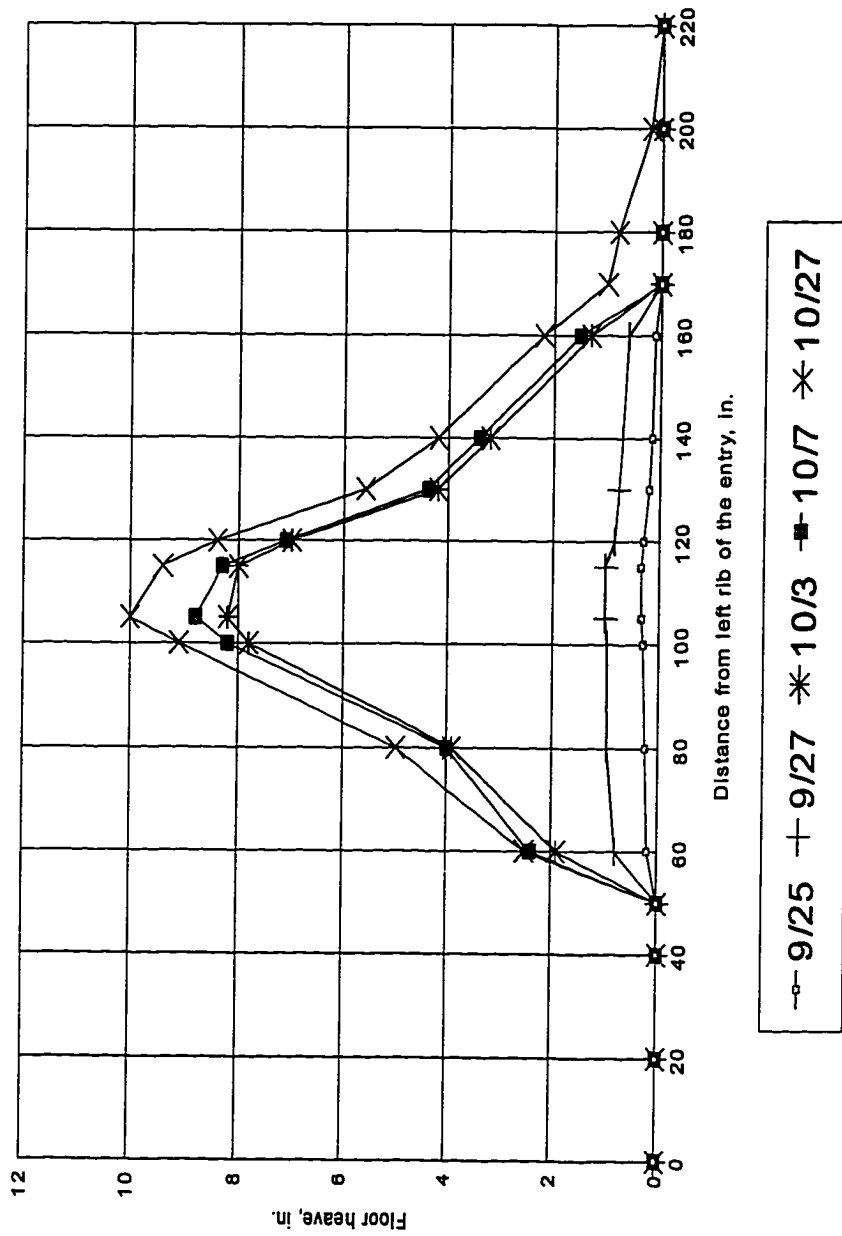
At site 1, station 1 and station 2 were installed at 1440 ft outby the pillaring line while station 3 was installed in the gob long after retreat pillaring had been completed in the second right panel (Fig. 2.3a). Fig. 2.5 shows the measured floor heave vs. the time at those three stations. The floor heave at station 1 and station 2 increased steadily as the pillar line was retreating toward the stations. Floor heave increased then sharply when the pillaring line was from 400 to 160 away. Clearly the pillar load increment due to the pillaring had very significant effect on the floor heave. Conversely, the floor heave at station 3 only increased a very small amount during the whole investigation period mainly because there was no mining activity nearby. Unfortunately, field monitoring was discontinued because the whole instrumentation area was sealed as a result of the unexpected emergency situation.

### **2. Floor Heave at Site 2**

Panel 1 Left has been developed for more than 10 years. Before pillar retreating, no floor heave was ever found. During and after retreating, the floor in some places heaved up suddenly. Fig. 2.3b shows the floor heave locations. The floor heaved up from 0.5 to 1.5 ft. Fig. 2.6 shows the observed floor heave at location B which was set up for monitoring on August 25, 1992. The panel retreat mining began from September 5. Before September 25 when the pillaring line was two blocks inby the station, floor deformation was very small.



**Fig. 2.5 Measured floor deformation at Site 1, Smoot Mine**



**Fig. 2.6 Observed floor heave at Site 2, Smoot Mine**

From September 27 when the pillaring line was one block inby the station, floor deformation increased significantly but no floor failure was observed. On October 3 when the pillaring line was two blocks outby the station, the floor failed and heaved up suddenly. After that and until October 27 the progressive floor heave increased 2 inches more. The floor behaved like a beam (Fig. 2.7). Also separation between the first and second layers during the period of floor heave was observed (Fig. 2.8). An observation hole drilled at the investigation site clearly showed differential horizontal displacement between floor rock layers of 0.5 to 1.5 in. (Fig. 2.9).

### **Summary**

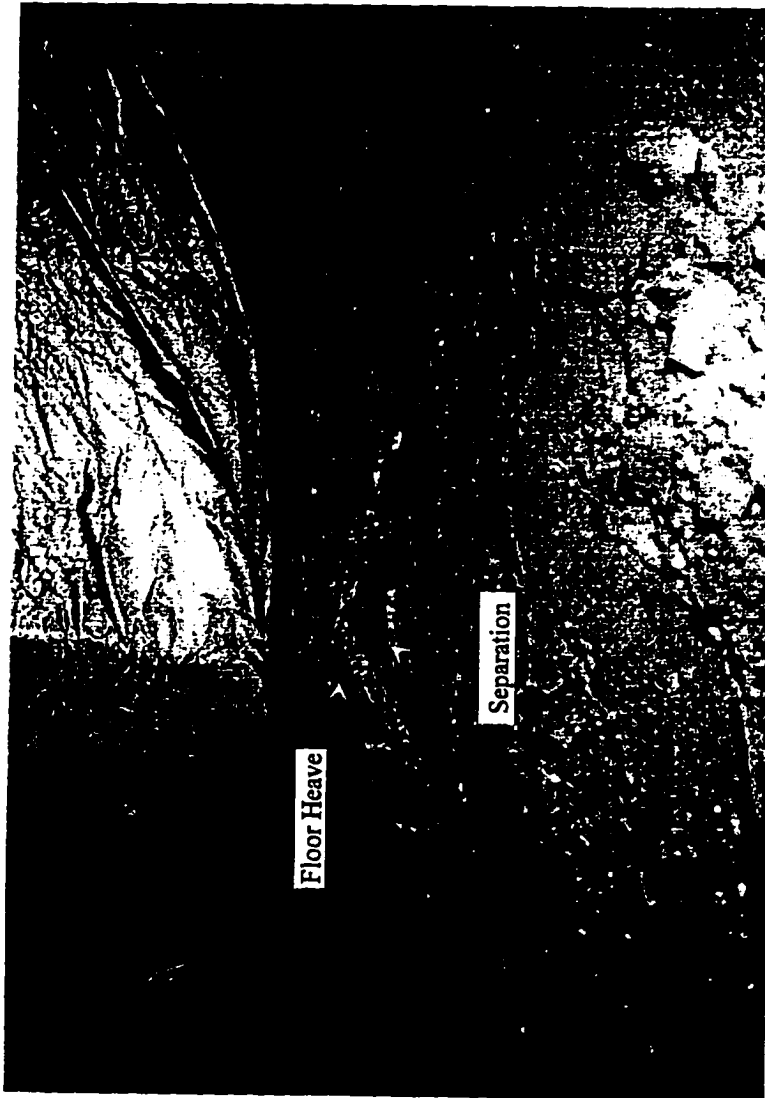
From the results of observations in Smoot mine, the basic conditions for the type 1 floor heave can be summarized as:

(1) Stress conditions: Both vertical and horizontal stresses must have been present and sufficiently large. Observations showed that most floor heaves occurred during the retreat pillaring stage, which means the abutment pressure transferred to the outby pillars increased the vertical stress and caused the floor to fail. However, the horizontal stress is more important in that it caused the broken floor to heave up. From the observations, it can be concluded that the final floor heave is caused by the buckling failure and horizontal movement of the floor layers.

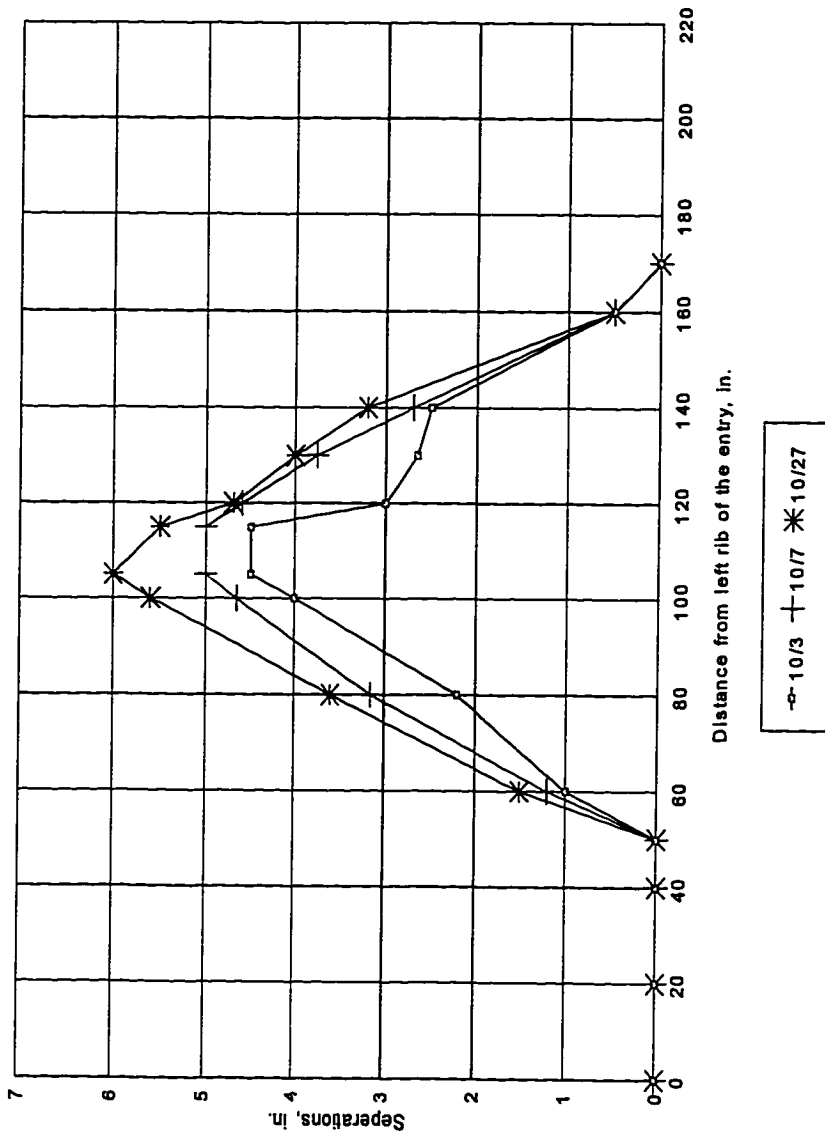
(2) Geological conditions: The floor consists of several thin layers of relatively strong rock, such as shale, sandstone etc.

The sequence of events for floor heave are:





**Fig. 2.7 Cross-section of floor heave at Site 2 in Smoot Mine**



**Fig. 2.8 Separation between layer 1 and layer 2 at Site B, Smoot Mine**



**Fig. 2.9 Differential horizontal displacement observed in an observation hole in mine floor at Site 2, Smoot Mine**

(1) During development, if the vertical stress is not high enough, the horizontal stress cannot cause the floor to heave.

(2) During retreat pillaring, the vertical stress increases through the transfer of abutment pressure to the pillars and the shear stresses on the bedding planes between the layers are also built up. Since the shear strength of the bedding plane is very low, shear failures on the bedding planes occur first (Fig. 2.10a).

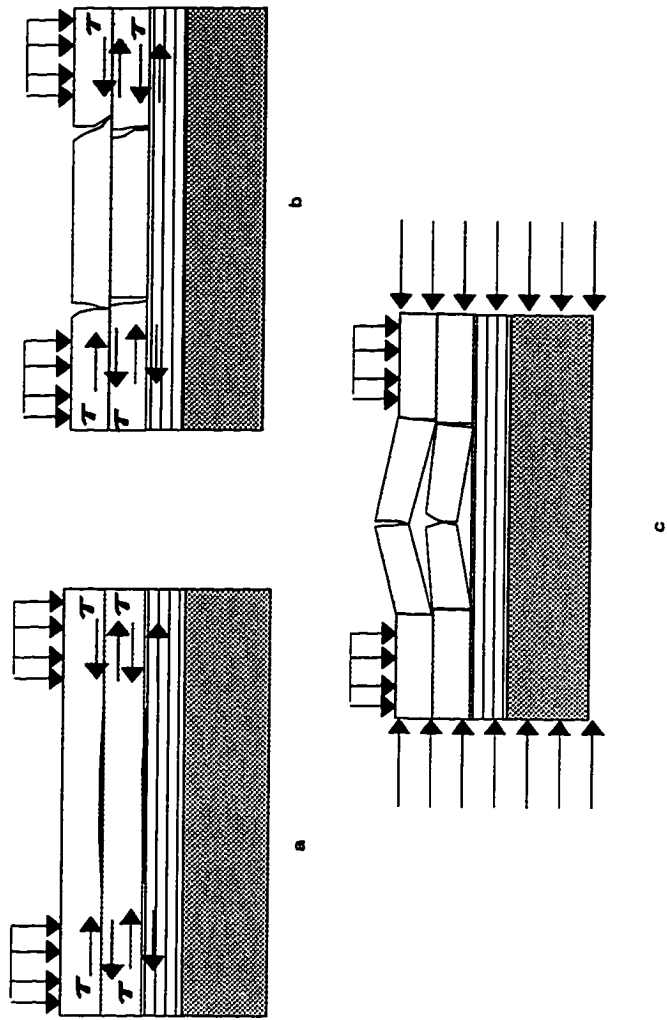
(3) Due to the shear failures of the bedding planes, the immediate floor will change from a composite floor beam into several individual beam members. This could cause tensile stress in each beam member to redistribute and increase. Therefore, tensile failure may occur as a result of redistributed tensile stress (Fig. 2.10b).

(4) If a high horizontal stress exists (usually caused by global tectonics structure), it will cause the floor to buckle and subsequent horizontal movement of the floor members will cause the floor to heave up (Fig. 2.10c).

## **2.2 Floor Heave in Marson Mine**

### **Geological and Mining Conditions**

The Marson coal mine (Fig. 2.11) near Helvetia, West Virginia, was selected for studying the Type II floor heave. This mine is in the Sewell seam, approximately 4 ft thick. The roof is firm shale with a uniaxial compressive strength of 7800 psi. The floor is mostly mudstone with a uniaxial compressive strength of 1300 psi. The geological column is shown



**Fig. 2.10 Floor heave sequence of events**

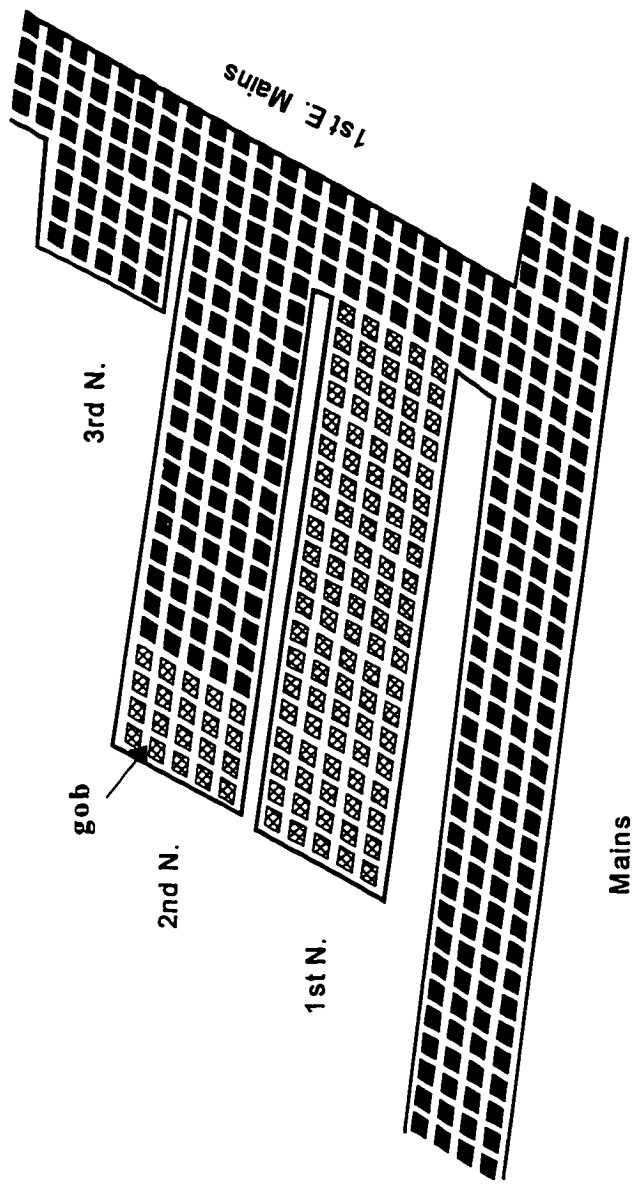
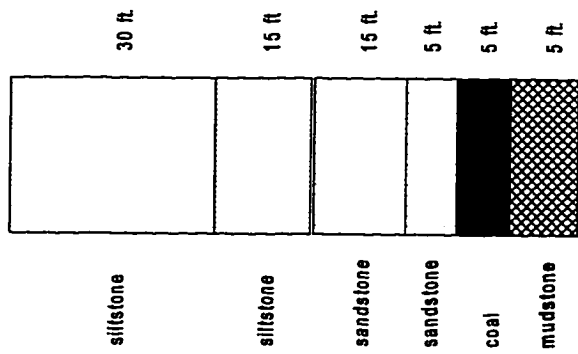


Fig. 2.11 Mine map of Marson Mine



**Fig. 2.12 Geological column of Marson Mine**

in Fig. 2.12. The overburden depth increased from 350 ft at the first North panel to more than 600 ft at the third North panel.

The Mains began with a four-entry and then five-entry system at 60 x 60 ft centers with a 20 ft wide entry. The first East Mains was five-entry system again at 60 x 60 centers.

### **Floor Heave Observations**

The first North panel was developed and retreat-pillared in four months with moderate floor heave near the panel turn off area. The second North panel was developed without any floor heave problems, but during retreat pillaring, the floor began to heave when the pillar line was halfway in the panel. At that time this panel was abandoned for fear that the heave might eventually prevent equipment retrieval. In the third North panel, it was during the development that the floor began to heave. Fig. 2.11 also shows the development face location when it was abandoned. The floor near the panel turn-off area heaved and reduced the entry height to 18-24 in (Fig. 2.13).

### **Summary**

From the observation results in Marson mine, the basic conditions for this kind of floor heave can be generalized as: (1) The immediate floor consists of massive soft rock material such as mudstone; and (2) the vertical stress is higher than the floor bearing capacity. The floor heave sequence can be generalized as:

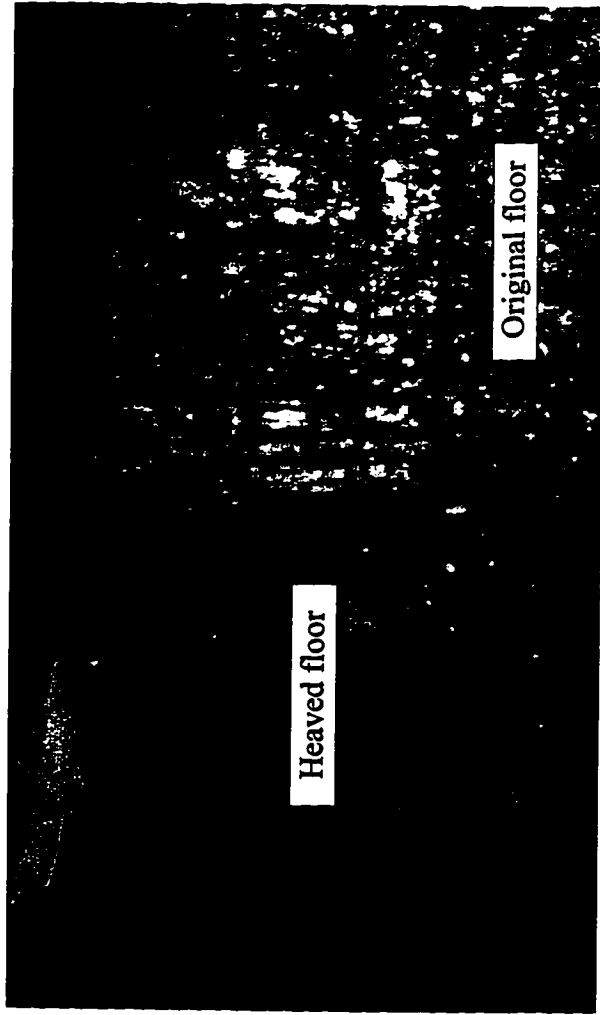
- (1) Once the vertical stress on the floor exceeded the bearing capacity of the floor, the



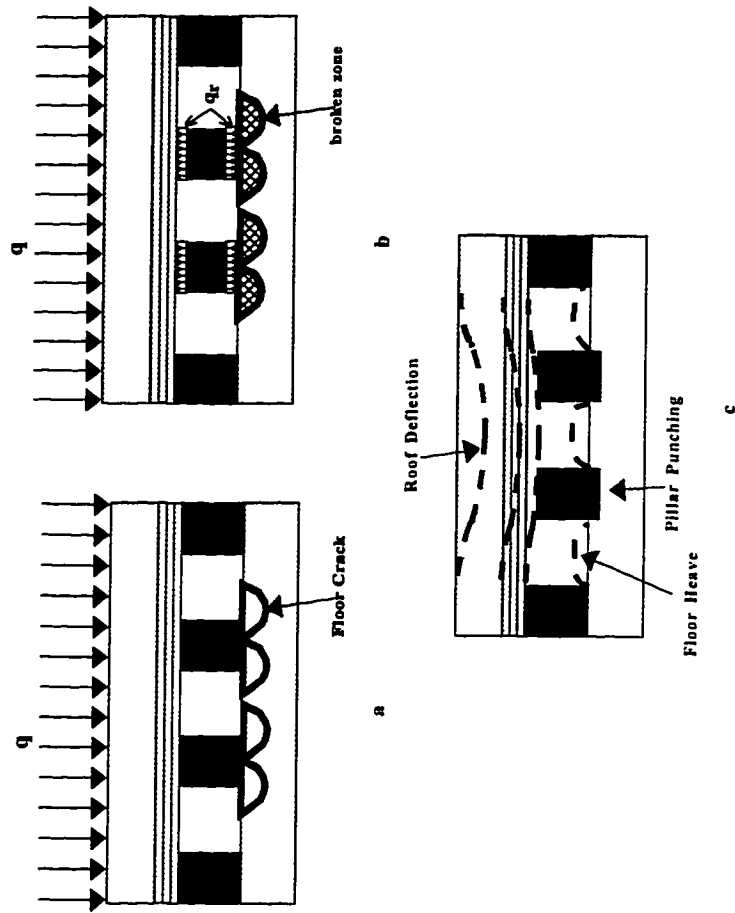
floor failed (Fig. 2.14a).

(2) After floor failure, the floor bearing capacity is reduced to the residual values which are more or less remains constant while the pillars continue to punch into the floor. The magnitude of the floor heave depends on how much pillars can punch into the floor (Fig. 2.14b).

(3) Because of pillar punching into the floor, pillar resistance to roof sagging is reduced to the residual value. Consequently, the roof both above the entries and pillars deflected. The magnitude of floor heave depends on the final roof deflection right above the pillars (Fig. 2.14c).



**Fig. 2.13 Floor heave in Marson Mine**



**Fig. 2.14 Sequence of floor heave**

**CHAPTER 3**  
**MECHANISM OF THE TYPE I FLOOR HEAVE**

---

---

**3.1 Modeling of Floor Strata as a Composite Slab Model**

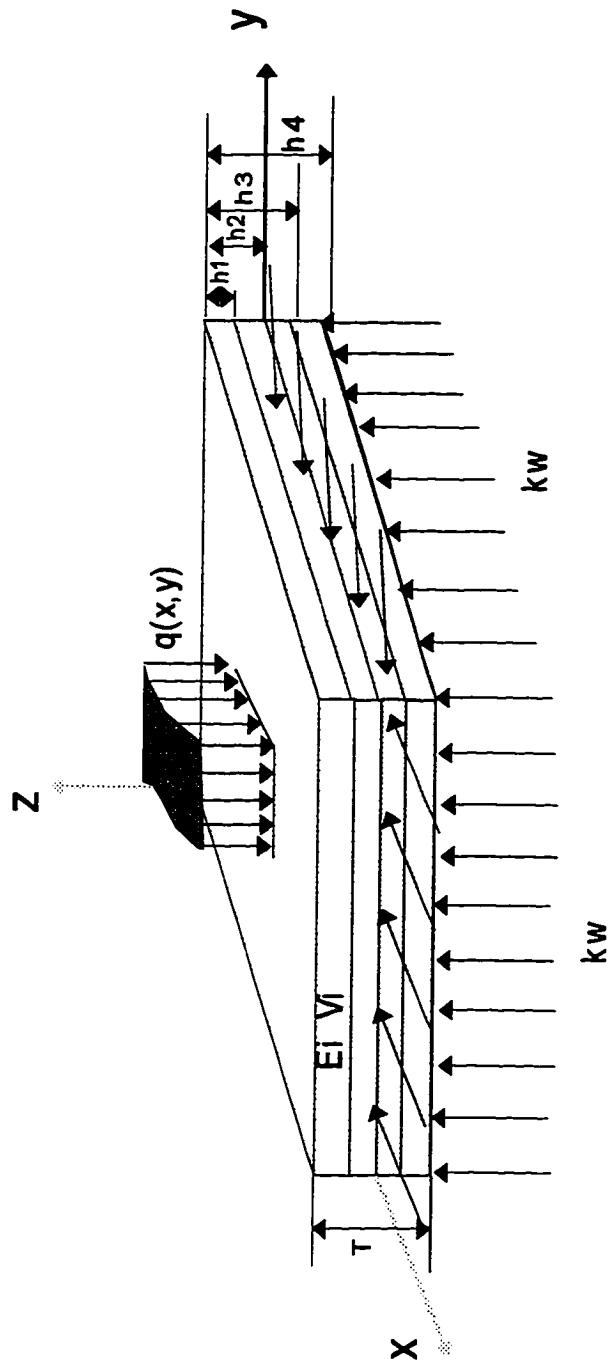
**3.1.1 Mechanistic Model of Floor Heave**

Based on the field study on the Type I floor heave, it is concluded that the immediate floor consists of several layers of relatively strong rock which behaves like a beam or a slab. The underlying main floor rock consists of a massive strong rock layer. Therefore it is reasonable to assume that:

- (1) The immediate floor is treated as a composite slab which may consist of  $n$  layers with different thicknesses  $t_i$ , Young's moduli  $E_i$  and Poisson's ratio  $\nu_i$ .
- (2) The main floor rock can be considered as a Winkler's foundation with the immediate floor rock resting on it.
- (3) Both the vertical stress and horizontal stress are acting on the floor.

Based on the assumptions described above, the composite slab model is shown in Fig.

3.1.  $q(x, y)$  is the stress transferred from pillar to the floor.



**Fig. 3.1 Mechanistic model of floor heave**

### 3.1.2 Elastic Solution

Based on the slab theory (Xu, 1986), the governing differential equation for this model is

$$\nabla^4 w + \frac{k}{D} w - \frac{1}{D} (N_x \frac{\partial^2 w}{\partial x^2} - N_y \frac{\partial^2 w}{\partial y^2}) = \frac{q}{D} \quad (3.1)$$

where  $w$  is the deflection of slab.

$k$  is the reaction factor of the main floor to the immediate floor, equation (3.2) was proposed by Woinowsky (Selvadurai, 1979) to determine  $k$ .

$$k = \frac{2.15}{h} \left( \frac{E_s^4}{E_b} \right)^{1/3} \quad (3.2)$$

where  $E_s$  and  $E_b$  are Young's moduli for subgrade material (main floor) and plate material (immediate floor), respectively.

$N_x$  and  $N_y$  are the horizontal load in the  $x$  direction and  $y$  direction, respectively.

$q$  is the vertical stress on immediate floor.

$D$  is the flexural rigidity of the composite slab which can be calculated as follows:

$$D = \frac{AB - C}{A} \quad (3.3)$$

$$A = \sum_{i=1}^n \frac{E_i}{1 - \nu_i^2} (h_i - h_{i-1}) \quad (3.4)$$

$$B = \sum_{i=1}^n \frac{E_i}{1-\nu_i^2} \frac{h_i^2 - h_{i-1}^2}{2} \quad (3.5)$$

$$C = \sum_{k=1}^n \frac{E_k}{1-\nu_k^2} \frac{h_k^3 - h_{k-1}^3}{3} \quad (3.6)$$

where  $h_i$  is the distance between the floor surface and the  $i$ th bedding plane.

$E_i$  is the Young's modulus of the  $i$ th layer, and

$\nu$  is the Poisson ratio of  $i$ th layer.

The bending moments and shear forces (Fig. 3.2) can be calculated as follows:

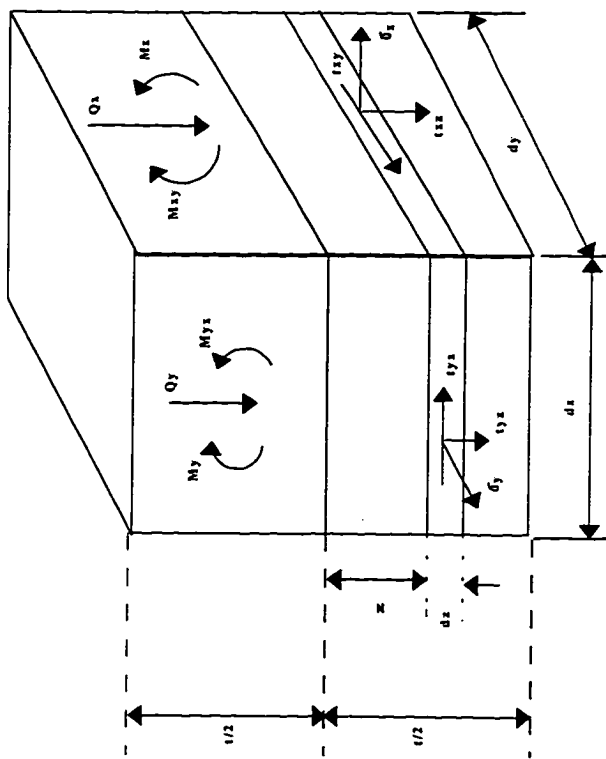
$$M_x = -D \left( \frac{\partial^2 w}{\partial^2 x} + \nu \frac{\partial^2 w}{\partial^2 y} \right) \quad (3.7)$$

$$M_y = -D \left( \frac{\partial^2 w}{\partial^2 y} + \nu \frac{\partial^2 w}{\partial^2 x} \right) \quad (3.8)$$

$$M_{xy} = -D(1-\nu) \frac{\partial^2 w}{\partial x \partial y} \quad (3.9)$$

$$Q_x = -D \frac{\partial}{\partial^2 x} \Delta^2 w \quad (3.10)$$

$$Q_y = -D \frac{\partial}{\partial^2 y} \Delta^2 w \quad (3.11)$$



**Fig. 3.2 Bending moment and shear stress**



The stresses can be calculated as follows:

$$\sigma_x = \frac{12M_x}{t^3} z \quad (3.12)$$

$$\sigma_y = \frac{12M_y}{t^3} z \quad (3.13)$$

$$\tau_{xy} = \tau_{yx} = \frac{12M_{xy}}{t^3} z \quad (3.14)$$

$$\tau_{xz} = \frac{6Q_x}{t^3} \left( \frac{t^2}{4} - z^2 \right) \quad (3.15)$$

$$\tau_{yz} = \frac{6Q_y}{t^3} \left( \frac{t^2}{4} - z^2 \right) \quad (3.16)$$

Where  $t$  is thickness of the composite slab.

### 3.2 Floor Failure Initiation and Propagation

Based on the composite slab model, the stresses can be determined. The failure initiation and propagation can be analyzed as follows:

(1) Bedding planes are the weakest part of the floor. If the shear stress on the bedding planes is higher than the shear strength of the bedding planes, shear failure will initiate on the bedding plane first and the layers of the composite slab will be dislocated.

Once the bonds between the layers are broken, each member of the immediate floor can act independently. Consequently the composite slab is divided into several individual slabs and the tensile stress will be redistributed. Generally this redistributed tensile stress is much larger than that existing in the composite slab.

(2) If the redistributed tensile stress is larger than the tensile strength of the floor strata, tensile failure will occur. Generally speaking, since the strength of the bond material in the bedding plane is very low, the bonds fail first and then the redistributed tensile stress causes the tensile failure in the layers.

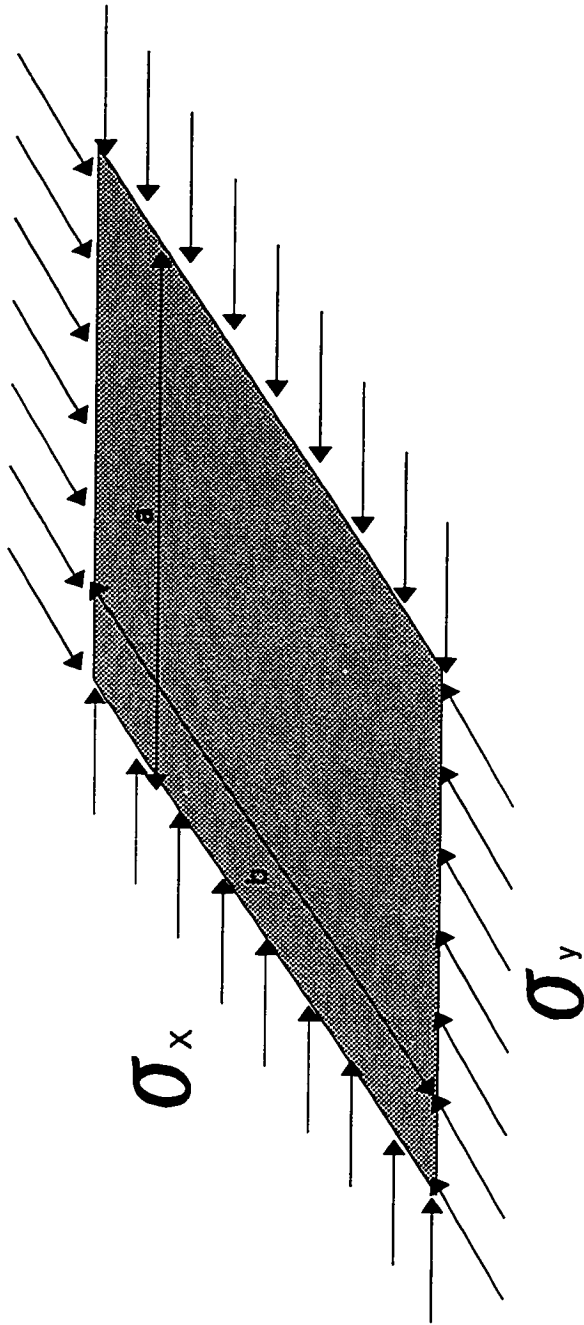
(3) High horizontal stress can also cause the buckling failure of floor members which will be studied in the next section.

### 3.3 Buckling Failure Analysis

The failure mentioned above only relieves the vertical stress in the floor but not the horizontal stress. The release of the horizontal stress may cause the floor to buckle. In order to study the floor behavior after failure initiation, a buckling model is used (Fig. 3.3). It treats the immediate floor as a series of simply supported slabs. According to the buckling theory of slab (Xu, 1986), the critical stress of slab  $P_{cr}$  is

$$P_{cr} = \frac{\pi^2 D}{a^2} \frac{\left(1 + \frac{a^2}{b^2}\right)^2}{1 + m \frac{a^2}{b^2}} \quad (3.17)$$

where  $m = \sigma_y / \sigma_x$ , and  $a$  and  $b$  are width and length of the slab, respectively.



**Fig. 3.3 Buckling failure model**

### 3.4 Floor Heave Analysis

After the buckling failure, the horizontal stress will be released and horizontal displacement occurs. This horizontal movement of the floor causes the broken floor to heave up (Fig. 3.4). Horizontal movement can be calculated by the following equations:

$$\Delta x = L_x \frac{\sigma_{hx} - \nu \sigma_{hy}}{E_i} \quad (3.18)$$

$$\Delta y = L_y \frac{\sigma_{hy} - \nu \sigma_{hx}}{E_i} \quad (3.19)$$

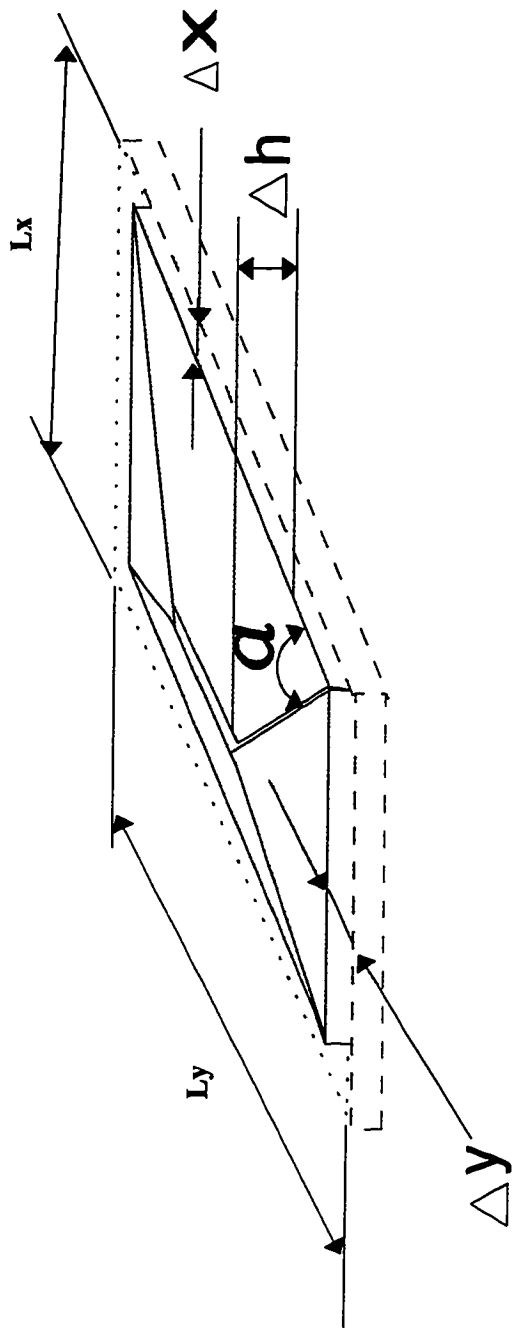
where  $\Delta x$  and  $\Delta y$  are horizontal displacement along x and y directions, respectively, and  $L_x$  and  $L_y$  are the parts of the floor rock slab in which the horizontal stress will be released.

The relationship between the horizontal movement and floor heave is

$$\Delta h = \sqrt{\frac{b^2}{4} - \left(\frac{b}{2} - \Delta x\right)^2} \quad (3.20)$$

$$\Delta h = \sqrt{\frac{a^2}{4} - \left(\frac{a}{2} - \Delta y\right)^2}$$

Where a and b are the width and length of the slab, respectively.



**Fig. 3.4 Floor heave model**

### 3.5 Numerical Solution of the Composite Slab Model

In order to solve the composite slab problems mentioned above, a computer program called FLOOR has been developed using the finite difference method. The basic principle behind this method is the replacement of the governing differential equations and the boundary conditions of a particular boundary value problem by their corresponding finite difference equations. This procedure then reduces the problem to the solution of a set of simultaneous algebraic equations.

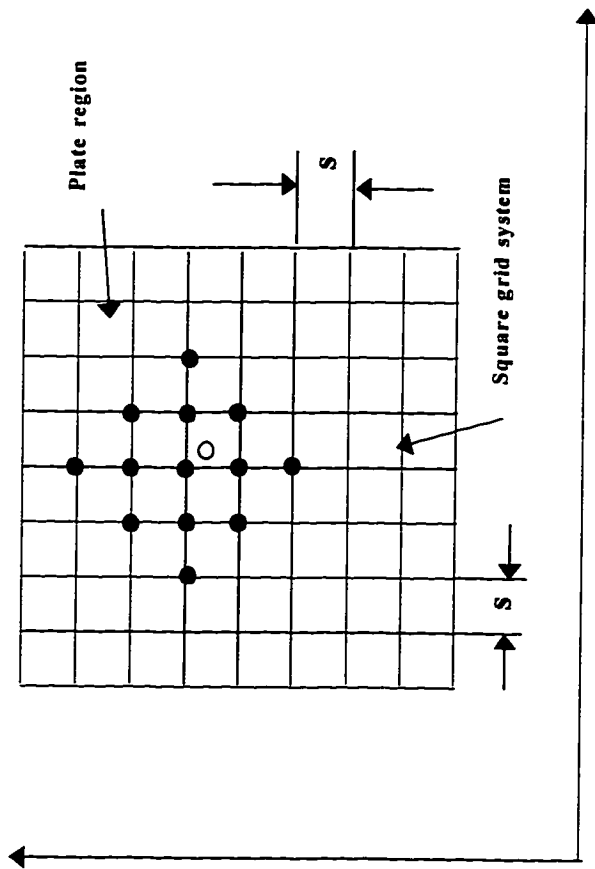
#### 3.5.1 Finite Difference Equation for Governing Differential Equation

In order to replace the governing differential equation, the domain of the elastic composite plate is divided into a finite difference grid as shown in Fig. 3.5, with equal grid line spacing,  $s$ , along both co-ordinate directions. The following finite difference relations for the derivatives of the composite plate deflection  $w(x, y)$ , at the location 0, are obtained.

$$\left[ \frac{\partial w}{\partial x} \right]_0 = \frac{1}{2s} [w_1 - w_3] \quad (3.21)$$

$$\left[ \frac{\partial w}{\partial x} \right]_0 = \frac{1}{2s} [w_2 - w_4] \quad (3.22)$$

$$\left[ \frac{\partial^2 w}{\partial x^2} \right]_0 = \frac{1}{s^2} [w_1 + w_3 - 2w_0] \quad (3.23)$$



**Fig. 3.5 Finite difference grid system**

$$\left[ \frac{\partial^2 w}{\partial y^2} \right]_o = \frac{1}{s^2} [w_2 + w_4 - 2w_o] \quad (3.24)$$

$$\left[ \frac{\partial^2 w}{\partial x \partial y} \right]_o = \frac{1}{4s^2} [w_5 - w_6 + w_7 - w_8] \quad (3.25)$$

$$\left[ \frac{\partial^3 w}{\partial x^3} \right]_o = \frac{1}{2s^3} [w_9 - 2w_1 + 2w_3 - w_{11}] \quad (3.26)$$

$$\left[ \frac{\partial^3 w}{\partial y^3} \right]_o = \frac{1}{2s^3} [w_{10} - 2w_2 + 2w_4 - w_{12}] \quad (3.27)$$

$$\left[ \frac{\partial^4 w}{\partial x^4} \right]_o = \frac{1}{s^4} [w_9 - 4w_1 + 6w_3 - 4w_5 + w_{11}] \quad (3.28)$$

$$\left[ \frac{\partial^4 w}{\partial y^4} \right]_o = \frac{1}{s^4} [w_{10} - 4w_2 + 6w_4 - 4w_6 + w_{12}] \quad (3.29)$$

$$\left[ \frac{\partial^4 w}{\partial x^2 \partial y^2} \right]_o = \frac{1}{s^4} [w_5 + w_6 + w_7 + w_8 + 4w_o - 2(w_1 + w_2 + w_3 + w_4)] \quad (3.30)$$

So, the governing differential equation can be represented in finite difference form as follows:



$$\begin{aligned}
& \left(20 + \frac{ks^4}{D} + \frac{2N_x s^2}{D} + \frac{2N_y s^2}{D}\right)w_0 + \left(8 - \frac{N_x^2}{D}\right)(w_1 + w_3) + \left(8 - \frac{N_y^2}{D}\right)(w_2 + w_4) \\
& + 2(w_5 + w_6 + w_7 + w_8) + (w_9 + w_{10} + w_{11} + w_{12}) - \frac{q_0 s^4}{D} = 0
\end{aligned} \tag{3.31}$$

### 3.5.2 Boundary Conditions

The finite difference expressions are derived for arbitrary points which are located far from the boundaries, i.e. for the case in which  $w_0, w_1, \dots, w_{12}$  all lie within the plate region.

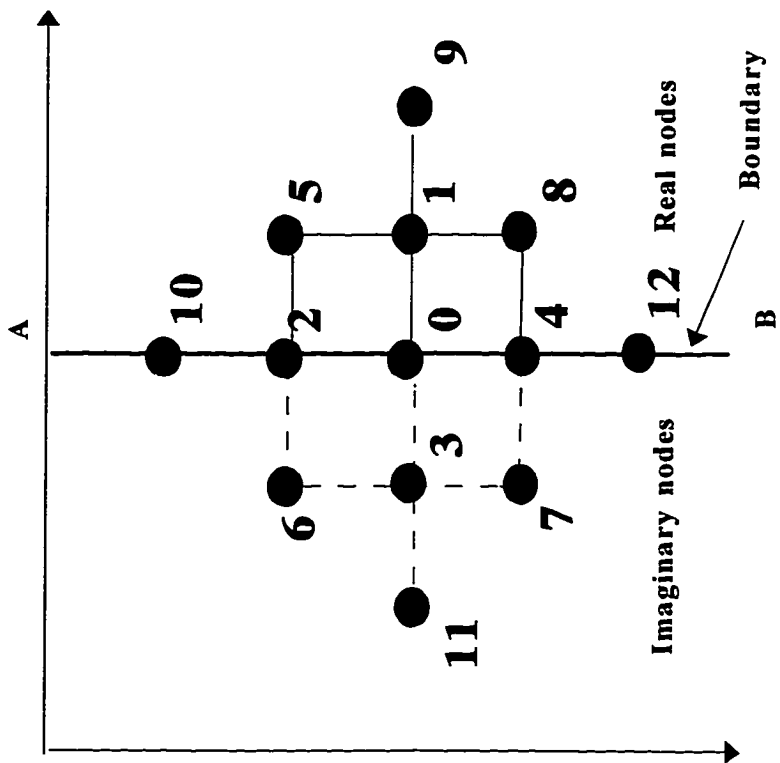
For a fixed boundary (Fig. 3.6), the boundary conditions on the edge where  $x=1$ , are

$$w(1, y) = 0$$

$$\left(\frac{\partial w}{\partial x}\right)_0 = \frac{w_1 - w_3}{2h} = 0 \tag{3.32}$$

So,  $w_1 = w_3$ , i.e. the deflection of an imaginary node is equal to that of the corresponding node inside the boundary. Therefore, the imaginary node outside the boundary can be expressed by its corresponding real node inside the boundary.

Consequently, the differential equation at any real point can be established.



**Fig. 3.6 Fixed boundary condition**

### 3.5.3 Stress Calculation

Once the deflection at each node is obtained, the bending moment and shear force can be expressed by the following finite difference equations in terms of the deflection.

$$(M_x)_0 = \frac{D}{s^2} [(2+2\nu)w_0 - (w_1 + w_3) - \nu(w_2 + w_6)] \quad (3.33)$$

$$(M_y)_0 = \frac{D}{s^2} [(2+2\nu)w_0 - (w_2 + w_4) - \nu(w_1 + w_3)] \quad (3.34)$$

$$(M_{xy})_0 = \frac{(1-\nu)D}{4s^2} [(w_5 + w_7) - (w_6 + w_8)] \quad (3.35)$$

$$(Q_x)_0 = \frac{D}{2s^3} [4(w_1 - w_3) - w_5 - w_6 + w_7 + w_8 - w_9 + w_{11}] \quad (3.36)$$

$$(Q_y)_0 = \frac{D}{2s^3} [4(w_2 - w_4) + w_5 - w_6 - w_7 + w_8 - w_{10} + w_{12}] \quad (3.37)$$

With bending moments and shear forces, the stresses can be calculated by equations 3.12-3.16.

Based on the finite difference equations, the computer program called "FLOOR" has been developed. The program can handle the following particular problems:

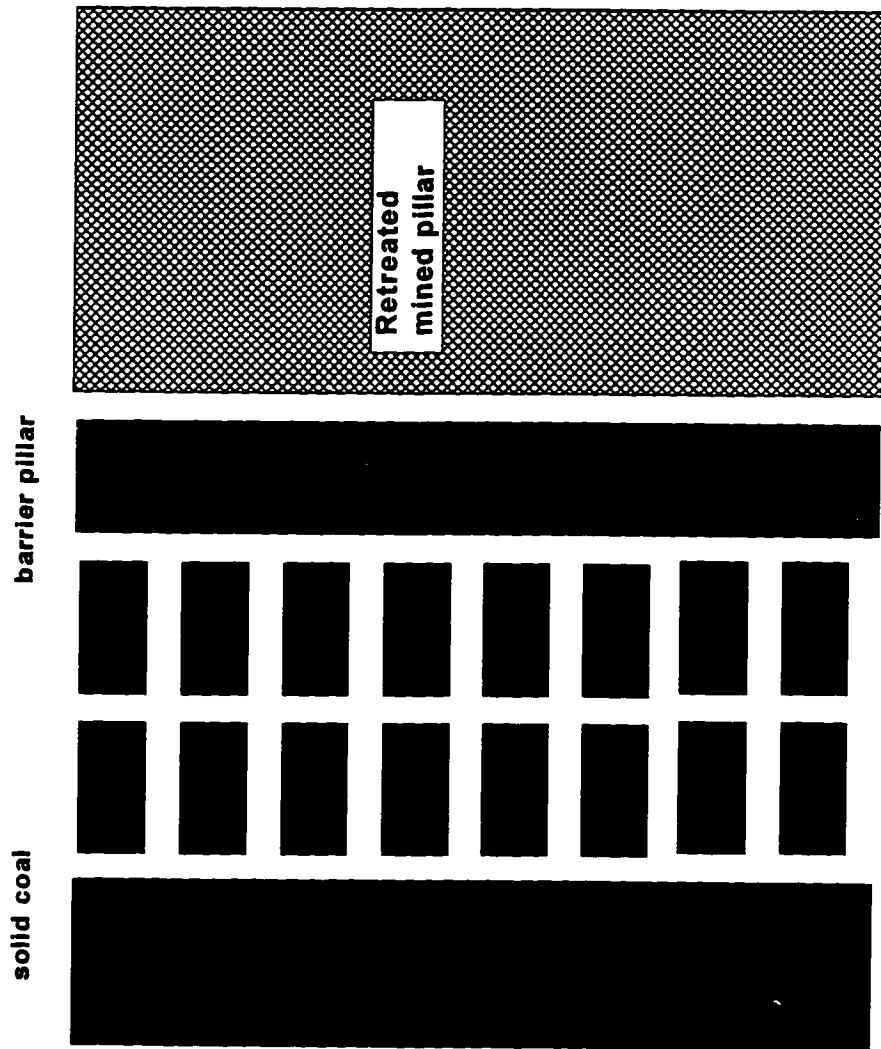
- (1) The immediate floor being a multiple-layered composite slab.
- (2) Any kind of load distribution.

(3) Calculation of the stresses and elastic deformations at any point of interest.

From the output results of the program, the model can predict when and where failure will be initiated in the floor and how failure will propagate further and finally lead to floor heave.

### **3.6 A Case Study - Floor Heave in Smoot Mine**

The geological and mining conditions of the Smoot mine were described earlier in chapter 2. Take Panel 1 left as an example (Fig. 3.7). The mine overburden depth is 800 ft. The mechanical properties of the floor material were tested in the laboratory and listed in Table 3.1. The shear strength on bedding planes were also tested and listed in Table 3.2. To simulate the floor behavior, two stage loadings corresponding to the mining operations are applied, i.e. before and after retreat pillaring. The load before pillaring is calculated based on the tributary loading method and the load on the floor after pillaring is based on an abutment angle of  $18^{\circ}$ . The maximum principal horizontal stress in this area is 2,973 psi and minimum principal horizontal stress is 1,466 psi (Aggson, 1978).



**Fig. 3.7 Panel 1 Left of Smoot Mine**

**Table 3.1 Mechanical Properties of Floor Rocks for Smoot Mine**

Rock	Young's modulus (10 <sup>6</sup> psi)	Poisson's Ratio	Compressive Strength (psi)	Tensile Strength (psi)
Shale	1.19	0.23	11,498	1,168
Bony coal	0.29	0.33	1,922	
Fireclay	1.85	0.27	5,720	811

### **Floor Failure Analysis**

(1) Before retreat pillaring. Figs. 3.8 and 3.9 show the deflection and maximum tensile stress distributions, respectively. The deflection distribution shows that the maximum elastic deformation of the floor is 1.85 in. at the center part of the pillar. The maximum tensile stress is 587 psi and the maximum shear stress which occurs on the bedding plane 1 is 81 psi as shown in Fig. 3.10. Therefore, before retreat pillaring both the tensile and shear stresses are less than the tensile and shear strength of the floor members and the bedding plane, respectively and no failure is initiated.

(2) After retreat pillaring. Figs. 3.11 and 3.12 show the deflection and maximum tensile stress distributions after retreat pillaring, respectively. Figures 3.13-3.15 show the shear stress

distribution on bedding planes 1, 2, and 3. Table 3.2 shows the maximum shear stress on the bedding planes. The maximum tensile stress which is 732 psi is still less than the tensile strength of the material. However the maximum shear stress on each bedding plane is larger than the shear strength. Therefore the shear failure initiates on the bedding plane first and separations between the layers occur. As a result, the composite slab is divided into several individual slabs which act independently and the tensile stress is redistributed. The maximum redistributed tensile stresses are shown in Fig. 3.16-3.21 and Table 3.3. It can be seen that the redistributed tensile stresses are greater than the tensile strength of the floor material. The floor will be broken along the maximum tensile stress line equivalent to the tensile strength. Thereafter, failure propagation and additional floor heave will depend on the magnitude of the horizontal stress and horizontal displacement in the floor.

Table 3.2 The Maximum Shear Stress on Each Bedding Plane

Bedding plane	1	2	3	4	5
Maximum shear stress (psi)	127	172	229	172	118
Shear strength (psi)	88	93	88	103	110

Table 3.3 Maximum Redistributed Tensile Stress on Each Layer

Layer	1	2	3	4	5
Tensile stress (psi)	1,539	1,213	1,894	1,894	1,376

## Buckling Analysis

The failure mentioned above only relieves the vertical stress, while the horizontal stress remains intact. This horizontal stress, if large enough, would cause the floor member to buckle. Table 3.4 is calculated from the buckling model. It can be seen that the immediate floor up to 24 inches deep will be broken by buckling failure of the slab.

Table 3.4 Buckling Failure Analysis

Floor strata	Thickness (in.)	$\sigma_x$	$\sigma_y$	$P_{cr}$ (psi)	Failure or not
Shale	4	2,793	1,466	621	yes
Bony coal	2	2,793	1,466	26	yes
Fireclay	6	2,793	1,466	918	yes
Bony coal	6	2,793	1,466	233	yes
Fireclay	3	2,793	1,466	230	yes
Fireclay	3	2,793	1,466	230	yes
Shale	48	2,793	1,466	8,943	no

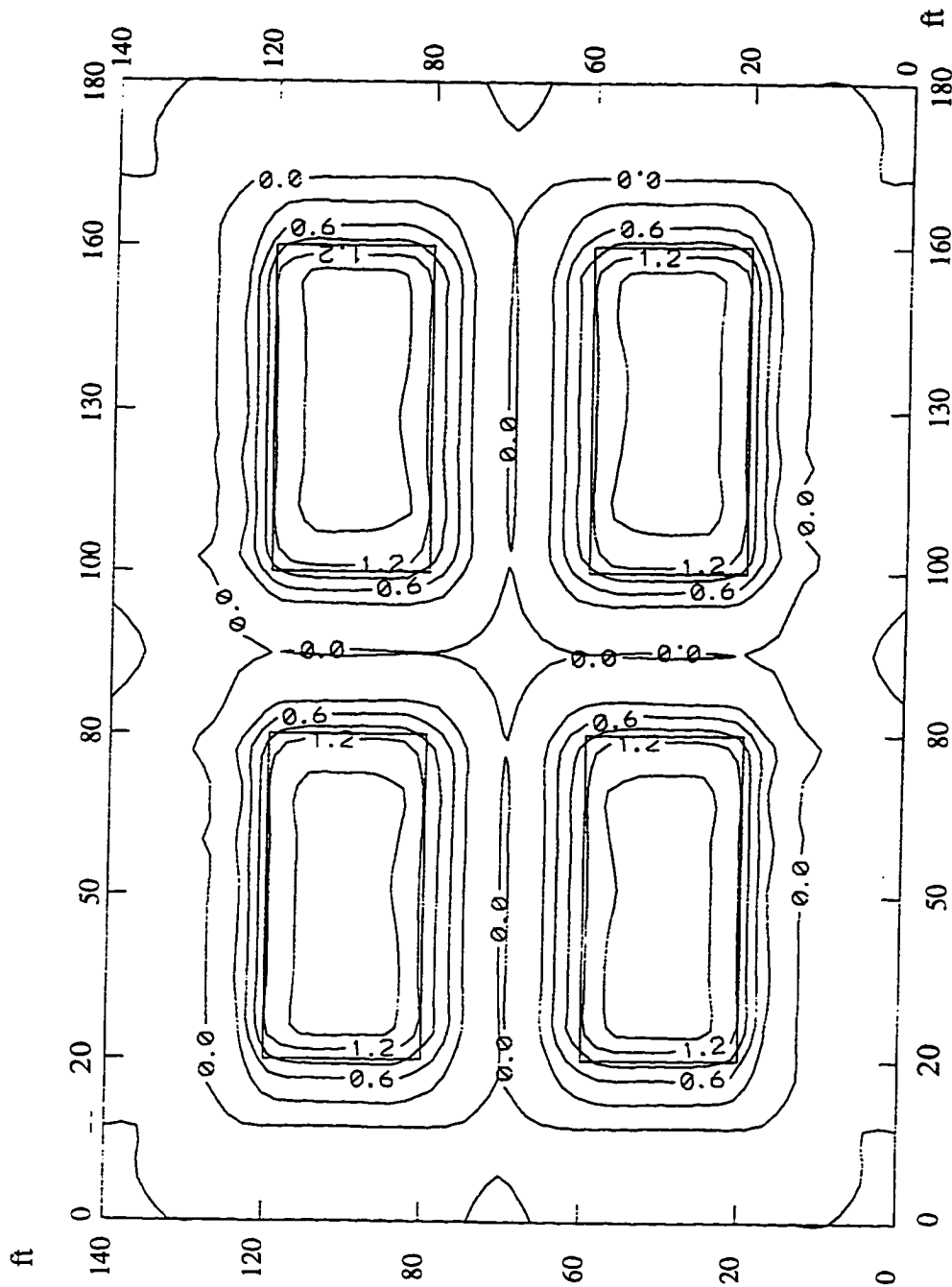


## Floor Heave

After buckling failure, the horizontal stress will be released and the floor will move toward the entry center. This horizontal movement eventually causes the broken floor to heave up. Table 3.5 shows the computed results of floor heave. The maximum floor heave at the center of the entry is 14 in. The separation between first layer and second layer is 6 in. The separation between the immediate floor and main floor is 4.4 in.

Table 3.5 Calculated Floor Heave

Floor strata	Thickness (in.)	$L_x$ (ft)	$\Delta x$ (in)	Floor Heave (in)	Separation (in)
Shale	4	15	0.4	14	0
Bony coal	2	16.6	2.0	14	0
Fireclay	6	13	0.21	8	6
Bony coal	6	13	0.85	8	0
Fireclay	3	15.7	0.24	4.4	3.6
Fireclay	3	15.7	0.53	4.4	0
Shale	48			0	4.4



**Fig. 3.8 Floor deflection (in inches) before pillar retreating**

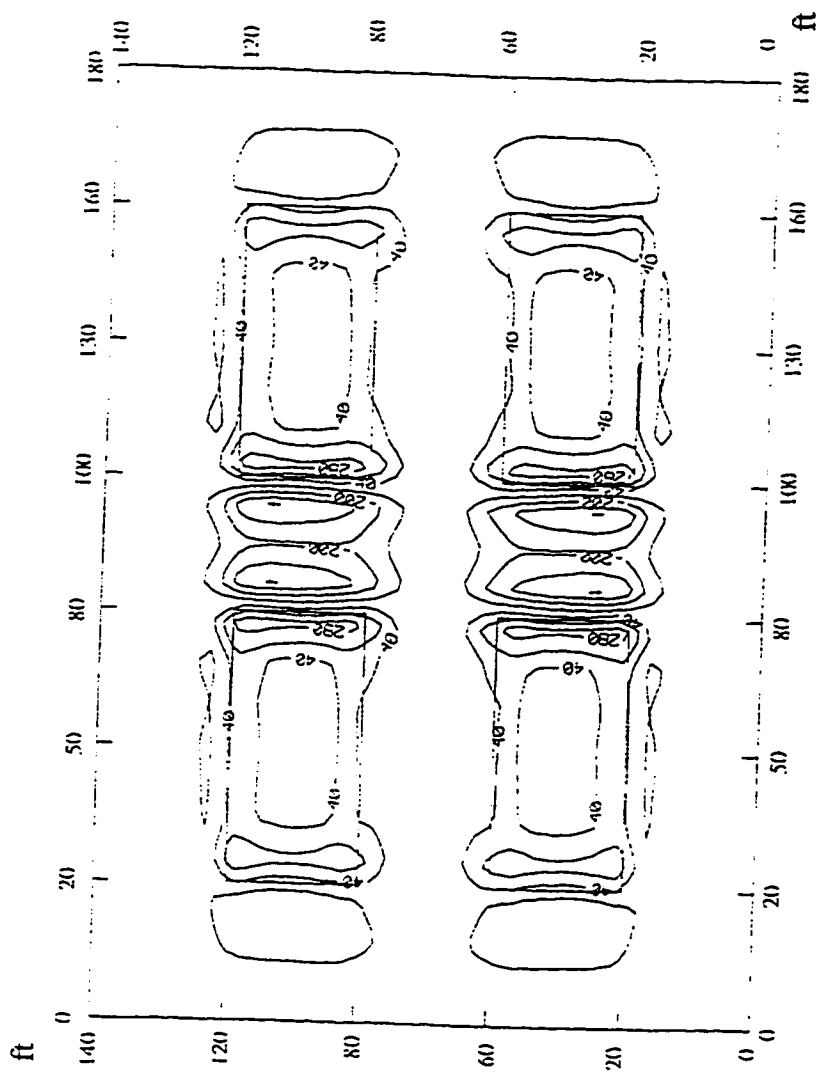


Fig. 3.9 Maximum tensile stress distribution (in psi) before pillar retreating

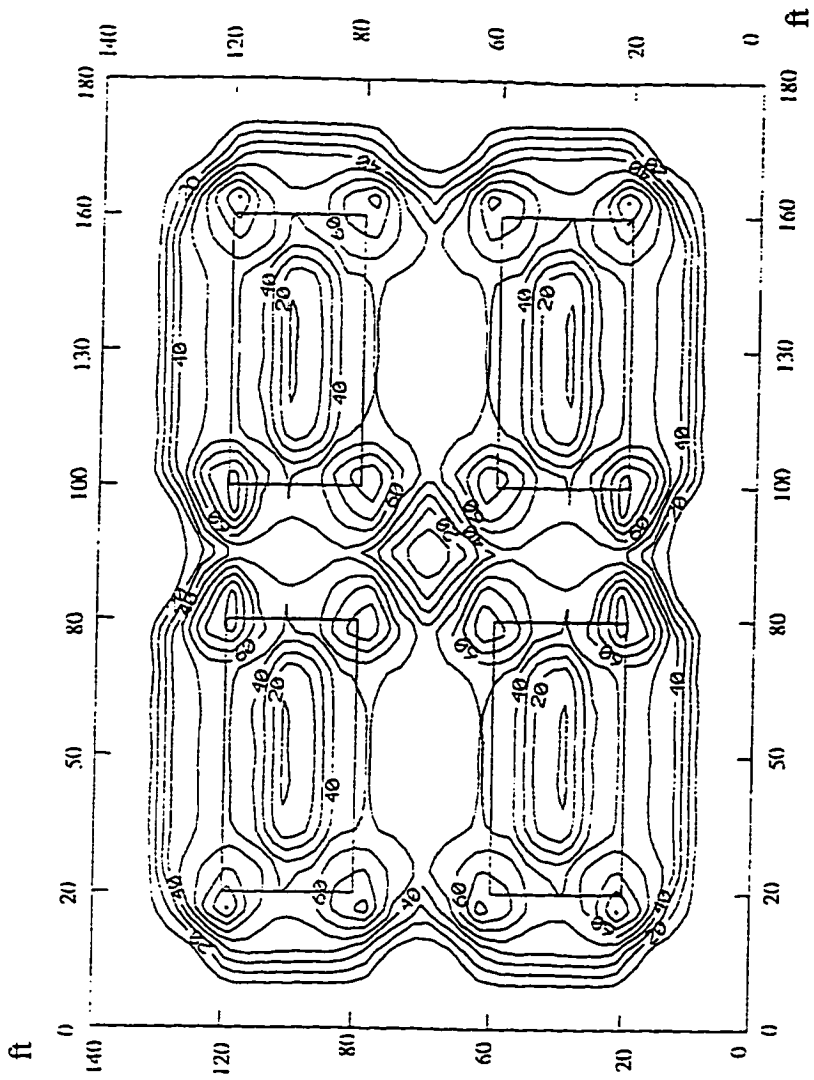


Fig. 3.10 Maximum shear stress distribution (in psi) on bedding plane 1 before pillar retreating

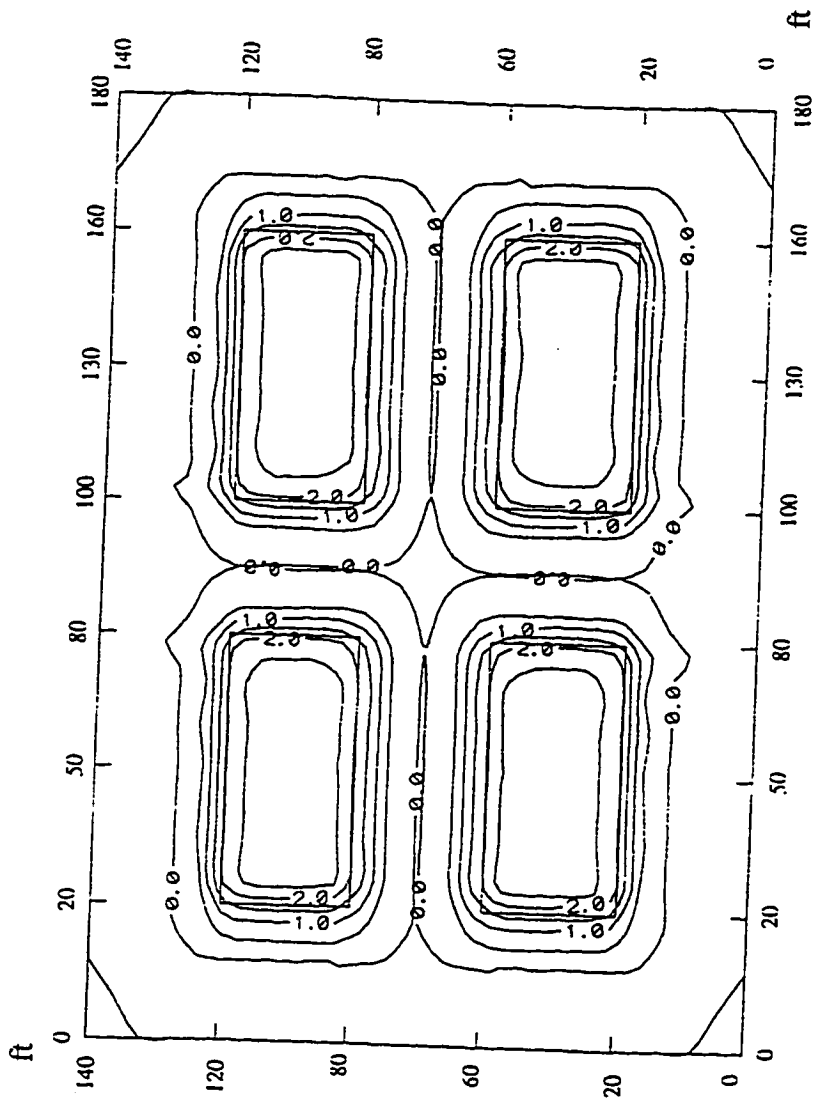


Fig. 3.11 Deflection (in inches) after pillar retreating

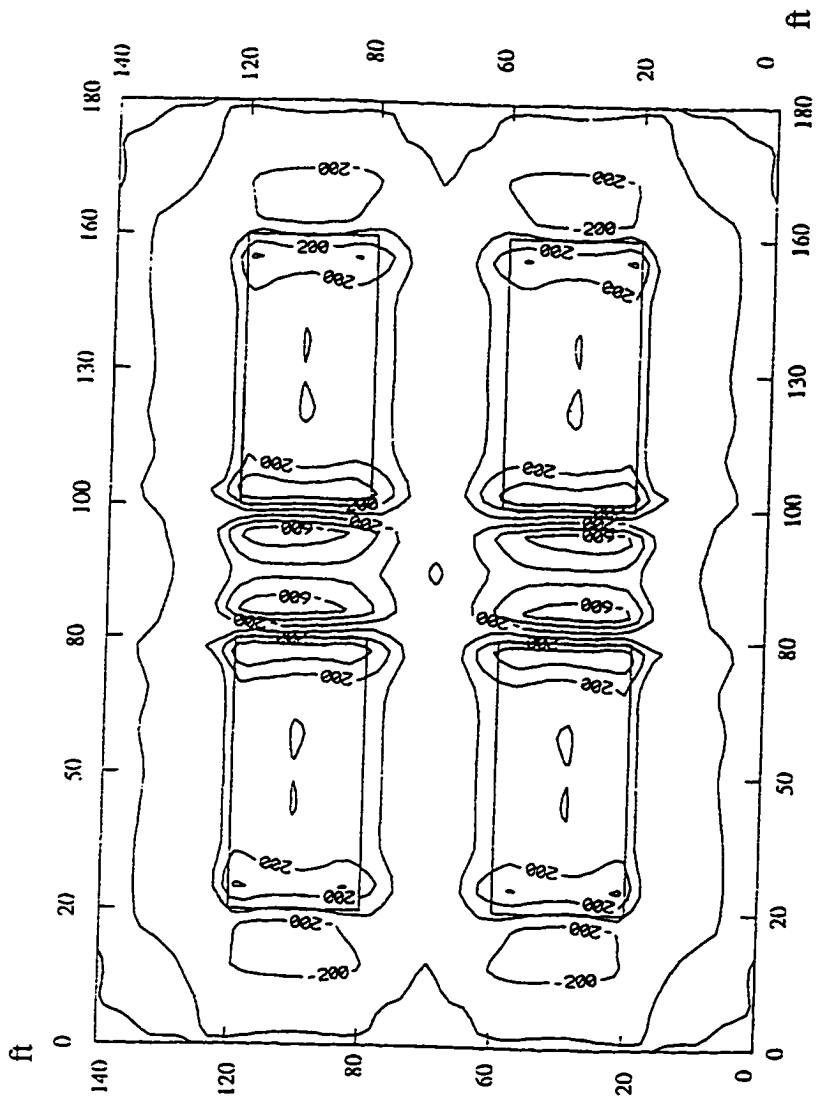


Fig. 3.12 Maximum tensile stress distribution (in psi) after pillar retreating

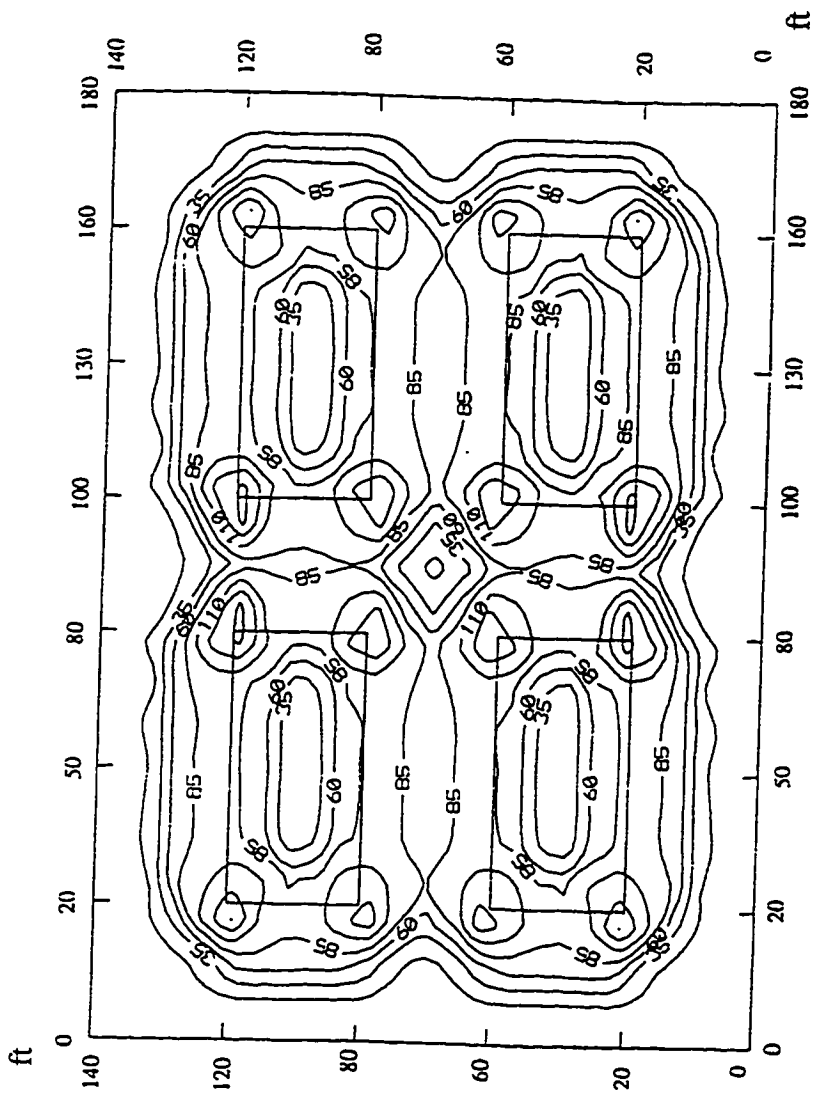


Fig. 3.13 Shear stress distribution (in psi) on bedding plane 1

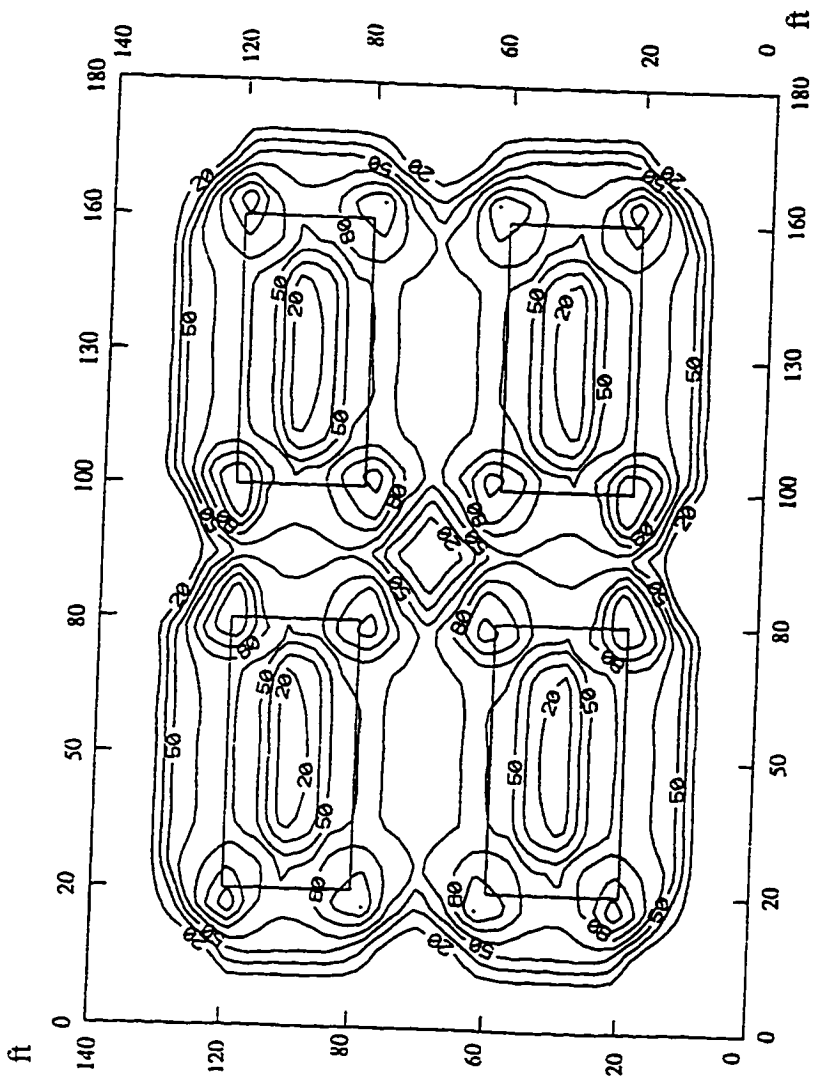


Fig.3. 14 Shear stress distribution (in psi) on bedding plane 2



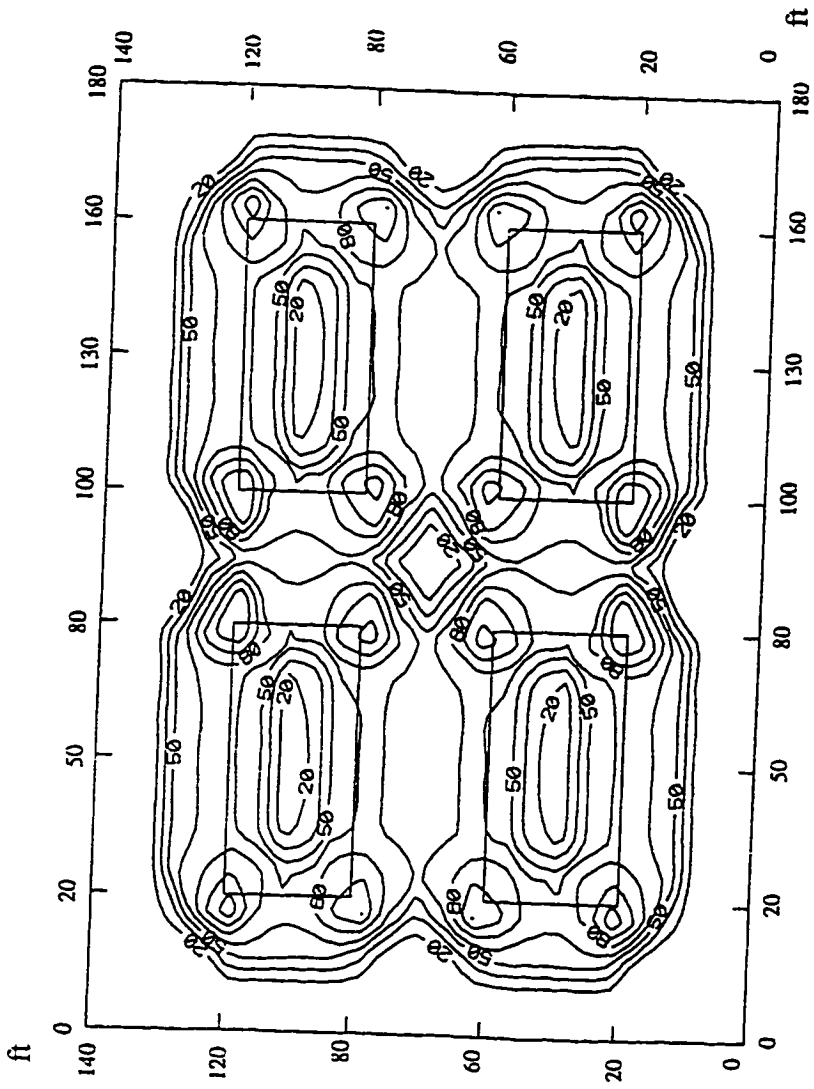


Fig. 3.15 Shear stress distribution (in psi) on bedding plane 3



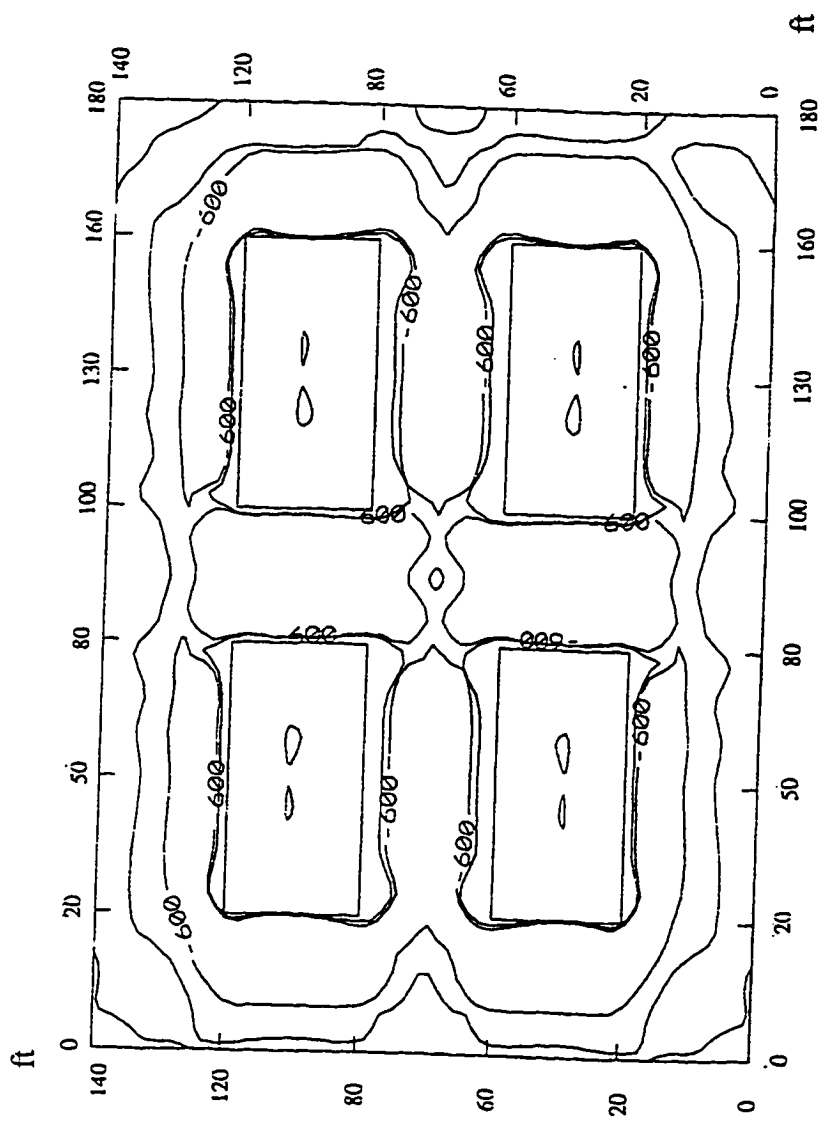


Fig. 3. 17 Maximum tensile stress (in psi) on layer 2

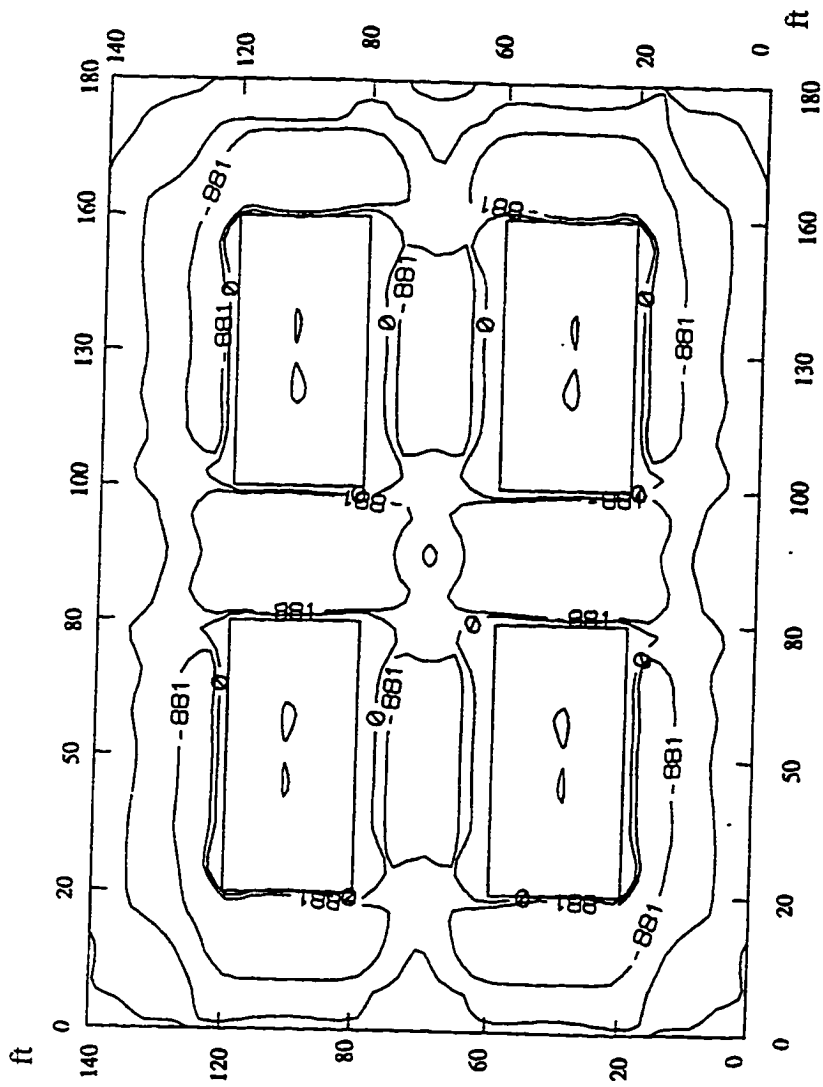


Fig. 3.18 Maximum tensile stress (in psi) on layer 3

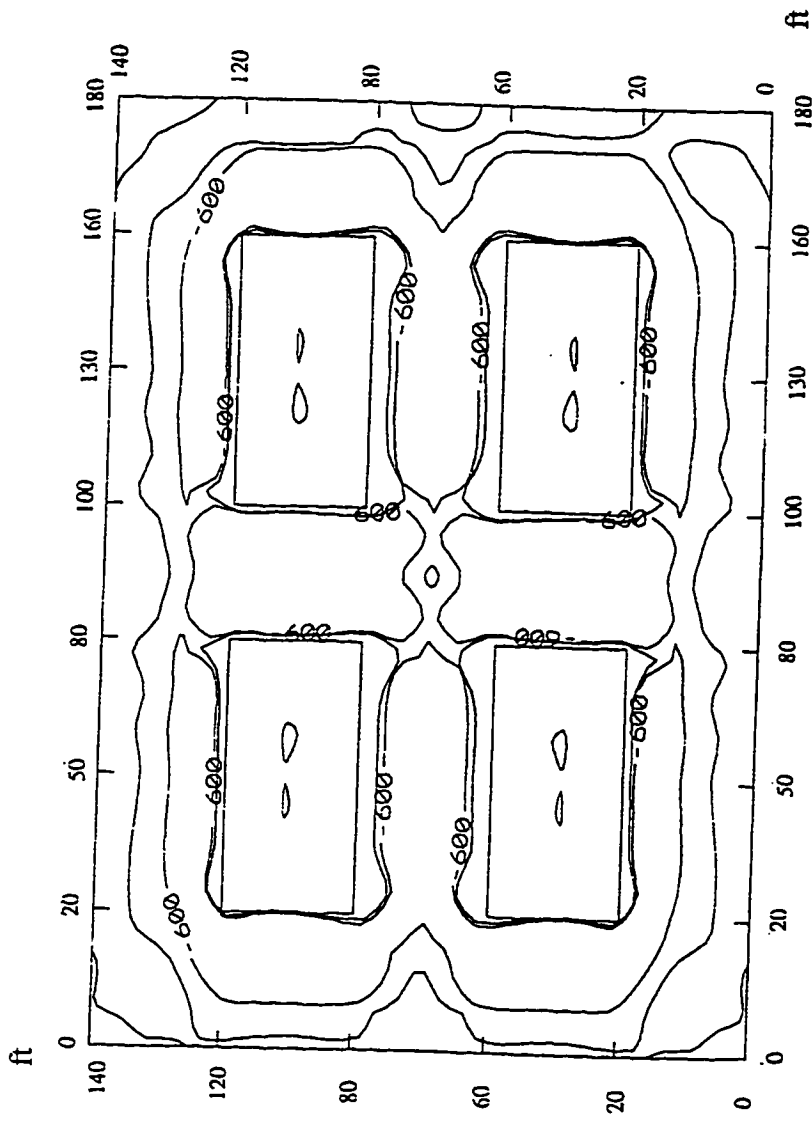


Fig. 3. 19 Maximum tensile stress (in psi) on layer 4

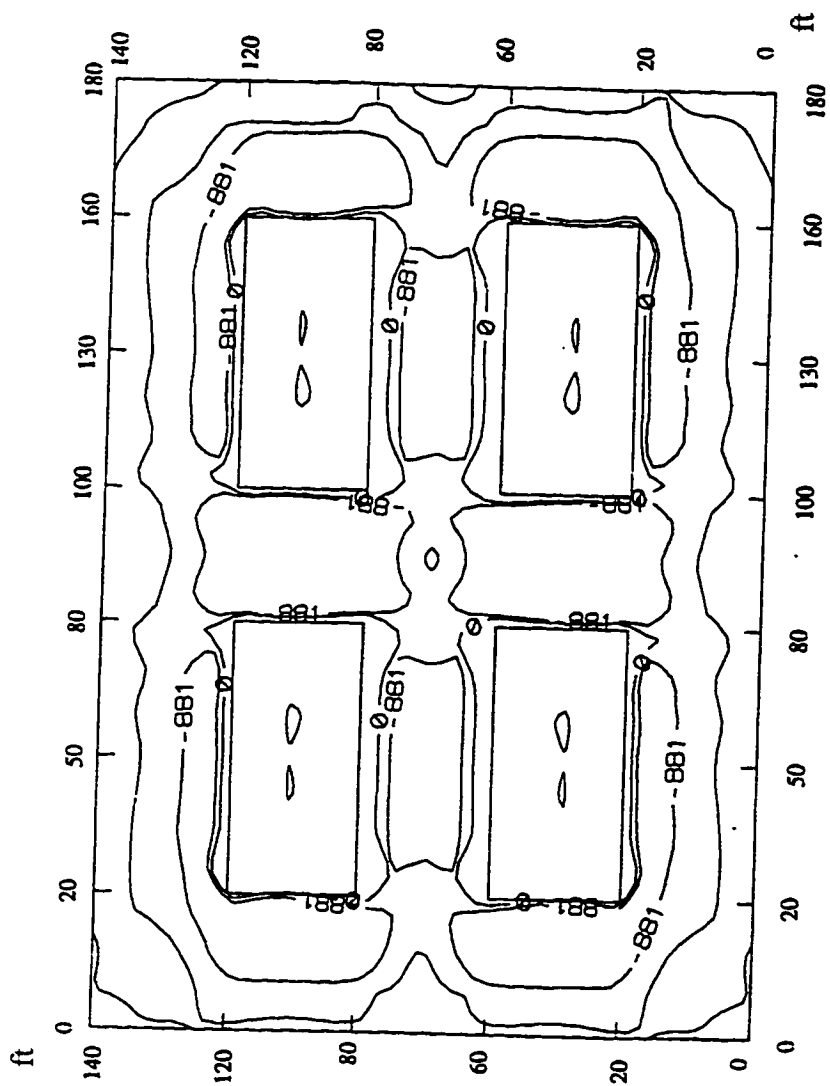


Fig. 3.20 Maximum tensile stress (in psi) on layer 5

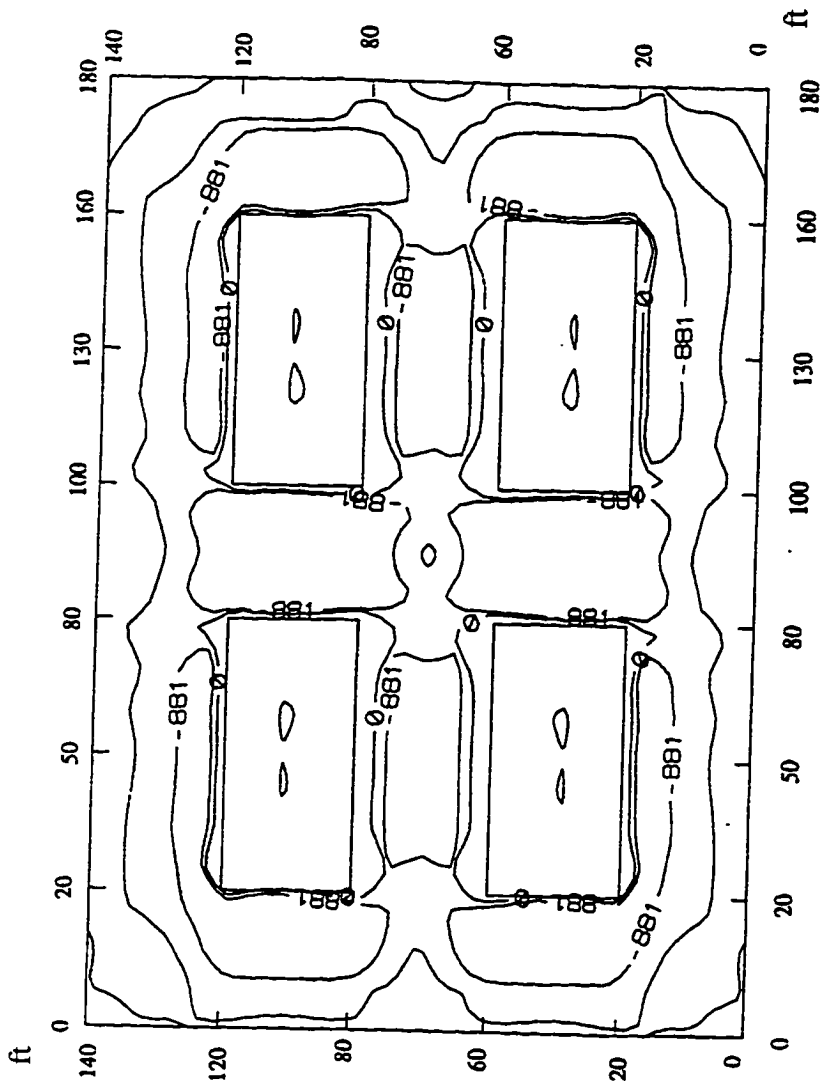


Fig. 3.21 Maximum tensile stress (in psi) on layer 6

## CHAPTER 4

### MECHANISM OF TYPE II FLOOR HEAVE

---

#### 4.1 MECHANISTIC MODEL OF FLOOR HEAVE

In-situ observations have shown that if the room-pillar system is designed improperly, floor heave often occurs in weak immediate floor consisting of massive fireclay, and mudstone when the overburden is sufficiently thick. The material in the heaved floor is usually broken and squeezed into the entry. The general floor heave sequence can be described as follows:

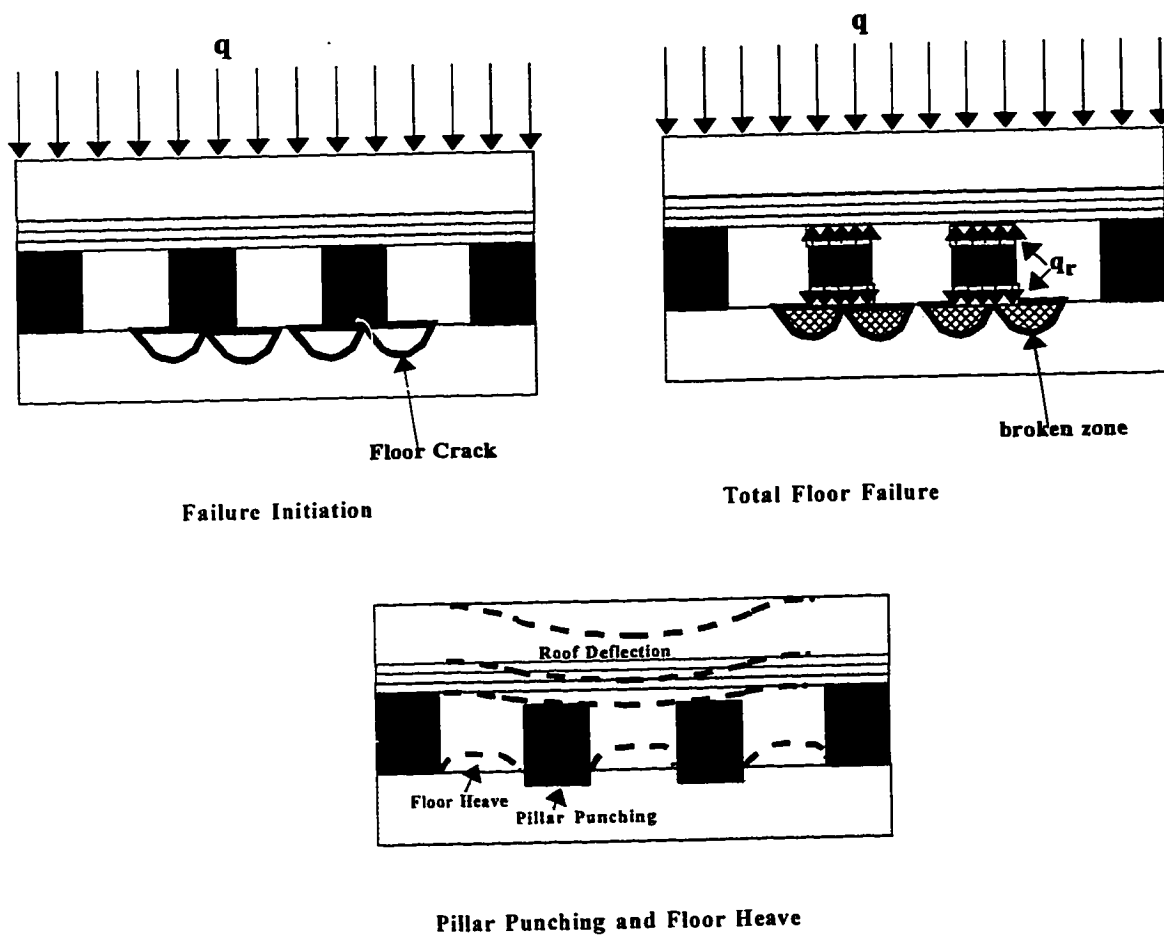
(1) Once the vertical stress on the floor exceeds the bearing capacity of the floor, the floor fails.

(2) After floor failure, the floor bearing capacity is reduced to the residual value which more or less remains constant while the pillars continue to punch into the floor. The magnitude of floor heave depends on how much the pillars can punch into the floor.

(3) Because of floor failure, the resistance of pillars to the roof is reduced to the residual value of the floor bearing capacity. Consequently, the roof both above the entries and pillars will deflect and force the pillar to punch into the floor.

Based on floor heave sequence, the mechanistic model of floor heave is shown in Fig. 4.1. Floor heave in the entry-pillar system depends on many factors such as the panel dimension, geometry of the entries and pillars within the system, floor properties, roof structure and overburden depth. All those parameters should be taken into account. The finite element





**Fig. 4.1 Mechanistic model of Type II floor heave**

analysis method will be used to solve this model. However, in order that floor failure and floor heave can be predicted and controlled, the following problems need to be analyzed and solved:

- 1) Floor bearing capacity;
- 2) Residual floor bearing capacity;
- 3) Relation between pillar punching and floor heave;
- 4) Final roof deflection and pillar punching;
- 5) Floor heave.

## **4.2 Floor Bearing Capacity**

### **4.2.1 Floor Failure Mechanism**

Based on the in-situ observation results described in chapter 2, this kind of floor heave is caused by plastic failure and plastic flow of the floor material. The slip-line field theory (Jiang, 1979) can be applied to analyze the floor failure mechanism. As shown in Fig. 4.2, the immediate floor consists of homogenous massive weak material; the pillars are very strong such that they can be considered a stiff material as compared to the floor. The width of a pillar is  $2B$ . The bearing capacity of the floor is  $q_b$ , which is the ultimate stress causing the floor to fail in plastic failure. According to the slip-line field theory, once the stress reaches the bearing capacity of the floor at each point of the immediate floor, the maximum shear stress exceeds the shear strength of the floor material and the material will slide along the direction of maximum

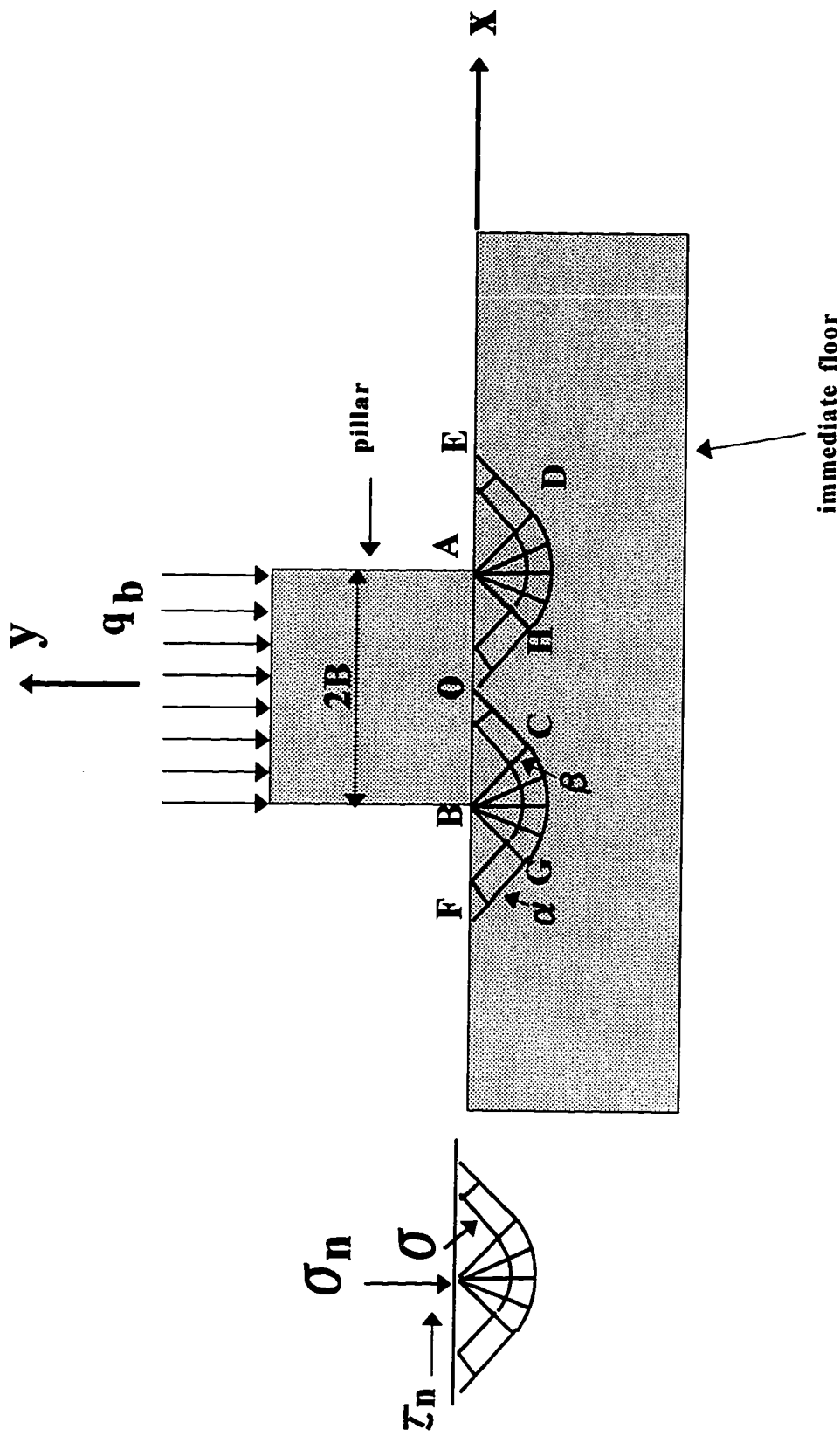


Fig. 4.2 Slip-line field

shear stress. There are two maximum shear stresses perpendicular to each other at each point. By connecting every point along the maximum shear stress directions, two sets of lines perpendicular to each other called slip-lines can be obtained. One is called the  $\alpha$  line and the other is called the  $\beta$  line. The slip-line field (Fig. 4.2) can be established as follows:

The boundary conditions are known as:

Along boundary AE,

$$\sigma_n = \sigma_y = 0, \quad \tau_n = \tau_{xy} = 0, \quad \psi = \frac{\pi}{2} \quad (4.1)$$

Along boundary AB,

$$\sigma_n = \sigma_y = -q, \quad \tau_n = \tau_{xy} = 0, \quad \psi = \frac{\pi}{2} \quad (4.2)$$

where  $\sigma_n$  is normal stress on the boundary,  $\tau_n$  is shear stress on the boundary and  $\psi$  is the angle between the normal stress on the boundary and the x axis. According to the boundary conditions and properties of the slip-lines, the slip-line field can be drawn as shown in Fig. 4.2. Zone AED and AOH are two uniform stress fields and AHD is a simple stress field.

Based on the slip-line field theory and the slip-line field established above, the stress distribution conditions area are given:

for zone AED:

$$\theta = \frac{\pi}{4}, \quad \sigma = -k, \quad \sigma_x = -2k \quad (4.3)$$

for zone AOH:

$$\theta = -\frac{\pi}{4}, \quad \sigma_x = -q_b + 2k, \quad \sigma = -q_b + k \quad (4.4)$$

for zone AHD

$$\sigma = 2k\left(\theta - \frac{\pi}{4} - \frac{1}{2}\right) \quad (4.5)$$

The floor bearing capacity can be derived based on the slip-line field characteristics, because along any slip line,  $\sigma/2k - \theta = \text{constant}$ . So,

$$\frac{\sigma_o}{2k} - \theta_o = \frac{\sigma_E}{2k} - \theta_E \quad (4.6)$$

Substituting  $\sigma$  and  $\theta$  into Equation 4.6

$$\frac{-q_b + k}{2k} + \frac{\pi}{4} = \frac{-k}{2k} - \frac{\pi}{4} \quad (4.7)$$

From Equation 4.7 the bearing capacity of the floor is

$$q_b = 2k\left(1 + \frac{\pi}{2}\right) \quad (4.8)$$

where  $\sigma$  is the normal stress perpendicular to the slip line at each point,  $\theta$  is the angle between the slip line and x axis, and k is shear strength of the floor material.

It must be noted that the slip-line field theory is based on the fact that the material is homogenous and pure plastic. However, for the floor rock material, the bearing capacity is not so simple as explained because of rock properties and inhomogeneous characteristics. In

foundation engineering, the bearing capacity of foundation has been developed considering the material properties, which will be described later.

## 4.2.2 Floor Bearing Capacity

### 1. General Floor Bearing Capacity Equation

Based on slip-line field theory, the method for determining the floor bearing capacity has been developed by Terzaghi (1943) considering the rock properties. Fig. 4.3 represents the formulation of the problem of bearing capacity. The failure region consists of three zones. Zone I is the active Rankine zone which pushes the Prandtl zone II laterally and forces the passive Rankin zone III in the upward direction. The failure boundary ACDE consists of lines AC and DE at  $45^\circ + \phi/2$  to the horizontal. The curved portion CD is a logarithmic spiral. Based on this formulation, the following equation was derived:

$$q_0 = S_0 N_c + q_s N_q + \frac{1}{2} \gamma B N_\gamma \quad (4.9)$$

where  $q_0$  = ultimate bearing capacity of floor.

$S_0$  = cohesion of floor material.

$q_s$  = surcharge load, which is equal to 0 for the mine floor problem.

$\gamma$  = unit weight of surcharge material.

$B$  = width of the floor under pillar.

$N_c, N_q, N_r$  = dimensionless bearing capacity factors.

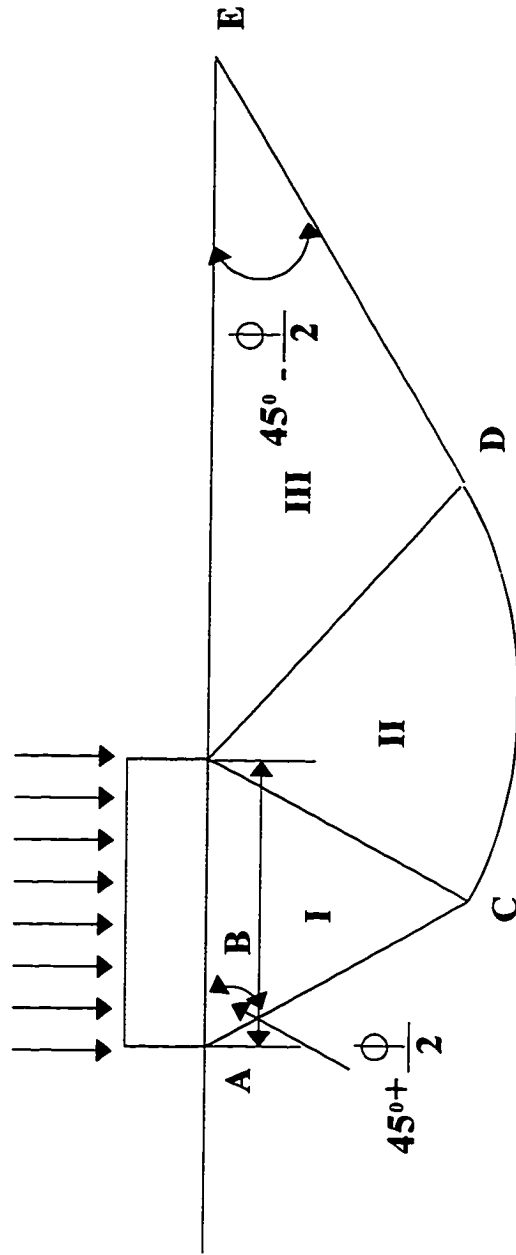


Fig. 4.3 The formation of the problem of bearing capacity

So, for mine floor problems, the bearing capacity can be simplified as:

$$Q_0 = S_0 N_c \quad (4.10)$$

$N_c$  can be calculated by the following equations:

$$N_q = e^{\pi \tan \phi} \tan^2 (\pi/4 + \phi/2) \quad (4.11)$$

$$N_c = (N_q - 1) \cot \phi \quad (4.12)$$

$\phi$  is angle of internal friction.

Equation (4.10) is only suitable for a long rectangular pillar. However, in underground coal mine, the pillar size varies from different mine layouts. On the basis of comparative loading tests with foundations of different sizes, Equation (4.10) has been modified by Vesic (1970) to account for the foundation shape and size:

$$Q_0 = S_0 N_c^* \quad (4.13)$$

$$N_c^* = N_c (1 + (B/L) (N_q/N_c)) \quad (4.14)$$

where  $L$  is the length of foundation.

## 2. Floor Bearing Capacity of Two Layered Floor Condition

Floor heave often occurs in a mine floor consisting of two layers. The top layer is usually soft rock such as fireclay and soft shale, and the second layer is strong rock. The



bearing capacity equation described above is only suitable for a homogeneous floor. For the two-layer floor structure, Brown (1969) proposed the following equation for the determination of bearing capacity for foundations on a soft stratum lying above a strong stratum, which is the case when the immediate floor consists of underclays overlying a strong shale or limestone.

$$q = c(1) \times N_m \quad (4.15)$$

where  $q$  is the floor bearing capacity,

$c(1)$  is the cohesive strength of the weak floor layer, and

$N_m$  is the modified bearing capacity factor. Vesic (1970) proposed the following equation for the determination of  $N_m$ :

$$N_m = \frac{r N_c^* (N_c^* + \beta - 1) [(r+1) N_c^{*2} + (1+\beta r) N_c^* + \beta - 1]}{[r(r+1) + r + \beta - 1] [(N_c^* + \beta) N_c^* + \beta - 1] - (r N_c^* + \beta - 1) (N_c^* + 1)} \quad (4.16)$$

where  $r$  is the strength ratio of the two layers, or

$$r = \frac{c(2)}{c(1)} \quad (4.17)$$

and where  $c(2)$  is the cohesive strength of main floor.

$$\beta = \frac{BL}{[2(B+L)t]} \quad (4.18)$$

where  $B$  is width of pillar,

$L$  is length of pillar, and

$t$  is thickness of the soft floor.

In order to calculate  $N_m$ , Equation 4.16 has been coded on spreadsheet.

### 3. Moisture Effect on Floor Bearing Capacity

The presence of moisture has a weakening effect on the bearing capacity of the mine floor. Jenkins (1958) found a decrease of 10% to 35% in the bearing capacity of an underclay mine floor when wet. Afrouze (1975) also report similar reductions.

In order to determine the bearing capacity reduction ratio due to moisture, in-situ bearing capacity test data under soaked floor conditions conducted by Chugh (1986, 1990) in two typical soft floor mines were used. Based on these data, the reduction ratio is calculated as shown in Table 4.1 and Table 4.2.

Table 4.1 Moisture Effect on Floor Bearing Capacity in Mine 1

Site	Floor Bearing Capacity (psi)		Reduction Ratio
	AS-mined	Soaked	
1	1,110	572	0.52
2	834	636	0.76
3	1,100	772	0.70
4	805	634	0.79
5	1,138	772	0.68
6	945	634	0.67
Average	989	670	0.69

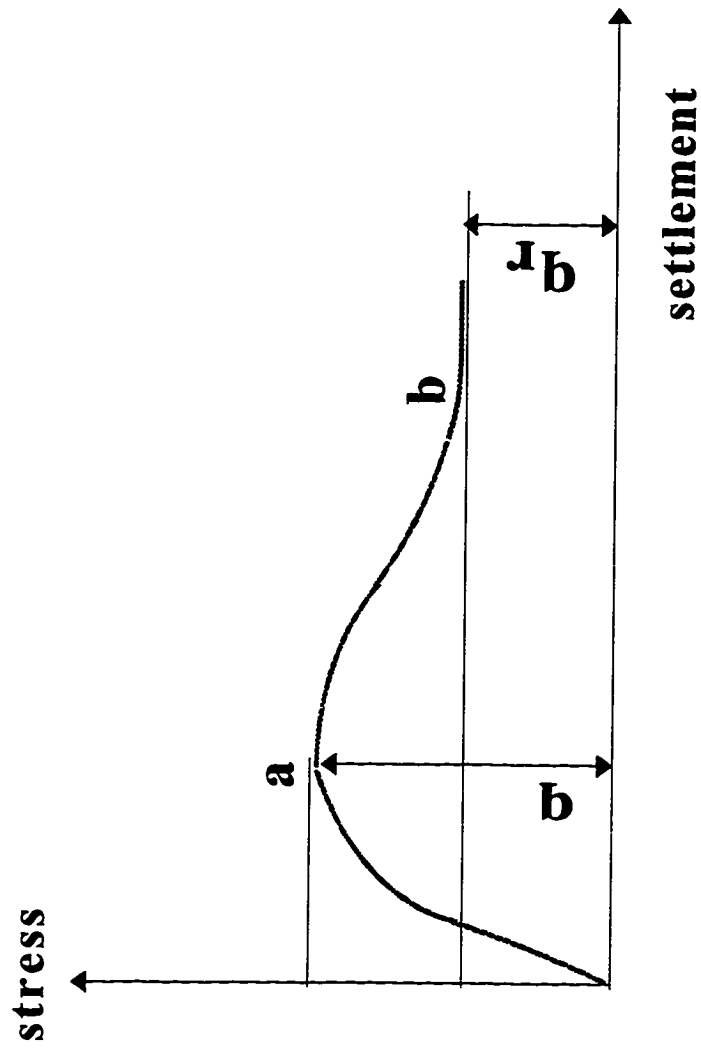
Table 4.2 Moisture Effect on Floor Bearing Capacity in Mine 2

Site	Floor Bearing Capacity (psi)		Reduction Ratio
	AS-mined	Soaked	
1	1,119	676	0.60
2	5,470	5000	0.91
3	1,147	808	0.70
4	676	647	0.96
5	1,333	560	0.42
6	1,340	536	0.40
7	1,272	617	0.49
Average	1,936	1,549	0.64

From this study, it can be seen that moisture can weaken the floor bearing capacity. The average reduction ratio for the soaked condition, which corresponds to the flooded condition in a mine, ranges 0.40-0.96 and averages 0.67. Generally, claystone is more sensitive to the moisture than shale. Therefore a small reduction ratio of 0.40 is recommended for the claystone (or fireclay), and the average reduction ratio of 0.67 is recommended for shale.

### **4.3 Residual Floor Bearing Capacity**

In-situ floor bearing capacity tests have shown that once the load on the floor exceeds the floor bearing capacity, the floor fails but still retains some bearing capability called the residual bearing capacity (Fig. 4.4). After failure, if the load on the floor is equal to (never larger than) the residual bearing capacity, the floor material will flow out into the entry. Unfortunately, although many in-situ floor bearing capacity tests have been conducted, residual floor bearing capacity has not been considered seriously. The reduction ratio of residual floor bearing capacity can be determined by in-situ floor bearing capacity test results. Table 4.3 shows the collected data from two mines (Chugh, 1986; Peng, 1981) and determined value of the reduction ration of residual floor bearing capacity.



**Fig. 4.4 Generalized curve of relation between floor stress and settlement  
(after Jiang, 1991)**

**Table 4.3 Determination of Reduction Ratio of Residual Floor Bearing Capacity**

Test No.	Mine	q (psi)	q <sub>r</sub> (psi)	Reduction Ratio
1	Mine 1	1,304	800	0.61
2	Mine 1	1,440	1,000	0.69
3	Mine 1	780	400	0.51
4	Mine 1	2,630	1,800	0.68
5	Mine 2	1,410	733	0.52
6	Mine 2	1,269	705	0.56
7	Mine 2	1,128	705	0.62
8	Mine 2	1,692	1,128	0.67
9	Mine 2	1,128	705	0.62
Average				0.61

Also, based on equation 4.15, if the peak and residual values of cohesion and angle of internal friction are known, the floor bearing capacity, residual floor bearing capacity, and reduction ratio can be calculated. Based on the data collected from in-situ borehole shear strength tests conducted by Chugh (1986), the reduction ratio is calculated and presented in Table 4.4

Table 4.4 Residual Floor Bearing Capacity Factor Calculation

Test Site	Pillar Size (ftxft)	t (ft)	C(2)	Residual Value			Peak Value			Reduction Ratio
				C(1)	$\phi$	$q_r$	C(1)	$\phi$	q	
1	30x30	2	1,357	75	33.3	635	198	35.4	1,611	0.40
2	30x30	2	1,357	210	28.6	1,704	398	28.2	3,089	0.55
3	30x30	2	1,357	284	30.8	2,265	361	32.4	2,827	0.80
4	30x30	2	1,357	312	19.1	2,472	487	20.3	3,698	0.67
5	30x30	2	1,357	2,614	26.9	1,203	146	26.7	2,093	0.57
6	30x30	2	1,357	170	27.5	520	61	26.7	1,392	0.40
Average										0.59

From the analysis above, it can be seen that the reduction ratio ranges 0.4-0.8 and averages about 0.60 of the peak bearing capacity. This is consistent with the conclusion drawn by Jiang (1991) for a particular mine that, *the residual bearing capacity is 59% of the floor bearing capacity*. So the residual bearing capacity can be calculated by:

$$q_r = c_r q_b \quad (4.19)$$

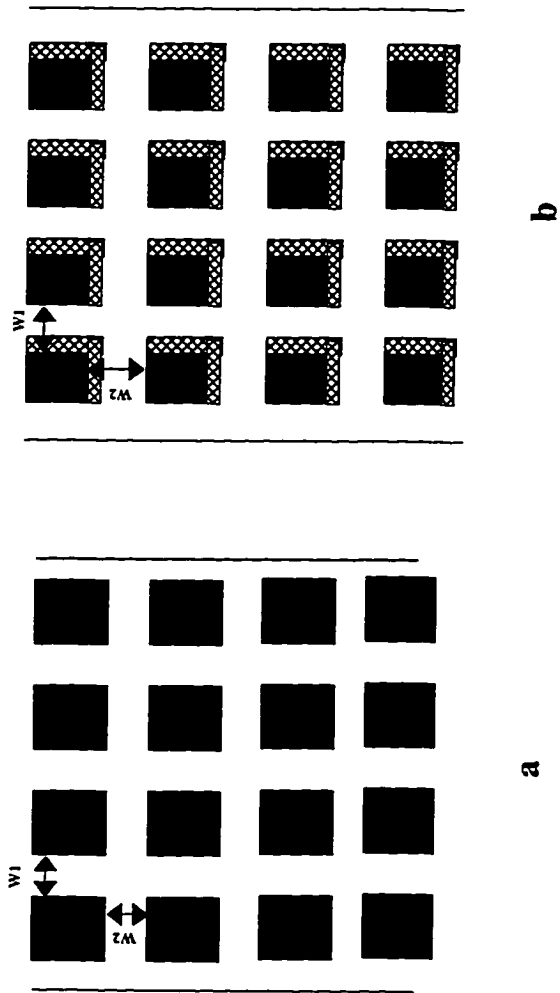
where  $q_r$  is the residual bearing capacity and  $c_r=0.4-0.8$  is the reduction ratio.

Conservatively,  $c_r=0.4$  is recommended for clay rock and  $c_r=0.6$  is recommended for the shale rock.

#### **4.4 Performance of Floor Bearing Capacity Equation in a Coal Mine**

In order to evaluate the performance of Equation 4.15 for the coal mine floor, a mine was selected to study the floor stability. The immediate floor of this mine consists of 2-6 ft of underclay. The overburden changes from 600 ft to 900 ft. The room and pillar mining method, with both partial pillar recovery and without pillar recovery, was used as shown in Fig. 4.5. In order to determine the floor rock material properties, the rock samples were randomly collected from different panels. The underclay material properties were tested in the laboratory as shown in Table 4.5. The floor performance and calculated floor stability factor based on the Equation 4.15 are listed in Table 4.6.





**Fig. 4.5 Mining method for the studied mine**

**a: No Pillar Recovery**  
**b: Partial Pillar Recovery**

Table 4.5 Floor Material Mechanical Properties

Sample	Cohesion (psi)	Angle of Internal Friction (degree)
#1	156	17.5
#4b	255	13.6
#4a	241	14.6
#4c	160	13.5
#2	302	N/A
#2	245	16.1
#2	208	30.1
#5	175	48
#10b	267	N/A
#11a	213	25
#10b	241	N/A
#9b	200	16
#9b	227	N/A
#10a	227	20
#7c	180	N/A
#7c	151	N/A
#5	213	30
#11b	142	N/A
#7b	142	14
#7	210	N/A
#11b	231	N/A
#11a	240	12
Average	213	20.6

Table 4.6 Pillar Performance and Stability Factor (SF)

Case	Pillar Size (ft)	Entry Width (ft)		Overburden (ft)	Floor Thickness (ft)	Stress (psi)	q (psi)	Floor Performance	SF
		W1	W2						
1	30x70	40	20	700	2	1,800	1,901	no heave	1.06
2	40x60	40	20	700	2	1,633	2,074	no heave	1.27
3	40x50	40	20	750	2	1,839	2,038	no heave	1.11
4	40x60	40	20	800	2	1,633	2,074	no heave	1.27
5	40x60	40	20	675	2	1,575	2,074	no heave	1.32
6	40x60	40	20	675	6	1,575	1,452	heave	0.92
7	50x50	40	40	625	4	1,630	1,804	heave	1.07
8	40x60	40	20	700	3	1,633	1,756	heave	1.12
9	50x50	40	40	625	3	1,406	1,706	heave	1.07
10	30x30	20	20	725	2	1,736	1,804	heave	1.04
11	30x30	20	20	725	8	1,856	1,459	heave	0.79
12	40x60	40	20	700	6	1,633	1,452	heave	0.89

From Table 4.6, it can be seen that all the unstable cases have stability factors of 1.10 or less with exception of case 8 whose SF is 1.12. All the stable cases have safety factors of 1.10 or larger with exception of case 1 whose SF is 1.06. Therefore the stability factor of 1.2 is recommended for mine design.

#### 4.5 Relation between Pillar Punching and Floor Heave

Floor heave is mainly caused by pillar punching into the floor and squeezing the floor material beneath the pillars out into the entries. Assume that during the pillar punching into the floor, the volume of floor material has no change. Therefore the total volume of the pillars that have punched into the floor is equal to the total volume of floor heave. The magnitude of floor heave can be calculated as shown in Fig. 4.6.

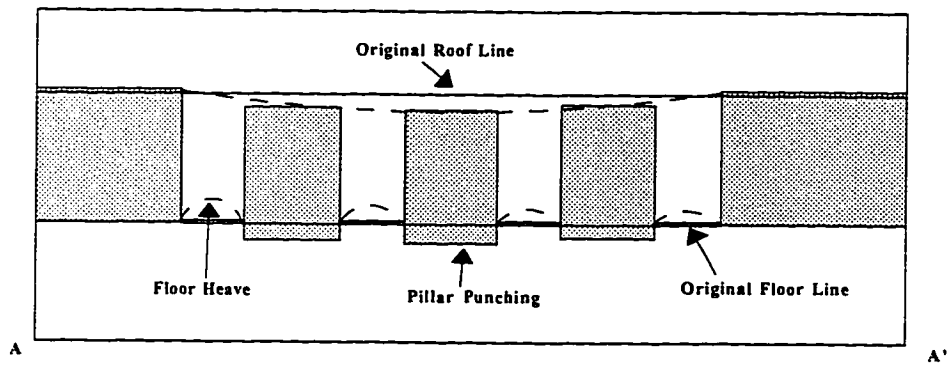
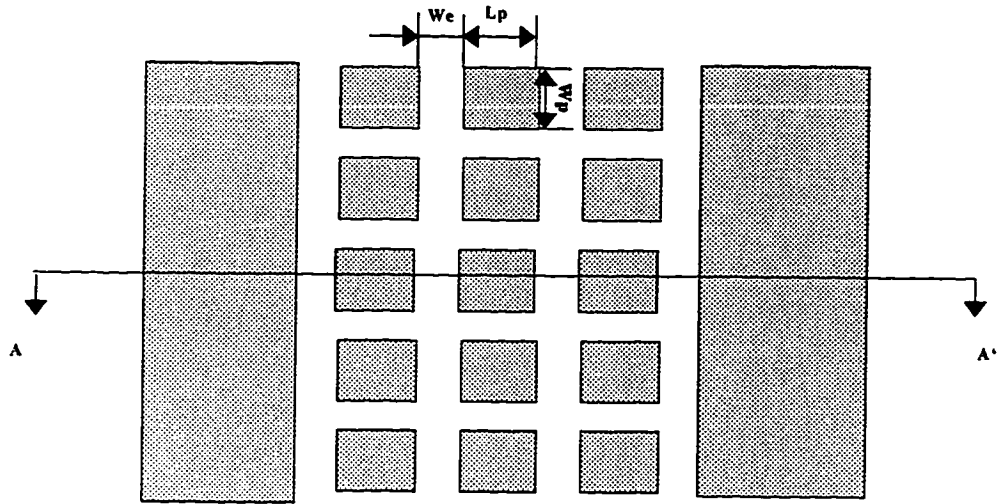
Volume of the pillar's punching into the floor:  $W_p \times L_p \times H_p$ .

Volume of the floor heave:  $[(W_p + W_e)(L_p + W_e) - W_p L_p] H_f$ .

So, the floor heave can be calculated by:

$$H_f = \frac{W_p L_p}{(W_p + W_e)(L_p + W_e) - W_p L_p} H_p \quad (4.20)$$

where  $W_p$  is pillar width;  $L_p$  is pillar length;  $H_p$  is depth of pillar punching;  $W_e$  is entry width; and  $H_f$  is the magnitude of floor heave.



**Fig. 4.6 Floor heave calculation**

#### **4.6 Floor Failure and Floor Heave Analysis and Control Method**

After the floor bearing capacity, residual floor bearing capacity, and relationship between floor heave and pillar punching are determined, the finite element analysis method can be used to analyze the floor failure, floor failure propagation, floor heave, and floor control methods.

The analytical procedures are described as follows:

1. Based on Equation 4.15, floor bearing capacity is calculated.
2. Based on Equation 4.19, residual floor bearing capacity is determined.
3. Finite element analysis.

Step 1: Based on mining and geological conditions, determine the average stress for all pillars.

Step 2: If the stresses on pillars are all smaller than the floor bearing capacity, neither floor failure nor floor heave will occur. Otherwise, take those pillars on which the stress is larger than the floor bearing capacity out and apply the floor residual bearing capacity value on the roof and floor where the stress on pillar is larger than the floor bearing capacity. Rerun the models to determine the average stress on the remaining pillars.

Step 3: Repeat step 2 until the stress on the remaining pillars is smaller than the floor bearing capacity. At this time, the floor failure propagation stops.

step 4: Determine the roof deflection and pillar punching based on the results

from step 3.

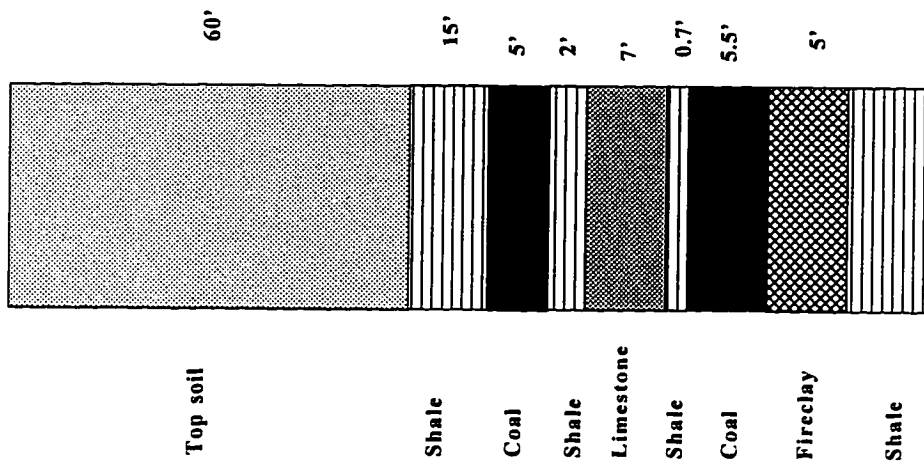
4. Calculate the amount of floor heave based on the relationship between pillar punching and floor heave.
5. Floor heave control measures. If the magnitude of floor heave is too large, using either of the following methods to control it:
  - a. Increase the pillar size such that the floor bearing capacity is larger than the applied stress. So neither failure nor heave occurs.
  - b. Use the same entry and pillar sizes but reduce the number of pillars and entries in a panel in such a way that the amount of floor heave can be reduced to some allowable value. In this case, both failure and heave occur but the amount of floor heave is too small to hinder any mining activities.

#### **4.7 Floor Heave Analysis and Mine Design - A Practical Application**

Based on the floor heave model and analysis approach described above, the floor heave case in a typical soft floor mine, namely Mine A, was analyzed and the panel was redesigned based on the results of analysis.

##### **4.7.1 Geological and Mining Condition in Mine A**

Mine A is in the No. 11 coal seam in Kentucky. The overburden depth is about 8.5 ft. Mining height is 5.5 ft. The immediate roof as shown in Fig. 4.7 consists of 0-8 in shale, 4-7 ft clayey limestone, 1-2 ft of shale, 2-5 ft of coal, and 5-18 ft of sandy shale. The mine floor



**Fig. 4.7 Geological column of Mine A**



is comprised of 4-7 ft fireclay underlain by sandy shale. The room and pillar mining method is used in this mine. The mine plan is shown as Fig. 4.8.

#### **4.7.2 Investigation of Floor Heave**

As Shown in Fig. 4.8, the floor heave occurred in the first west section and a portion of the north mains. The first west section consists of eight entries on 50x54 ft centers while the North mains were driven in a seven-entry system on 54x60 ft centers. The history of floor heave is described as follows:

During the development of North mains, no floor failure was ever observed. After First West section had been developed, to a size covering nine rows of pillars, water was found to gush out of the mine floor on the left side of the section as shown in Fig. 4.9. In order to keep the section dry, the water was pumped to the inby side of the North mains and then in turn pumped out to the surface. Therefore the floor in the First West section and outside the First West section mouth in the North mains were flooded. After the floor was flooded, floor cracks were first observed on both sides of the central entries of the First West section and then propagated to the other areas. Soon after pillars in this area began to punch into the mine floor causing the floor to heave up. Due to the extreme floor heave, the section had to be sealed off at location A of North Mains (Fig. 4.8). Several months after the section was sealed off, the sealed-off location was examined in detail. In the area outby the seal location, the fireclay floor was under natural moisture conditions and no wet area was found. However, no evidence of floor failure and floor heave was observed both inby and outby the sealed area. On the surface, a large crack was found as shown in Fig. 4.9.

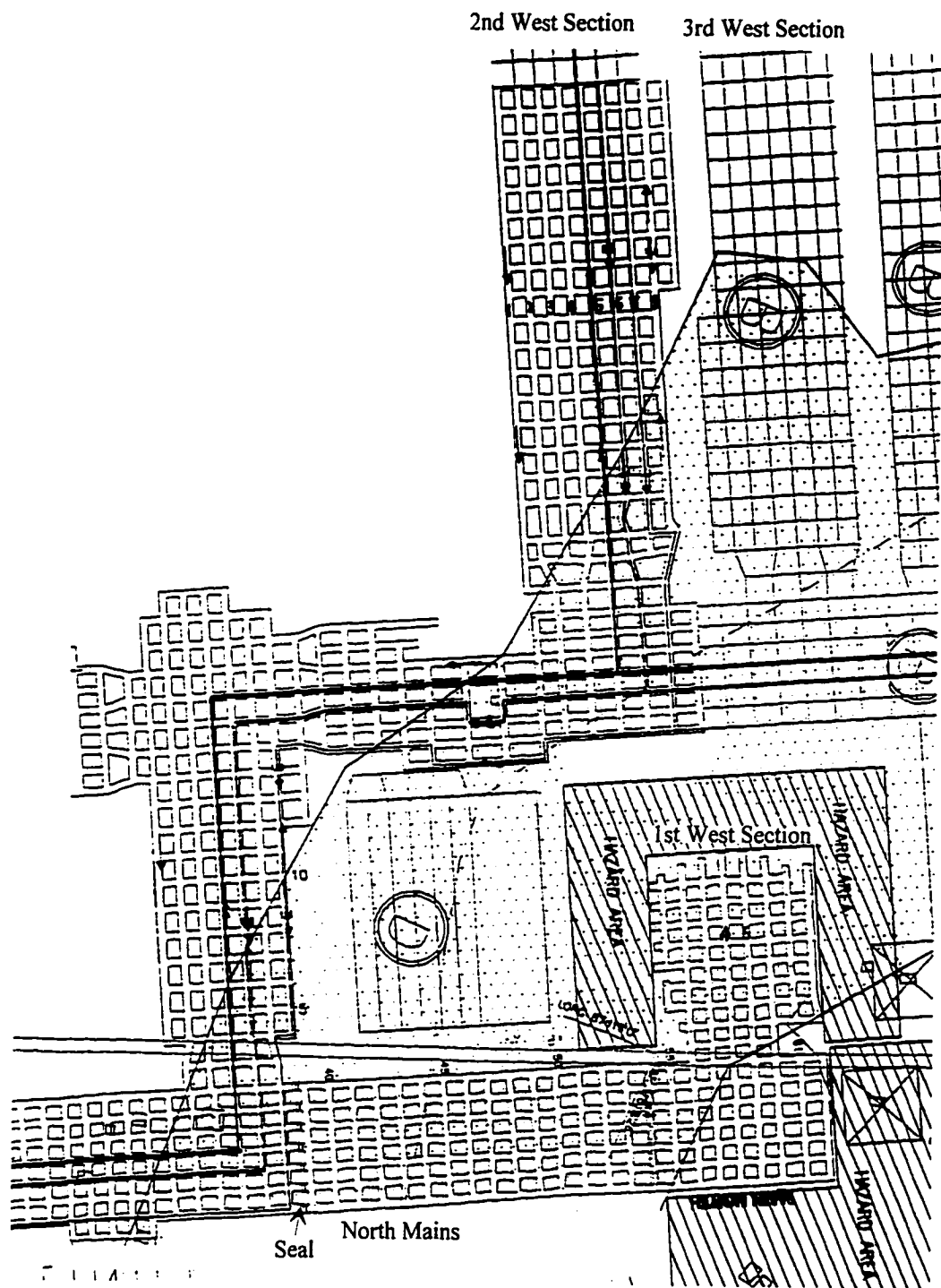


Fig. 4.8 The mine map of mine A (Not to scale)

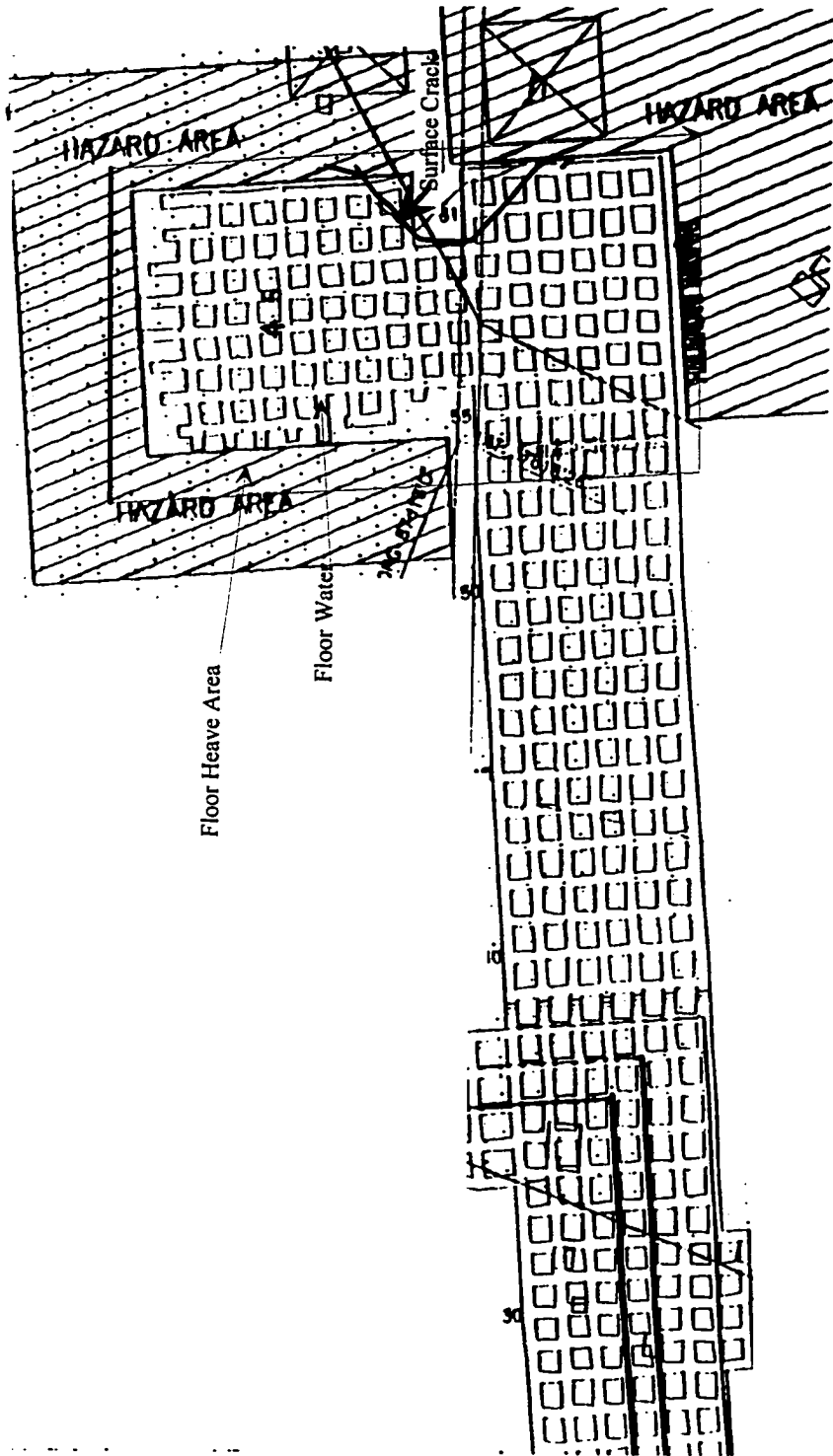


Fig. 4.9 Floor heave in first West section (Not to scale)

Based on the floor heave history described above, it can be determined that two factors played an important role in the process of floor heave. One is the thick fireclay layer of the immediate floor and the other is presence of water in this section.

#### **4.73 Rock Properties**

##### **1. Floor rock properties**

Floor rock blocks were collected from four different sites and tested in the laboratory.

The results are listed in Table 4.7.

Table 4.7 Floor Fireclay Properties

Site	Sample	Shear Strength* (psi)	Moisture Content (%)
1	1	217	6.8
	2	180	
	3	167	
2	1	180	6.5
	2	192	
3	1	340	8.5
	2	330	
	3	259	
4	1	293	7.1
	2	295	
Average		228	7.3

\* Direct shear test

## 2. Roof Rock and Coal Properties

Roof and Coal Properties are listed in Table 4.8.

Table 4.8 Rock Properties

Rock Type	Young's Modulus (10 <sup>6</sup> psi)	Poisson's Ratio	Strength (psi)		
			Compressive	Tensile*	Shear**
Coal	0.53	0.24	949	103	104
Shale	3.1	0.12	1,752	154	376
limestone	11.1	0.15	4,742	244	640

\* Indirect tensile strength, Brazilian test

\*\* Direct shear test

### 4.7.4 Floor Bearing Capacity

Based on Equation 4.15, floor bearing capacity under natural and flooded condition is calculated and listed in Table 4.9. Reduction ratio used for the flooded condition is 0.4.

**Table 4.9 Floor Bearing Capacity**

Pillar Size (ft x ft)	Bearing Capacity (psi)	
	Dry	Flooded
34x30	663	265
35x40	715	286
35x55	705	282
35x50	707	282
50x65	764	305

**4.7.5 Residual Bearing Capacity of Floor**

Based on Equation 4.19, the residual floor bearing capacity of the floor is calculated and listed in Table 4.10. The Reduction ratio of 0.4 is used due to the fact that the immediate floor is extremely soft and thick.

Table 4.10 Residual Floor Bearing Capacity

Pillar Size (ft x ft)	Residual Floor Bearing Capacity (psi)	
	Dry	Flooded
34x30	265	106
35x40	286	114
35x55	282	112
35x50	282	112
50x65	305	122

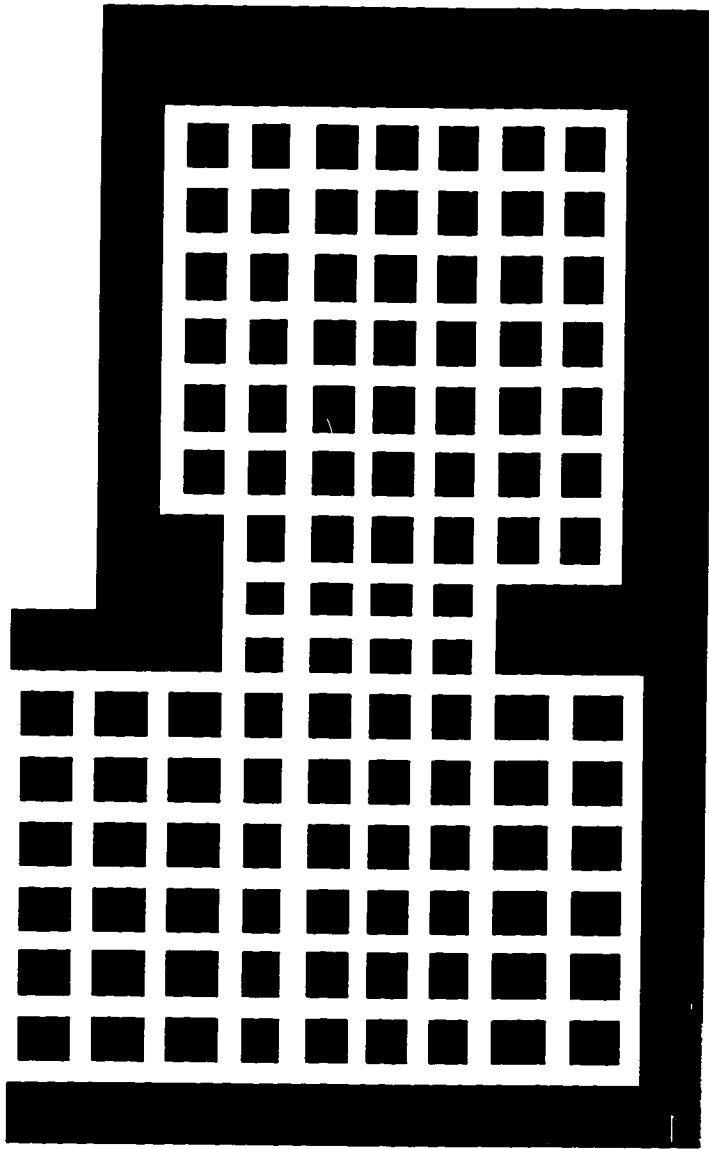
#### 4.7.6 Finite Element Modeling

The 3-D finite element method was used to simulate the floor failure and heave in the First West section, and then the panel was redesigned based on the two approaches described earlier.

##### 1. Floor Failure Initiation

A 3-D finite element model is established to simulate floor failure initiation as shown in Fig. 4.10. The model covers the whole First West section and a portion of North Mains. The overburden strata are simulated up to the surface. The pillars are 30x34 ft in size and the entries are 20 ft wide. The mining height is 5.5 ft.





**Fig. 4.10 Simulation of floor failure initiation**

Fig. 4.11 shows the vertical stress distribution on the mine floor before failure initiation and Fig. 4.12 shows the average stress on the mine floor. It can be seen that stress on the shadowed floor area is larger than the floor bearing capacity of 265 psi under flooded condition but much smaller than the floor bearing capacity of 663 psi under dry condition. Therefore, the floor failure on the shadowed area will be initiated due to a flooded condition. During this stage, only the cracks on floor can be observed without obvious floor heave.

## 2. Floor Failure Propagation

After failure initiation, the floor bearing capacity is reduced to its residual value of 106 psi. As a result, part of the stress will be transferred to the neighboring pillars and cause the propagation of floor failure. A 3-D finite element model is established to simulate the floor failure propagation and the amount of floor heave after floor failure initiation (Fig. 4.13). In this model pillars on the failed floor area are taken out and a constant stress equal to the residual floor bearing capacity of 106 psi is applied to the roof and floor.

Fig. 4.14 shows the stress distribution after failure initiation and Fig. 4.15 shows the average stress on the floor. It can be seen that the stress values on the floor beneath the neighboring pillars are all larger than the floor bearing capacity. Therefore floor failure will be propagated to the neighboring area. The maximum floor heave at this stage is only 3.3 in.

Fig. 4.16 shows the tensile stress distribution in the limestone roof layer. The maximum tensile stress is 166 psi which is less than its tensile strength of 244 psi. Therefore, the roof and overburden are still stable at this stage.

Consequently, the floor in all the flooded area will fail.

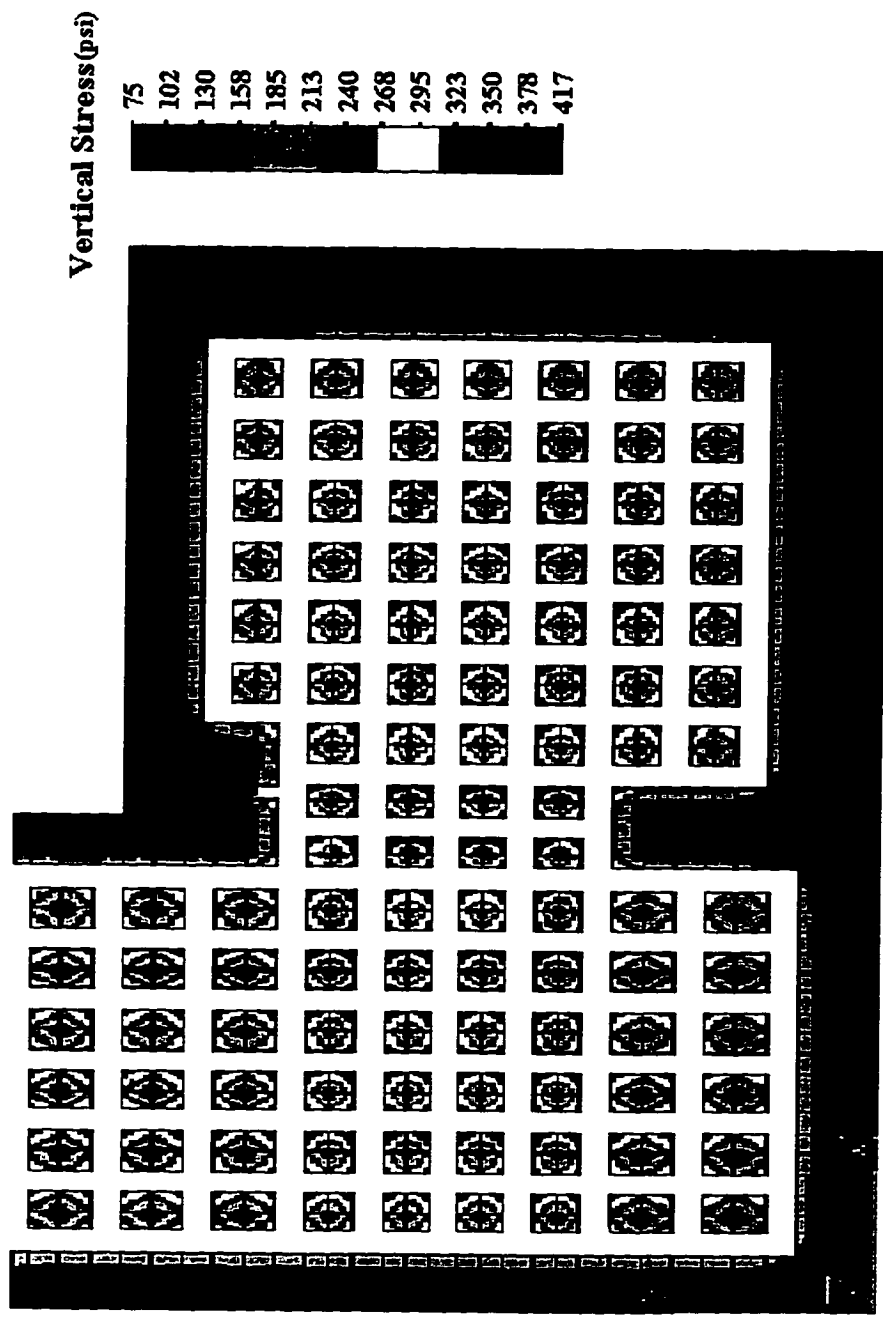
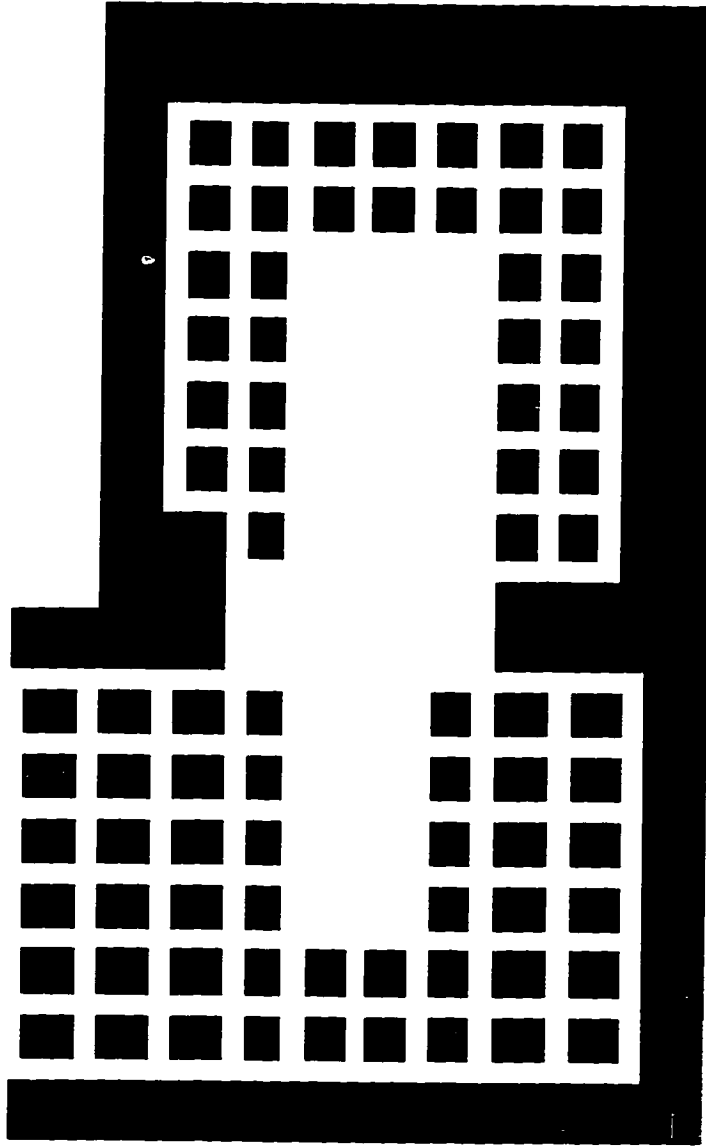


Fig. 4.11 Vertical stress distribution on the floor before failure Initiation





**Fig. 4.13 Simulation of floor failure propagation**

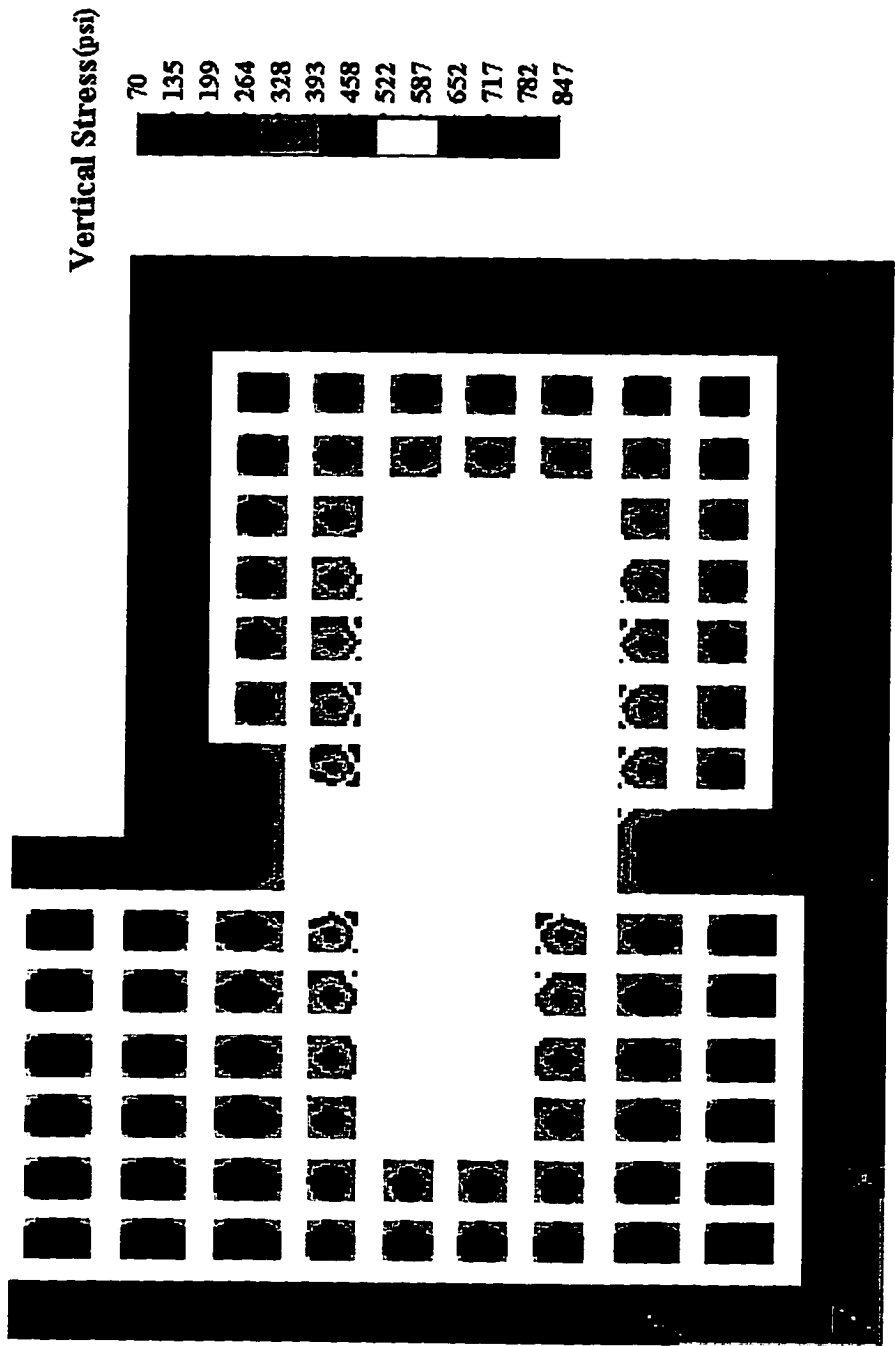
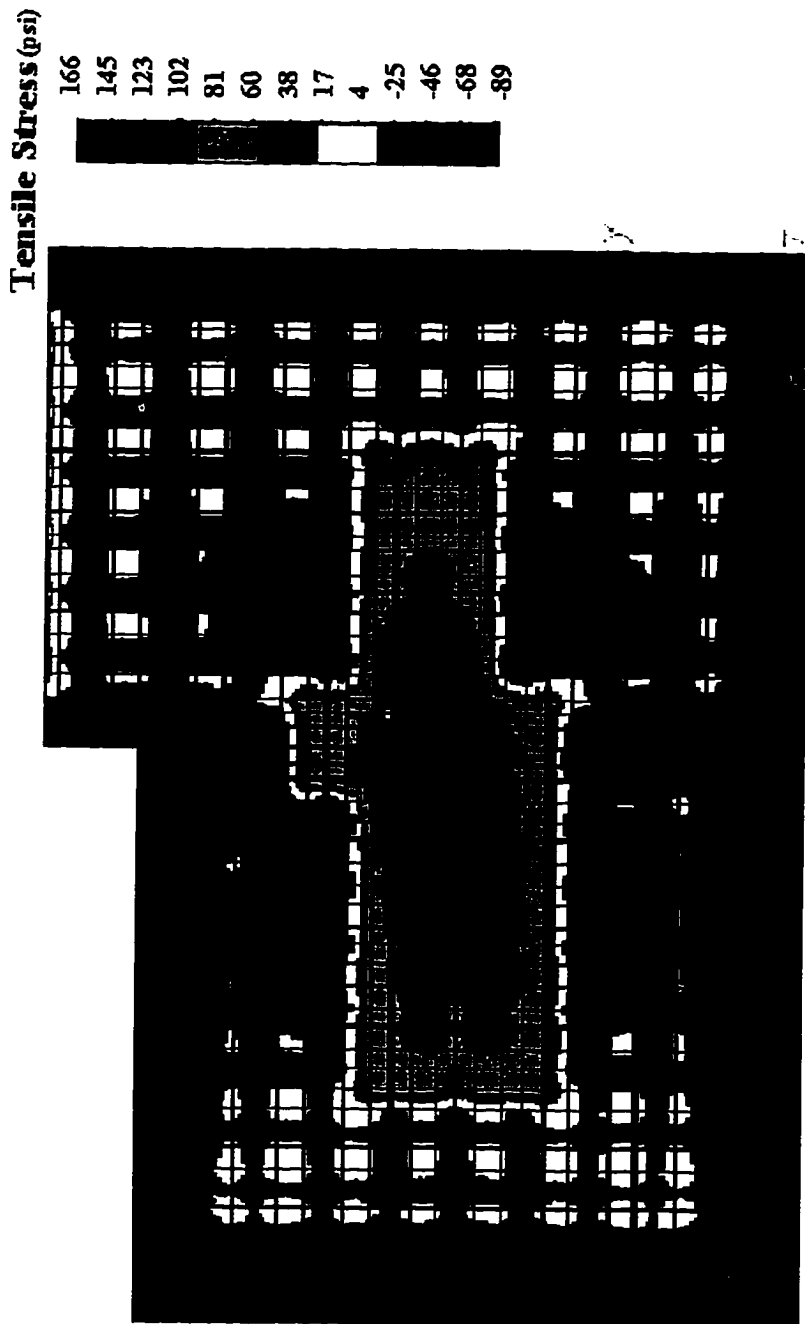


Fig. 4.14 Vertical stress distribution after failure initiation





**Fig. 4.16 Tensile stress distribution in the immediate roof after floor failure initiation**

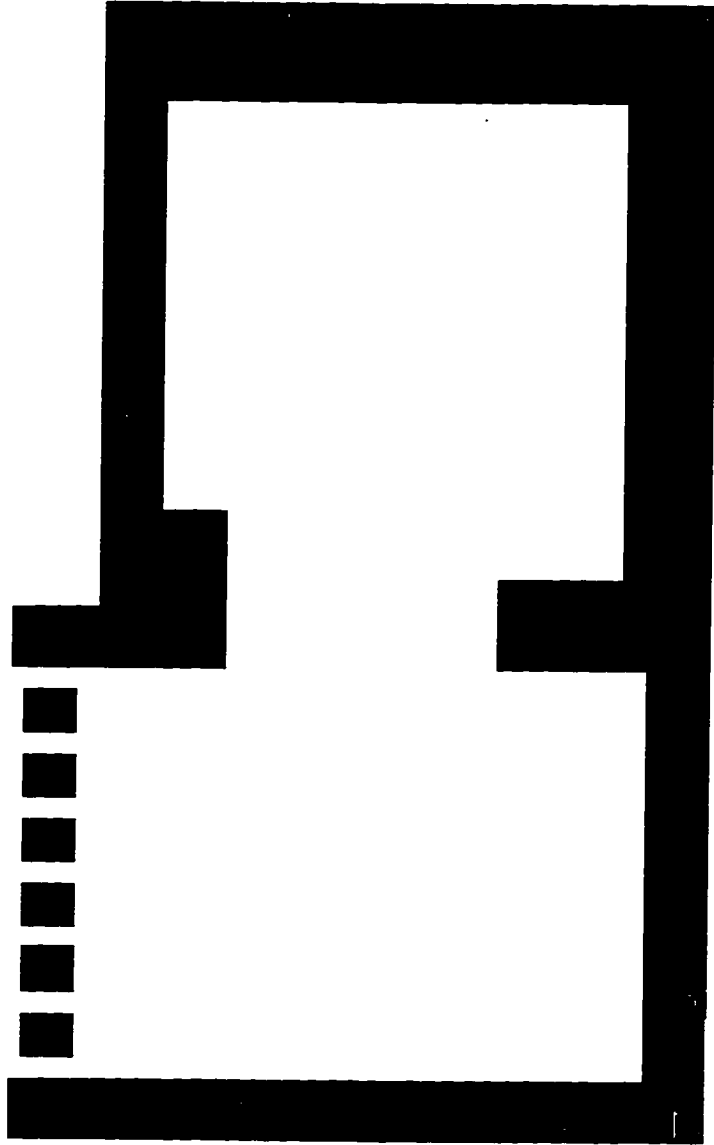


### 3. Final Floor Heave Area and Overburden Failure Analysis

After the floor in the flooded area fails, part of the stress will be transferred to the dry area. A 3-D finite element model is established to simulate if the floor failure can stop in dry area (Fig. 4.17). In this model, pillars in the flooded area are all taken out and a constant stress equal to the floor residual capacity of 106 is applied to the roof and floor where pillars are taken out.

Fig. 4.18 and Fig. 4.19 show the stress distribution and average stress on the floor in the dry area after all of the wet floor fails, respectively. The stresses on the dry pillars are all less than the floor bearing capacity under natural moisture conditions. Therefore the floor failure and floor heave will stop at the location where the mine floor is under a natural moisture condition. The maximum floor heave is 0.6 ft if the overburden is still stable.

Fig. 4.20 shows the tensile stress distribution in the immediate roof and the maximum tensile stress on the limestone layer is 422 psi, which is larger than the tensile strength on the central part of section. Therefore the limestone roof will have tensile failure on the central area of the panel. Fig. 4.21 shows the maximum shear stress distribution in the immediate roof. The maximum shear stress around the panel boundary is larger than the shear strength of the limestone, so the shear failure will occur around the panel boundary. After the limestone layer fails, the whole overburden rock which is very soft will fail along the maximum shear stress plane. Fig. 4.22 is the maximum shear stress distribution on the surface. The immediate roof will collapse and shear failure will occur all the way through the overburden. The potential failure line on the surface is shown in Fig. 4.22. Because of the overburden failure, the weight of the whole overburden in the floor failure area will be transferred to the floor. Obviously, the



**Fig. 4.17 Simulation of floor heave**

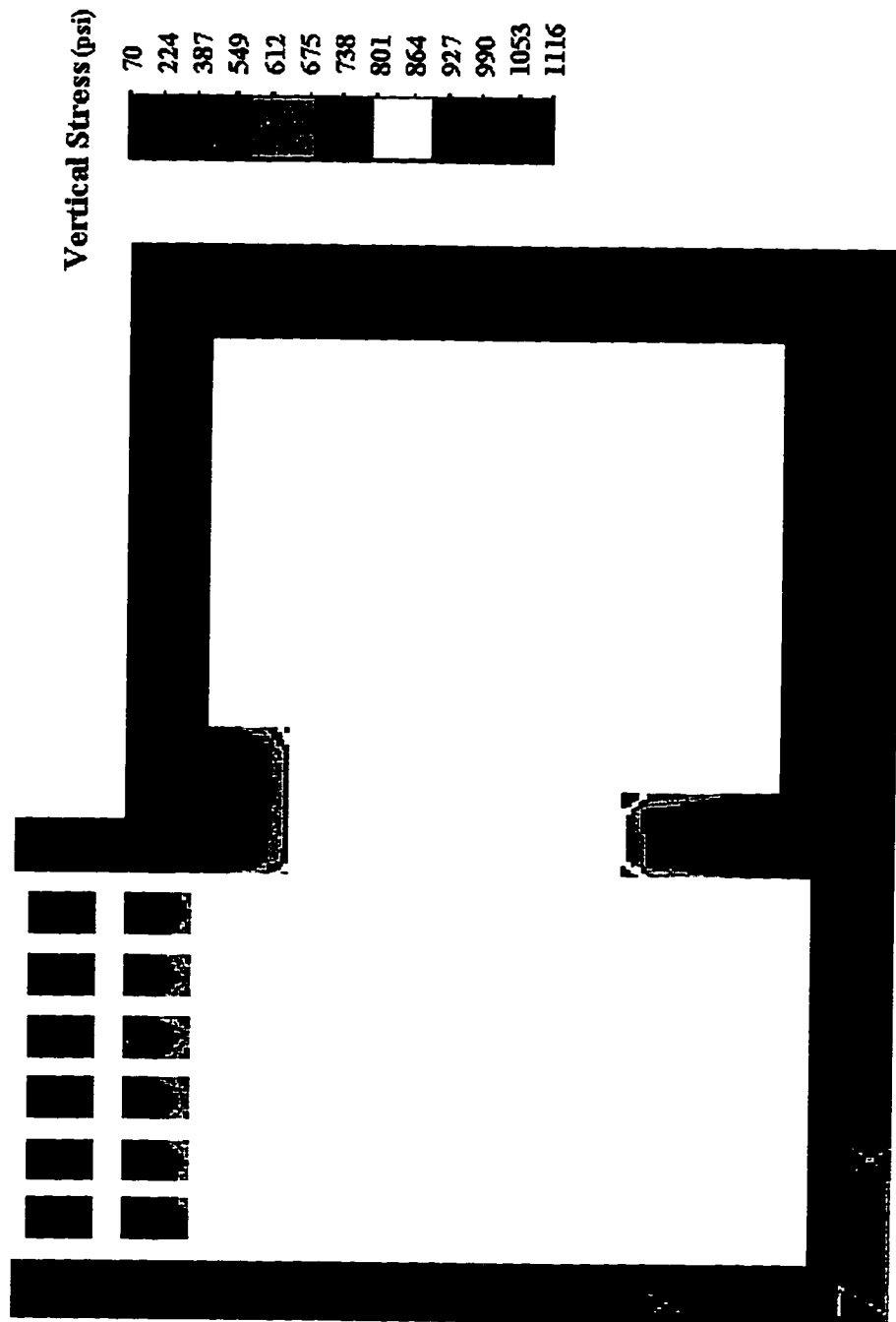


Fig. 4.18 Vertical stress distribution after the wet floor area fails



Tensile Stress (psi)

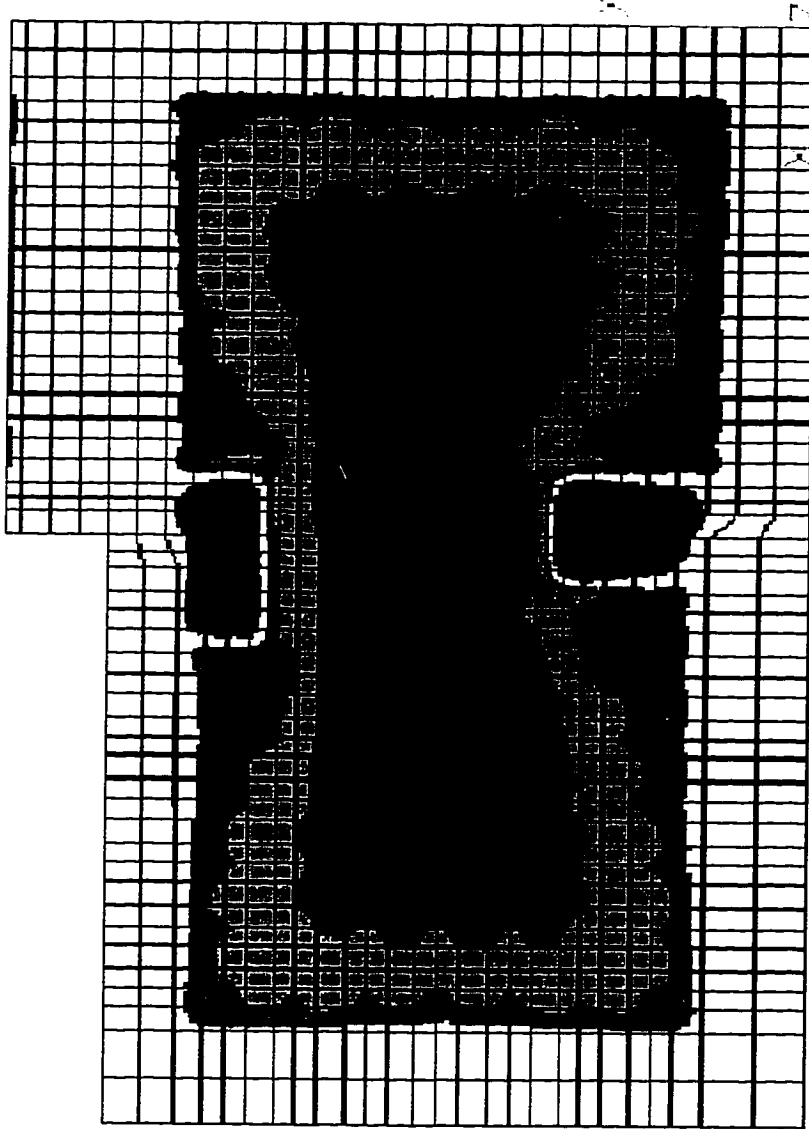
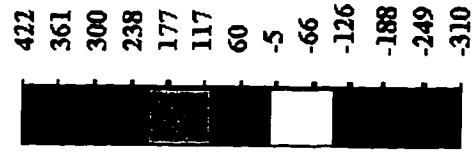


Fig. 4.20 Tensile stress distribution in the immediate floor after the wet floor area fails

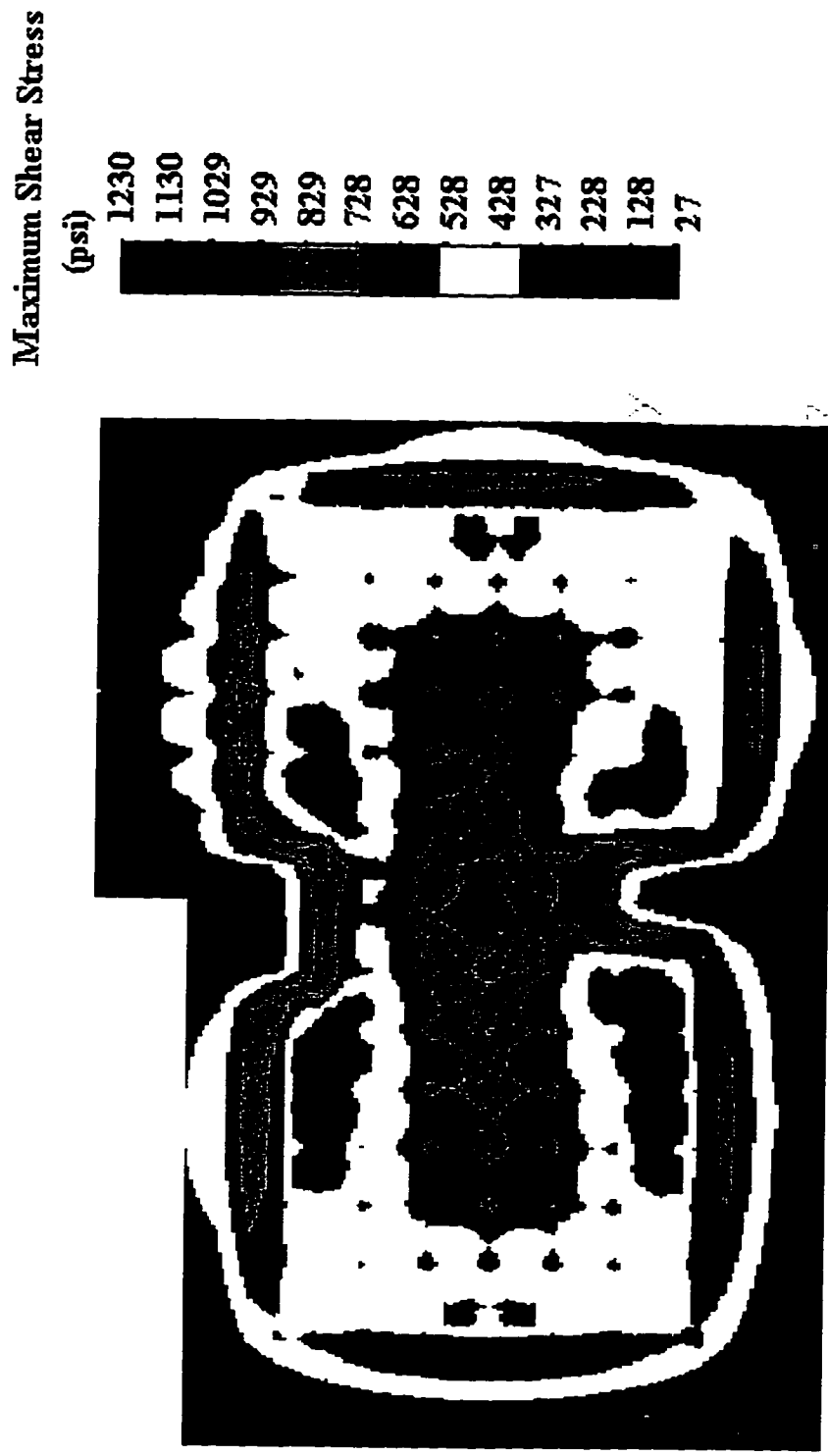


Fig. 4. 21 Maximum shear stress distribution in the immediate roof after the wet floor area fails

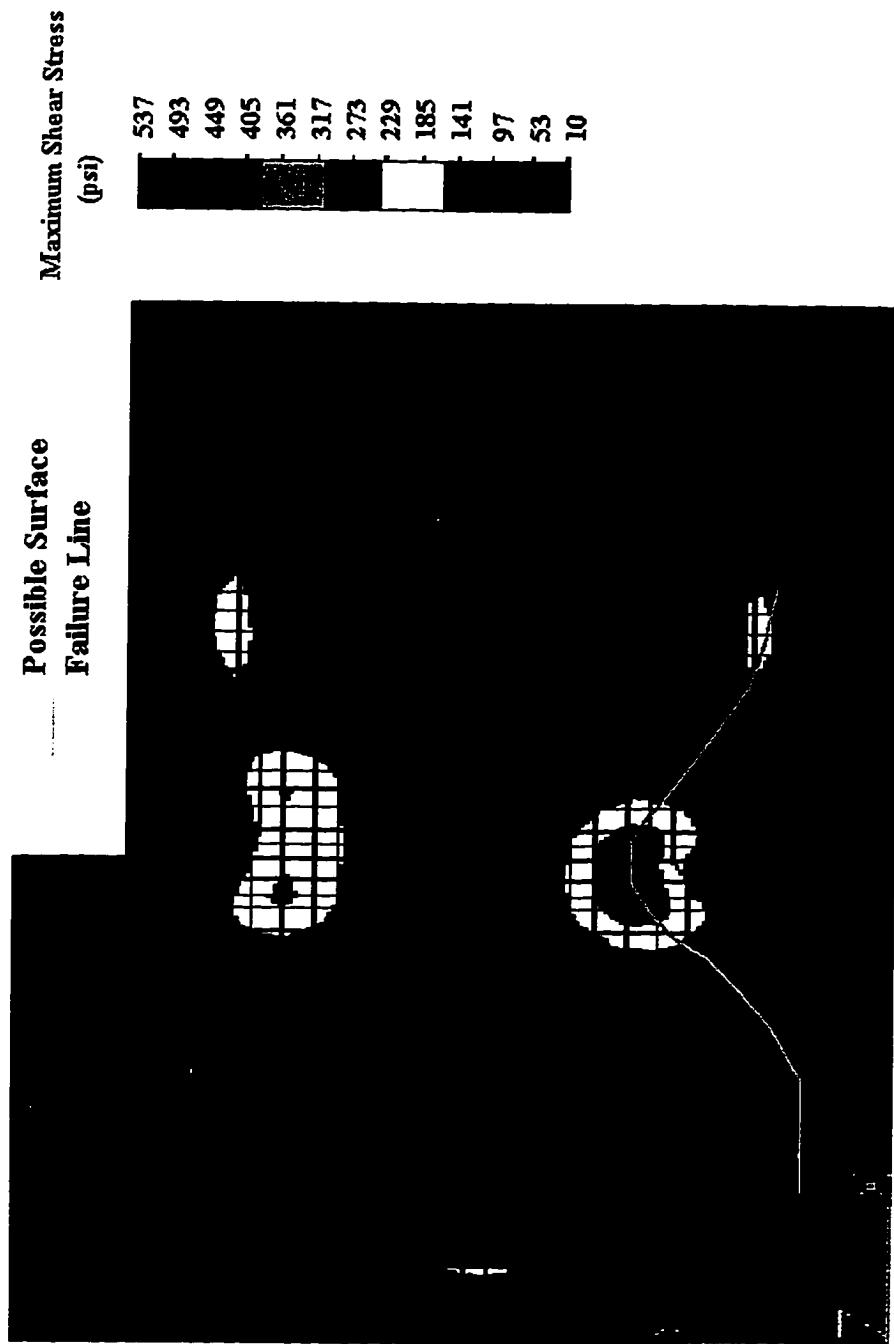


Fig. 4.22 Maximum shear stress distribution on the surface after the wet floor fails

residual bearing capacity of the floor is much less than the stress caused by the whole overburden. Pillars will punch into the floor until the entry is filled up.

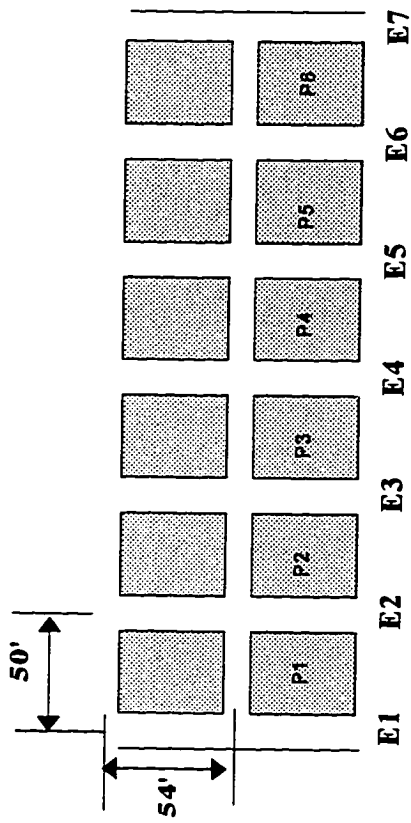
#### 4. Re-design of the Mine Plan to Control the Floor Failure and Floor Heave

Based on the floor heave mechanism described previously, two control methods are tested: One is to reduce the panel size while the pillar size remains the same, so that some floor failure is allowed but the amount of floor heave is controlled to some allowable value. The other is to increase the pillar size so that the floor bearing capacity is larger than the stress on the floor. In this case, neither floor failure nor floor heave will occur.

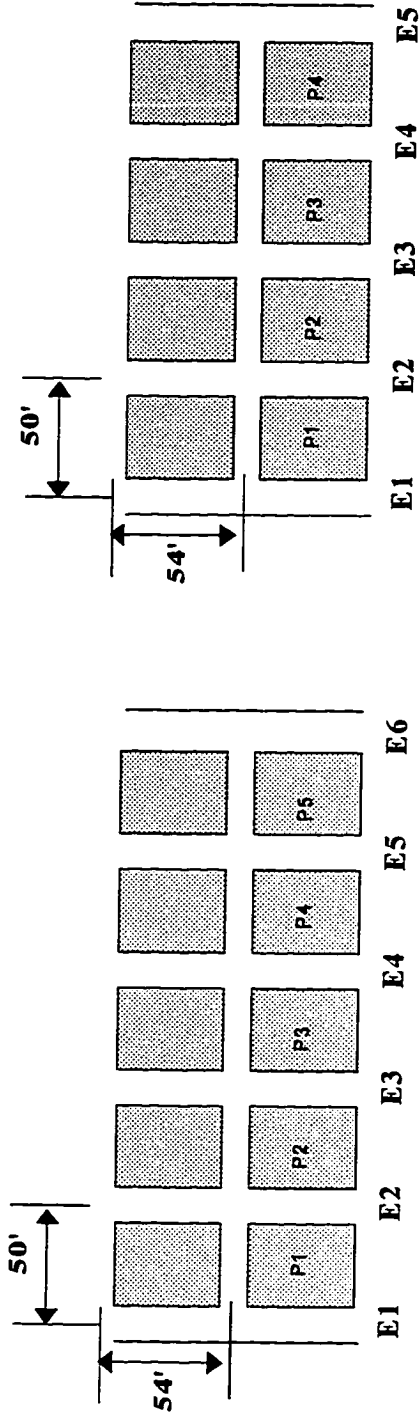
##### 1) Reduce the Panel Size

By reducing the panel size, the roof deflection can be reduced, thereby reducing the pillar punching and floor heave. Using 3-D finite element analysis, three mine plans, seven-entry, six-entry and five-entry systems (Fig. 4.23) are analyzed. Fig. 4.24 shows the amount of pillar punching, floor heave, and roof to floor convergence for the seven-entry system. It can be seen that the maximum pillar punching, which occurs in pillar 3, is 0.58 ft; the maximum floor heave, which occurs in entry 4, is 0.4 ft; and the maximum roof-to-floor convergence, which is also in entry 4, is 0.98 ft. Therefore, the seven-entry system cannot be employed because of too much floor heave and roof-to-floor convergence. Fig. 4.25 shows the amount of pillar punching, floor heave and roof to floor convergence for the six-entry system. It can be seen that





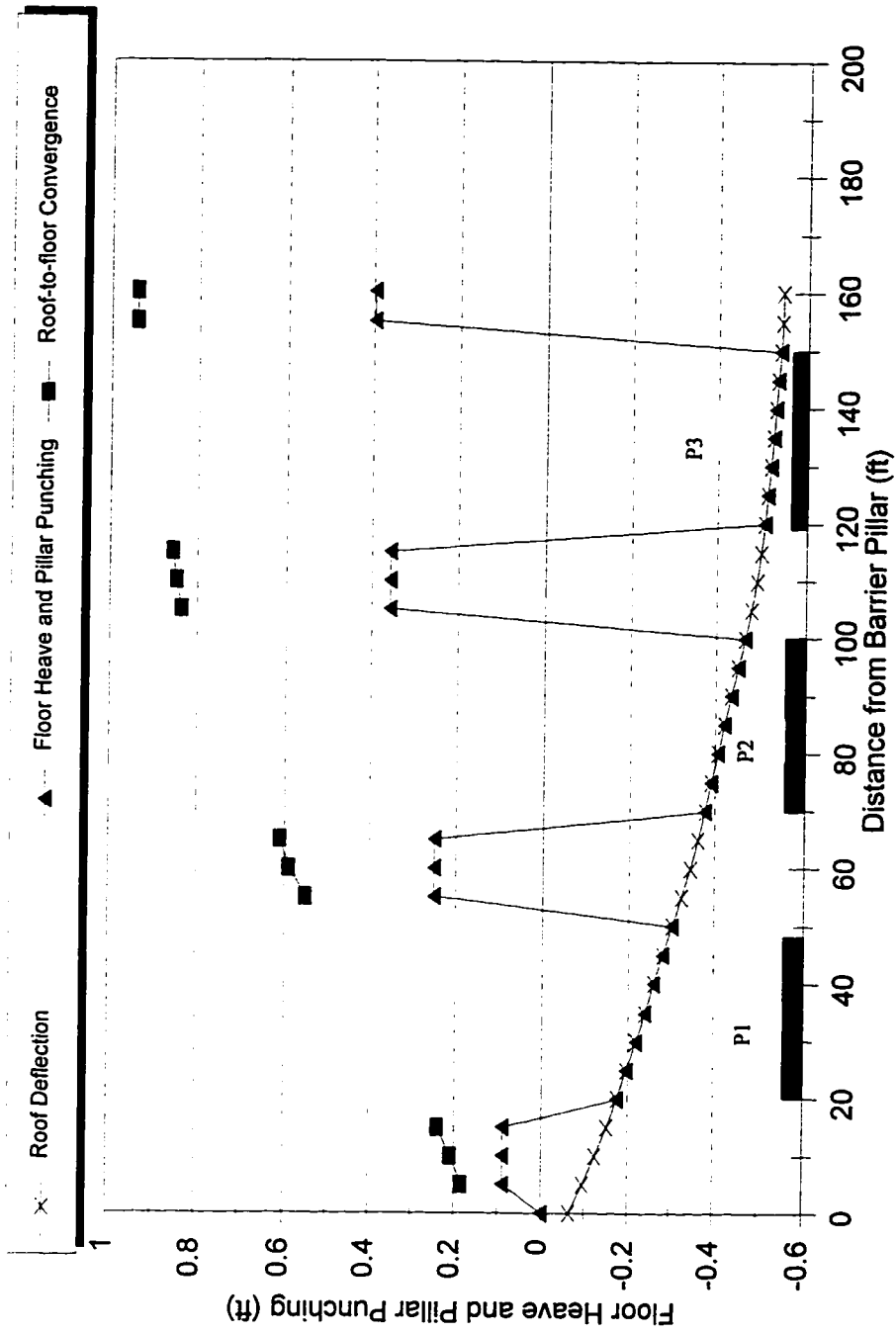
7-Entry System



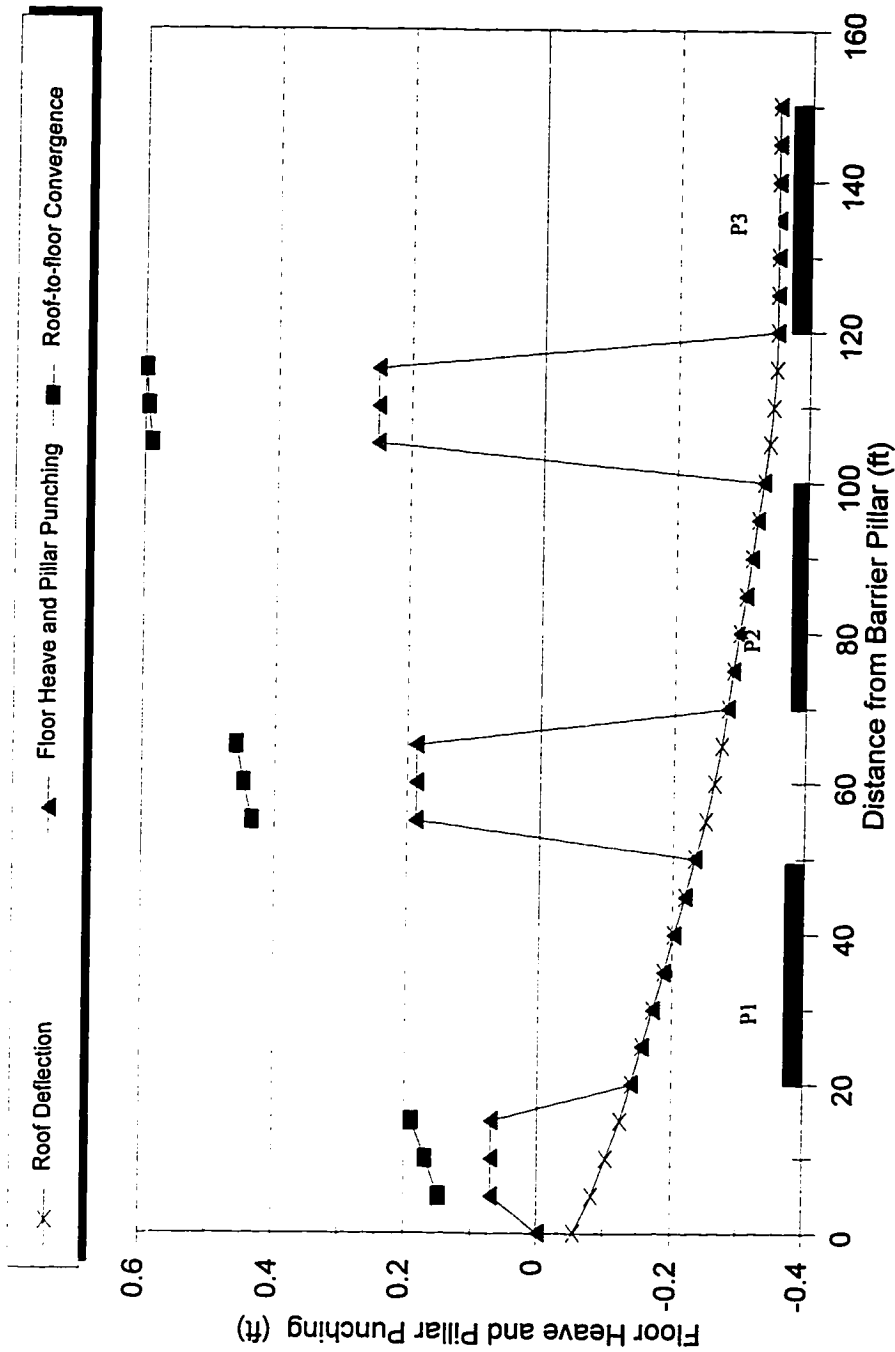
6-Entry System

5-Entry System

Fig. 4.23 Mining plan analysis



**Fig. 4.24 Floor heave and pillar punching in seven-entry system**



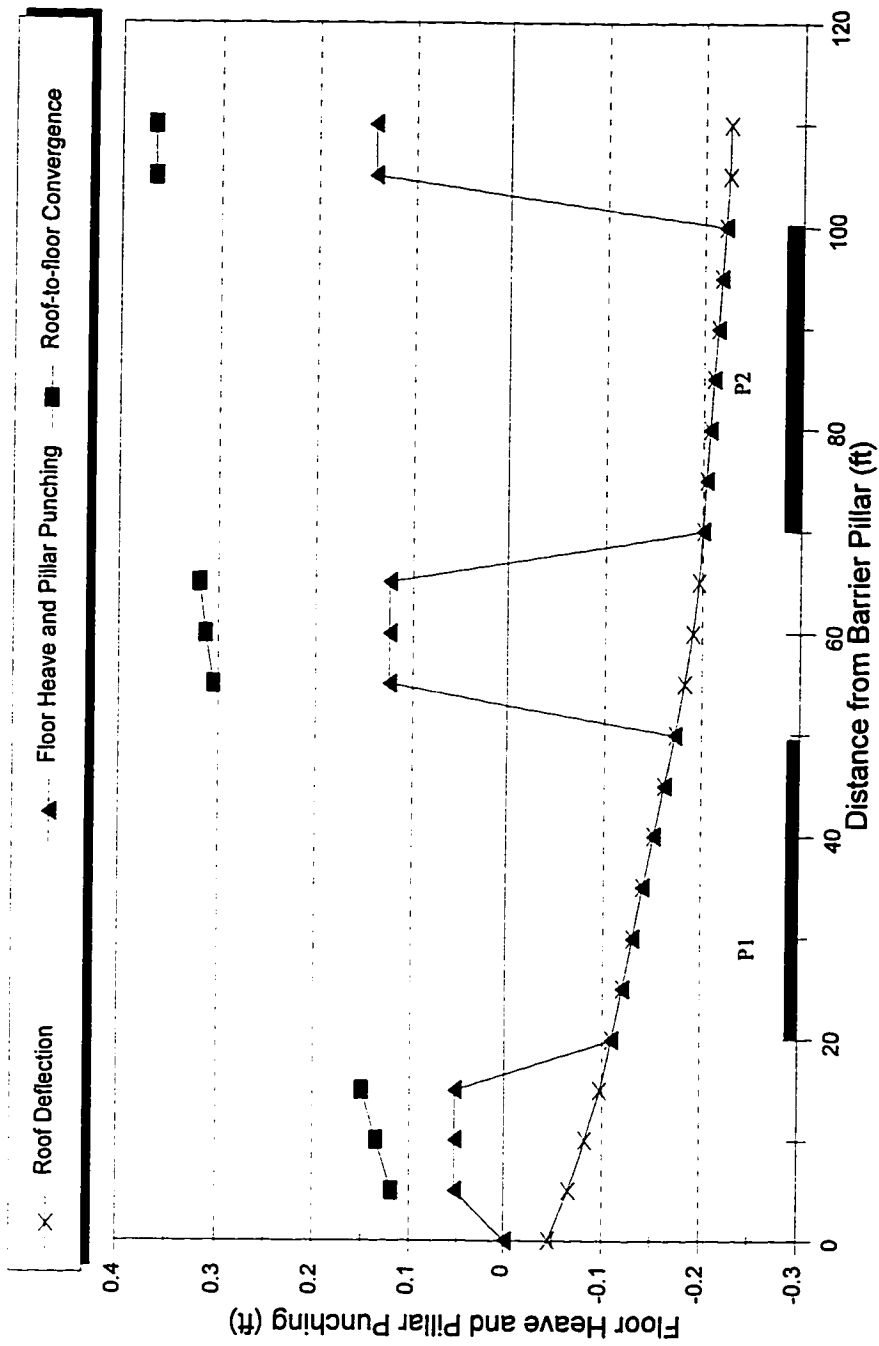
**Fig. 4.25 Floor heave and pillar punching in six-entry system**

the maximum pillar punching, which occurs in pillar 3, is 0.35 ft; the maximum floor heave, which occurs in entry 3, is 0.25 ft; and the maximum roof-to-floor convergence, which is also in entry 3, is 0.60 ft. Therefore, the six-entry system cannot be employed either because of too much floor heave and roof-to-floor convergence. Fig. 4.26 shows the amount of pillar punching, floor heave, and roof-to-floor convergence for the five-entry system. It can be seen that the maximum pillar punching, which occurs in pillar 2, is 0.22 ft; the maximum floor heave, which occurs in entry 3, is 0.15 ft; and the maximum roof-to-floor convergence, which is also in entry 3, is 0.37 ft. This amount of roof to floor convergence may not affect mining activity at all. Therefore, by reducing the panel size to a five-entry system, although the floor still fails, the amount of floor heave and roof-to-floor convergence is too small to hinder any mining activity.

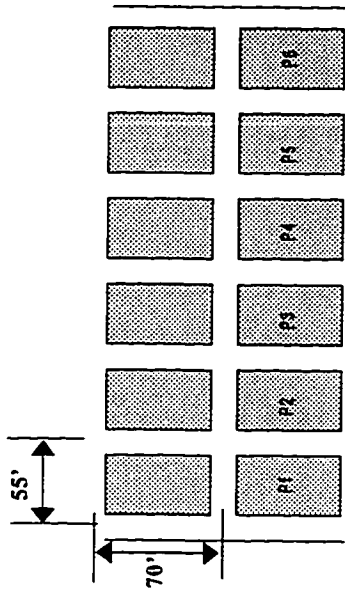
Based on this study, it is recommended that if the same pillar size is used, the panel size should be reduced from the eight-entry system to the five-entry system.

## 5. Enlarging the Pillar Size

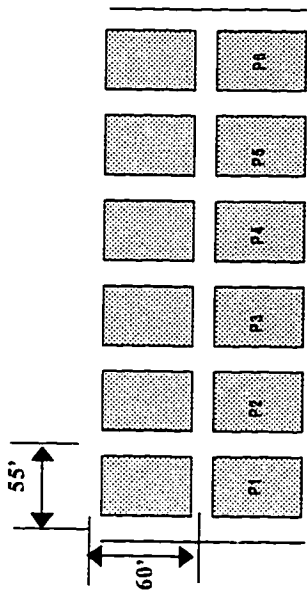
For the convenience of mining operations, four mining plans, namely Type A, B, C, and D, are proposed as shown in Fig. 4.27. Pillar size in Type A is enlarged from 30x34 ft rib-to-rib to 35x40 ft rib-to-rib; pillar size in Type B is enlarged from 30x34 ft to 35x50 ft rib-to-rib; pillar size in Type C is enlarged from 30x34 ft to 35x55 ft rib-to-rib; in mining plan D, the boundary pillar size is 65x50 ft rib-to-rib and the size of middle pillars is 35x50 ft rib-to-rib. To evaluate the floor stability, a 3-D finite element analysis was conducted for each mining plan.



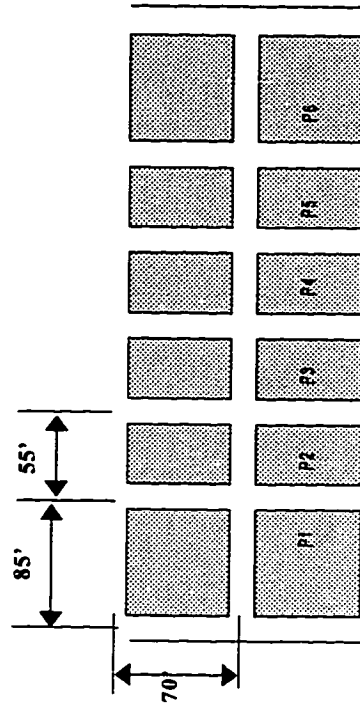
**Fig. 4.26 Floor heave and pillar punching in five-entry system**



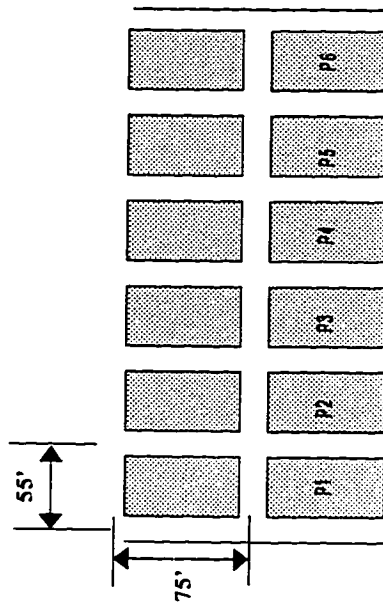
**B**



**A**



**D**



**C**

**Fig. 4.27 Proposed mining plans**

Table 4.11 shows the results of floor stability analysis for all four mining plans.

Table 4.11 Floor Safety Factors for Mining Plans Shown in Fig. 4.27

Mining Plan	Floor Condition	Pillar Number		
		1	2	3
A	Wet	1.23	1.15	1.14
	Dry	3.65	3.42	3.40
B	Wet	1.3	1.23	1.23
	Dry	3.73	3.52	3.51
C	Wet	1.33	1.26	1.26
	Dry	3.76	3.57	3.55
D	Wet	1.49	1.23	1.23
	Dry	4.50	3.51	3.51

Safety factors for the proposed mining plans in Table 4.11 indicate that all mining plans are safe to be used except Type A under wet condition.

Based on the analysis above, either of the two floor heave control methods can be employed in this mine: One is to reduce the panel size from the eight-entry system to the five-

entry system while using the same pillar size (30x34 ft rib-to-rib). In this case, floor failure and floor heave will occur but the magnitude of floor heave is too small to hinder any mining activities. The other is to increase the pillar size to at least 35x50 ft rib-to-rib. In this case, neither floor failure nor floor heave will occur.

It was decided by mining management that in order to run a super panel of a seven-entry system a block pillar size 35x50 ft needed to be used. As shown in Fig. 4.8 during the development of Third West section, the same water condition as in the First West section was encountered. The water was gushing out from the floor during panel development. However, due to the enlarged pillar, neither floor failure nor floor heave was ever observed. This section has been successfully mined out without any floor heave problems.



## **CHAPTER 5**

### **CONCLUSIONS**

---

---

Mechanisms and control of floor heave have been studied in this research. Through underground observations, two types of floor heave, namely Type I and Type II were identified. Correspondingly, two mechanical models for the two types of floor heave have been developed. The major results are concluded as follows:

#### **Type I Floor Heave**

1. **Floor Strata Properties.** The floor usually consists of several thin layers of relatively strong rock where this type of floor heave has occurred.
2. **Stress conditions.** Observations have shown that most floor heave occurred during the pillar recovery stage, which means the abutment pressure transferred to the outby pillars increases the vertical stress and causes the floor to fail. However, high horizontal stress is most important in that it causes the broken floor to heave up. The final floor heave is caused by the buckling failure of floor and horizontal movement of floor layers.
3. **Floor Heave Sequence and Analysis.** During development, if the vertical stress is not high enough, the horizontal stress cannot cause the floor to heave. During retreat pillaring, the vertical stress increases through the transfer of abutment pressure to the pillars, and the shear stresses on the bedding planes between the layers are also built up. Since the shear strength of

the bedding planes is very low, shear failures on the bedding planes occur first. Due to the shear failures of the bedding planes, the immediate floor will change from a composite floor beam into several individual beam members. This could cause tensile stress in each beam members to redistribute and increase. Therefore, tensile failure may occur as a result of redistributed tensile stress. If a high horizontal stress exists, it will cause the floor to buckle and subsequent horizontal movement of the floor members will cause the floor to heave up.

4. **Mechanistic Modelling of Floor Heave.** Based on the floor heave observation and analysis, a mechanical model for Type I floor heave has been established using composite slab theory. This model was used to simulate the floor heave in the Smoot mine. The results have shown that the predicted floor heave was fairly accurate.

## **Type II Floor Heave**

1. **Geological and Mining Conditions.** The immediate floor consists of massive soft rock material such as mudstone. Floor heave often occurs during pillar recovery stage which results in higher vertical stress concentration.

2. **Floor Heave Sequence:** Based on underground observations, the floor heave sequence can be described and analyzed as follows:

(1) Once the vertical stress on the floor exceeds the bearing capacity of the floor, the floor fails.

(2) After floor failure, the floor bearing capacity is reduced to the residual values which more or less remain constant while the pillars continue to punch into the floor.

The magnitude of the floor heave depends on how much pillars can punch into the floor.

(3) Because of pillar punching into the floor, pillar resistance to the roof is reduced to the residual value. Consequently, the roof both above the entries and pillars will deflect and the magnitude of roof deflection depends on the panel size and roof condition. The magnitude of floor heave depends on the final roof deflection right above the pillars.

3. Determination of Floor Bearing Capacity. Floor bearing capacity was determined by the Vesic equation which was validated by floor heave cases in underground coal mines by the author. The residual floor bearing capacity was studied and the reduction ratio of residual floor bearing capacity ranges 0.4-0.8. The moisture effect on floor bearing capacity was also studied and the reduction ratio for the flooded mining condition was determined to range 0.40-0.96.

4. Determination of Relation between Pillar Punching and Floor Heave. The relation between pillar punching and floor heave was determined assuming that the volume of the floor material is not changed before and after floor heave.

5. Floor Heave Modeling and Mine Design. Using the analysis approach and floor control method described in Chapter 4.5, the 3-D finite element analysis technique was used to simulate a floor heave case. The results showed that the predicted floor failure and floor heave are fairly accurate and that the redesigned panel has eliminated floor heave problems.

The major contributions of the author are:

1. Through the in-situ observations, the author systematically studied the floor heave in

different floor rock conditions. Two types of floor heaves were identified based on the case studies. By mechanistic modeling, the magnitudes of both types of floor heave were predicted. No one has ever predicted floor heave before.

2. For the type I floor heave, the model combines the immediate floor and main floor by winkler foundation and slab theory and then uses buckling theory to analyze the stress distribution in the floor and predict the floor heave. Compared with the finite element method, this model can predict floor heave and separations between floor rock layers while finite element method cannot.

3. For the type II floor heave, the author identified the factors affecting floor failure and floor heave. Among these factors, for the first time the author pointed out that the floor failure depends on the stress and floor bearing capacity while the floor heave depends on the panel size, residual bearing capacity of floor, and roof structure. Using 3-D finite element method, floor failure initiation and propagation, and floor heave have been analyzed.

## REFERENCES

- Afrouze, A. Yield and Bearing Capacity of Coal Mine Floors. *International J. of Rock Mechanics and Mining Science*, Vol. 12, 1975, pp. 241-253.
- Aggson, J. R. Coal Mine Floor Heave in the Beckley Coalbed, An Analysis. U. S. Bureau of Mines, RI 8274, 1978, 32 pp.
- Brown, J. D. Experimental Study of Bearing Capacity in Layered Clays. *Proceedings of Seventh International Conference in Soil Mechanical Engineering, Mexico City*, Vol. 2, 1969, pp. 45-51.
- Chugh, Y. P. Effect of Soft Floor Interaction on Room and Pillar Mining. *International Journal of Mining and Geological Engineering*, 1990, Vol. 8, pp. 111-130.
- Chugh, Y. P. Insitu Strength Characteristics of Coal Mine Floor Strata in Illinois, 1986, Research Report, Illinois Mine Subsidence Research Program, 120 pp.
- Conover, D., Hanna, K., and Vandergrift, T. Floor Failure at King #4 Mine, Utah. U. S. Bureau of Mines, Interim Report, October, 1988, 91 pp.
- Freer, J. Mine Creeps. *Illinois Min. Inst. J.*, Vol. 1, No. 3, 1892, pp. 238-243.
- Hall, R. D. Squeezes in Mines and Their Causes. *Mines and Miner.*, Vol. 30, No. 5, 1909, pp. 286-287.
- Holland, C. T. Design of Pillars for Overburden Support-- part I, *Min. Congr. J.*, Vol. 48, No. 3, 1962, pp. 24-28.
- Jones, E. The Control of Creeps. *Colliery Eng. and Met. Monit.*, Vol.18, No. 3, 1897, pp. 111-113.

- Jenkins, J. D. The Bearing Capacities of Mine Floors. *Colliery Guardian*, Vol. 195, No. 5039, 1957, pp. 397-400.
- Jenkins, J. D. Some Investigations into the Floor Bearing Capacities of the Floors in the Northumberland and Durham Coalfields. *Trans. Inst. Min. Eng.*, Vol. 117, Part II, 1958, pp. 725-738.
- Jenkins, J. D. A Laboratory and Underground Study of the Bearing Capacity of Mine Floors. Paper in Proceedings of Third International Conference of Strata Control (Paris, France, May 1960). Cerchar Research Center, 1960, pp. 227-240.
- Jiang, Y. M. Floor Characteristics and its Bearing Capacity. *Rock Mechanics as a Multidisciplinary Science*, Proceedings of the 32nd U.S. Symposium. J. Roegiers(ed.), 1991, pp. 833-842.
- Jiang, Y. Q. Introduction to the Plastic Mechanics. Mechanical Engineering Publishing House, Beijing, China, 1979, 256 pp. (in Chinese).
- Nelson, A. Floor Movement and Their Control. *Iron and Coal trades Rev.*, Vol. 154, No.4136, 1947, pp. 38-40.
- Peng, S. S. and Wang, Y. J. An Improved Model For Floor Heave. Proceedings of 11th Annual Workshop of Generic Technology Center for Mining System Design and Ground Control, Held at University of Alabama, October, 1993, pp. 45-55.
- Peng, S. S. Tsang, Po and Wang, Y. J. Mechanism of Floor Heave-- A Case Study. Proceedings of 10th Annual Workshop of Generic Technology Centers for Mine System Design and Ground Control. Held at the University of Idaho. Nov., 1992, pp. 53-64.
- Peng, S. S. Coal Mine Ground Control. John Wiley & Sons, Inc. 1986, 491 pp.

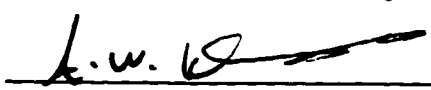
- Peng, S. S. Report on Bearing Capacity of Floor Rock in Big John #4 Mine and Twin Poplar Mine, 1981, unpublished report, pp 33. West Virginia University, Morgantown, WV.
- Selvadurai, A. P. S. Elastic Analysis of Soil Foundation Interaction. Elsevier, 1979, pp. 481.
- Terzaghi, K. Theoretical Soil Mechanics, 1943, Wiley and Sons, New York, 170 pp
- Vesic, A. S. Research on Bearing Capacity of Soils, 1970, Unpublished Report, 32 pp.
- Wilson, M. J. The Origin and Geological Significance of the South Wales Underclays. J. Sediment. Petro., Vol. 35, No. 1, 1965, pp. 26-31.
- William, J. W. Controlling Coal Mine Floor Heave: An Overview. U. S. Bureau of Mines, IC 9326, 1992, 17 pp.
- Xu, Z. L. Theory of Elasticity. The education publishing House, 1986, 842 pp. (in Chinese).
- Young, C. M. Percentage of Extraction of Bituminous Coal with Special Reference to Illinois Conditions. Univ. Illinois Bull. Eng. Expt. Stn. No. 100, 1917, pp. 175.


## VITA

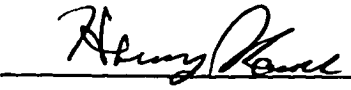
The author was born on October 25, 1962 in China. He started his college education in September 1979 and received his Bachelor of Engineering degree in Mining Engineering in July 1983 from Fuxin Coal Mining College in China. Then he began his graduate study in Beijing Graduate School of China University of Mining and Technology (CUMT). He received the Master of Science degree in Mining Engineering in July 1986. After graduation, he worked as an assistant professor at the Department of Mining Engineering in Beijing Graduate School, CUMT. In January 1992, he started his graduate program towards a Doctor of Philosophy degree in Mining Engineering at West Virginia University.




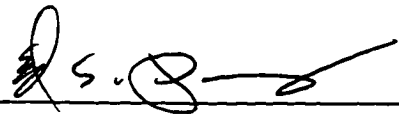
**APPROVAL OF THE EXAMINING COMMITTEE**

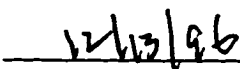
  
A. W. Khair, Ph.D., Professor  
Department of Mining Engineering

  
Mo. Gabr, Ph.D., Professor  
Department of Civil Engineering

  
H. Rauch, Ph.D., Professor  
Department of Geology Engineering

  
D. Thompson, Ph.D., Professor  
Department of Mining Engineering

  
S. S. Peng, Ph.D., Professor & Chairman  
Department of Mining Engineering  
Chairman of the Examining Committee

  
Date